1260770

THE UNITED STATES OF AMERICA

TO ALL TO WHOM THESE PRESENTS SHALL COME:

UNITED STATES DEPARTMENT OF COMMERCE

United States Patent and Trademark Office

December 13, 2004

THIS IS TO CERTIFY THAT ANNEXED HERETO IS A TRUE COPY FROM THE RECORDS OF THE UNITED STATES PATENT AND TRADEMARK OFFICE OF THOSE PAPERS OF THE BELOW IDENTIFIED PATENT APPLICATION THAT MET THE REQUIREMENTS TO BE GRANTED A FILING DATE.

APPLICATION NUMBER: *60/513,582*
FILING DATE: *October 24, 2003*
RELATED PCT APPLICATION NUMBER: *PCT/US04/35143*

Certified by

Jon W Dudas

Acting Under Secretary of Commerce
for Intellectual Property
and Acting Director of the U.S.
Patent and Trademark Office

IN THE UNITED STATES PATENT AND TRADEMARK OFFICE

REQUEST FOR FILING PROVISIONAL PATENT APPLICATION
Under 35 USC 111(b)
(Not for DESIGN cases)

Box: PROVISIONAL APPLICATION

The Asst. Commissioner of Patents
and Trademarks
Washington, D.C. 20231

PROVISIONAL APPLICATION
Under Rule 53(c)

Sir:

Herewith is a PROVISIONAL APPLICATION

Title: **SPECTRAL IDENTIFICATION OF NEW STATES OF HYDROGEN, LAB NOTEBOOK OF RANDELL L. MILLS**

Our Order No. 50-0687	62226		
	C#	M#	
Atty. Dkt.	62226-P-SI-1		
	M#	Client Ref	

including:

Date: 24 October 2003

1. Specification: 89 pages 2. [ ] Specification in non-English 3. [x] Drawings: 19 sheet(s)

4. The invention [ ] was [X] was not made by, or under a contract with, an agency of the U.S. Government.
If yes, Government agency/contact # = _____

5. [ ] Attached is an assignment and cover sheet. Please return the recorded assignment to the undersigned.

6. [X] Applicant(s) claims "small entity" status under Rules 9 & 27.

7. [ ] Attached:

8. This application is made by the following named inventor(s) (Double check instructions for accuracy.):

(1) Inventor	**Randell**	**L.**	**Mills**
	First	Middle Initial	Family Name
Residence	**Cranbury**		**New Jersey**
	City		State/Foreign Country

(2) Inventor			
	First	Middle Initial	Family Name
Residence			
	City		State/Foreign Country

(3) Inventor			
	First	Middle Initial	Family Name
Residence			
	City		State/Foreign Country

(4) Inventor			
	First	Middle Initial	Family Name
Residence			
	City		State/Foreign Country

(5) Inventor			
	First	Middle Initial	Family Name
Residence			
	City		State/Foreign Country

	Large/Small Entity		Fee Code
10. Filing Fee	$80	$80	114/214
11. If "non-English" box 2 is X'd, add Rule 17(k) processing fee	$	+	139
12. If "assignment" box 5 is X'd, add recording fee	$		581
13. TOTAL FEE ENCLOSED =		$80	

CHARGE STATEMENT: The Commissioner is hereby authorized to charge any fee specifically authorized hereafter, or any missing or insufficient fee(s) filed, or asserted to be filed, or which should have been filed herewith or concerning any paper filed hereafter, and which may be required under Rules 16-17 (missing or insufficient fee only) now or hereafter relative to this application or credit any overpayment, to our Account/Order Nos. shown in the heading hereof for which purpose a duplicate copy of this sheet is attached.

Manelli Denison & Selter, PLLC By: Atty: **Jeffrey S. Melcher** Reg. No. **35,950**

Customer No.: 20736

Sig: Fax: (202) 887-0336

Tel: **(202)261-1045**

NOTE: File in duplicate with 2 post card receipts & attachments

APPLICATION UNDER UNITED STATES PATENT LAWS

Invention: **SPECTRAL IDENTIFICATION OF NEW STATES OF HYDROGEN, LAB NOTEBOOK OF RANDELL L. MILLS**

Inventor(s): Randell L. Mills
493 Old Trenton Road
Cranbury, NJ 08512

Attorney Docket No: 62226-P-SI-1

Jeffrey S. Melcher
Manelli, Denison & Selter P.L.L.C.
Customer No.: 20736
2000 M Street, N.W.
7th Floor
Washington, D.C. 20036-3307

THIS IS A PROVISIONAL PATENT APPLICATION

SPECIFICATION

Spectral Identification of New States of Hydrogen

R. L. Mills, Y. Lu, J. He, M. Nansteel, P. Ray, X. Chen, A. Voigt, B. Dhandapani
BlackLight Power, Inc., 493 Old Trenton Road, Cranbury, NJ 08512

ABSTRACT

Novel emission lines with energies of $q \cdot 13.6\,eV$ where $q = 1,2,3,4,6,7,8,9,$ *or* 11 were previously observed by extreme ultraviolet (EUV) spectroscopy recorded on microwave discharges of helium with 2% hydrogen [R. L. Mills, P. Ray, "Extreme Ultraviolet Spectroscopy of Helium-Hydrogen Plasma", J. Phys. D, Applied Physics, Vol. 36, (2003), pp. 1535-1542]. These lines matched $H(1/p)$, fractional Rydberg states of atomic hydrogen wherein $n = \frac{1}{2}, \frac{1}{3}, \frac{1}{4}, ..., \frac{1}{p}$; ($p \leq 137$ is an integer) replaces the well known parameter n = integer in the Rydberg equation for hydrogen excited states. Evidence supports that these states are formed by a resonant nonradiative energy transfer to He^+ acting as a catalyst. Ar^+ also serves as a catalyst to form $H(1/p)$; whereas, krypton, xenon, and their ions serve as controls. $H(1/p)$ may react with a proton and two $H(1/p)$ may react to form $H_2(1/p)^+$ and $H_2(1/p)$, respectively, that have vibrational and rotational energies that are p^2 times those of the species comprising uncatalyzed atomic hydrogen. A series of over twenty peaks in the 10-65 nm region emitted from low-pressure helium-hydrogen (90/10%) and argon-hydrogen (90/10%) microwave plasmas matched the energy spacing of 2^2 times the vibrational energy of H_2^+ with the series ending on the bond energy of $H_2(1/4)^+$. Rotational lines were observed in the 145-300 nm region from atmospheric pressure electron-beam excited argon-hydrogen plasmas. The unprecedented energy spacing of 4^2 times that of hydrogen established the internuclear distance as 1/4 that of H_2 and identified $H_2(1/4)$. $H_2(1/p)$ gas was isolated by liquefaction at liquid nitrogen temperature and by decomposition of compounds found to contain the corresponding hydride ions $H^-(1/p)$. The $H_2(1/p)$ gas was dissolved in $CDCl_3$ and characterized by ^1H NMR. Considering solvent effects, singlet peaks upfield of H_2 were observed with a predicted integer spacing of 0.64 ppm at 3.47, 3.03, 2.18, 1.47, 0.85, and 0.22 ppm which matched the consecutive series $H_2(1/2)$, $H_2(1/3)$, $H_2(1/4)$, $H_2(1/5)$, $H_2(1/6)$, and $H_2(1/7)$, respectively. Excess power was absolutely measured from the helium-hydrogen plasma. For an input of 41.9 W, the total plasma power of the helium-hydrogen plasma measured by water bath calorimetry was 62.1 W corresponding to 20.2 W of excess power in 3 cm^3. The excess power density and energy balance were high, 6.7 W/cm^3 and $-5.4\,X10^4\,kJ/mole\,H_2$ ($280\,eV/H\,atom$), respectively. In addition to power applications, battery and rocketry propellant reactions are proposed that may be transformational, and observed excited vibration-rotational levels of $H_2(1/4)$ could be the basis of a UV laser that could significantly advance photolithography.

Keywords: fractional-principal-quantum-level atomic and molecular hydrogen and hydrogen molecule ion, vibrational series, rotational series, LN-condensable hydrogen, NMR series, exothermic plasma catalysis reaction

I. Introduction

A. Theoretical Predictions

The basic spectral emission of pure helium and hydrogen light sources have been well known for about a century. Recently, however, unique vacuum ultraviolet (VUV) emission lines were found at predicted wavelengths and reported in numerous publications [1-5]. For example, extreme ultraviolet (EUV) spectroscopy was recorded on microwave discharges of helium with 2% hydrogen. Novel emission lines were observed with energies of $q \cdot 13.6\,eV$, $q = 1,2,3,7,9,11$. or $q \cdot 13.6\,eV$, $q = 4,6,8$ less $21.2\,eV$ corresponding to inelastic scattering of these photons by helium atoms due to excitation of $He(1s^2)$ to $He(1s^1 2p^1)$. These strong emissions are not found in any single gas plasma, and cannot be assigned to the known emission of any species of the single gases studied such as H, H^-, H_2, H_2^+, H_3^+, He, He_2^*, and He^+, known species of the mixture such as He_2^+, HeH^+, HeH, HHe_2^+, and HHe_n^+ and He_n, or possible contaminants [1]. However the results can be explained by a novel catalytic reaction involving atomic hydrogen [1-5].

J. R. Rydberg showed that all of the spectral lines of atomic hydrogen were given by a completely empirical relationship:

$$\bar{\nu} = R\left(\frac{1}{n_f^2} - \frac{1}{n_i^2}\right) \tag{1}$$

where $R = 109{,}677\ cm^{-1}$, $n_f = 1,2,3,\ldots$, $n_i = 2,3,4,\ldots$ and $n_i > n_f$. Bohr, Schrödinger, and Heisenberg each developed a theory for atomic hydrogen that gave the energy levels in agreement with Rydberg's equation.

$$E_n = -\frac{e^2}{n^2 8\pi\varepsilon_o a_H} = -\frac{13.598\,eV}{n^2} \tag{2a}$$

$$n = 1,2,3,\ldots \tag{2b}$$

where e is the elementary charge, ε_o is the permittivity of vacuum, and a_H is the radius of the hydrogen atom. The excited energy states of atomic hydrogen are given by Eq. (2a) for $n > 1$ in Eq. (2b). The $n = 1$ state is the "ground" state for "pure" photon transitions (i.e. the $n = 1$ state can absorb a photon and go to an excited electronic state, but it cannot release a photon and go to a lower-energy electronic state). However, an electron transition from the ground state to a lower-energy state may be possible by a resonant nonradiative energy transfer such as multipole coupling or a resonant collision mechanism. Processes such as hydrogen molecular bond formation that occur without photons and that require collisions are common [6]. Also, some commercial phosphors are based on resonant nonradiative energy transfer involving multipole

coupling [7].

The theory reported previously [1-5, 8-13] predicts that atomic hydrogen may undergo a catalytic reaction with certain atoms, excimers, and ions which provide a reaction with a net enthalpy of an integer multiple of the potential energy of atomic hydrogen, $E_h = 27.2\ eV$ where E_h is onc hartree. Specific species (e.g. He^+, Ar^+, and K) identifiable on the basis of their known electron energy levels are required to be present in plasmas with atomic hydrogen to catalyze the process. In contrast, species such as atoms or ions of Kr or Xe do not fulfill the catalyst criterion—a chemical or physical process with an enthalpy change equal to an integer multiple of E_h that is sufficiently reactive with atomic hydrogen under reaction conditions. The reaction involves a nonradiative energy transfer followed by $q \cdot 13.6\ eV$ emission or $q \cdot 13.6\ eV$ transfer to H to form extraordinarily hot, excited-state H [11-17] and a hydrogen atom that is lower in energy than unreacted atomic hydrogen that corresponds to a fractional principal quantum number. That is

$$n = \frac{1}{2}, \frac{1}{3}, \frac{1}{4}, ..., \frac{1}{p}; \quad p \le 137 \text{ is an integer} \tag{2c}$$

replaces the well known parameter $n = \text{integer}$ in the Rydberg equation for hydrogen excited states. The $n = 1$ state of hydrogen and the $n = \frac{1}{\text{integer}}$ states of hydrogen are nonradiative, but a transition between two nonradiative states, say $n = 1$ to $n = 1/2$, is possible via a nonradiative energy transfer. Thus, a catalyst provides a net positive enthalpy of reaction of $m \cdot 27.2\ eV$ (i.e. it resonantly accepts the nonradiative energy transfer from hydrogen atoms and releases the energy to the surroundings to affect electronic transitions to fractional quantum energy levels). As a consequence of the nonradiative energy transfer, the hydrogen atom becomes unstable and emits further energy until it achieves a lower-energy nonradiative state having a principal energy level given by Eqs. (2a) and (2c).

Prior related studies that support the possibility of a novel reaction of atomic hydrogen which produces hydrogen in fractional quantum states that are at lower energies than the traditional "ground" ($n = 1$) state include extreme ultraviolet (EUV) spectroscopy [1-5, 10-13, 16-27], characteristic emission from catalysts and the hydride ion products [12-13, 18-20, 22-23], lower-energy hydrogen emission [1-5], chemically formed plasmas [10-13, 18-23], Balmer α line broadening [1, 2, 11-18, 20, 22-23, 25-26], population inversion of H lines [22-25], elevated electron temperature [14-16, 26], anomalous plasma afterglow duration [21], power generation [2, 4, 16, 26], and analysis of novel chemical compounds [28-30].

$H(1/p)$ may react with a proton and two $H(1/p)$ may react to form $H_2(1/p)^+$ and $H_2(1/p)$, respectively. The hydrogen molecular ion and molecular charge and current density functions, bond distances, and energies were solved previously [9] from the Laplacian in

ellipsoidal coordinates with the constraint of nonradiation.

$$(\eta-\zeta)R_\xi\frac{\partial}{\partial\xi}(R_\xi\frac{\partial\phi}{\partial\xi})+(\zeta-\xi)R_\eta\frac{\partial}{\partial\eta}(R_\eta\frac{\partial\phi}{\partial\eta})+(\xi-\eta)R_\zeta\frac{\partial}{\partial\zeta}(R_\zeta\frac{\partial\phi}{\partial\zeta})=0 \tag{3}$$

The total energy of the hydrogen molecular ion having a central field of $+pe$ at each focus of the prolate spheroid molecular orbital is

$$E_T=-p^2\left\{\frac{e^2}{8\pi\varepsilon_o a_H}(4\ln 3-1-2\ln 3)\left[1+p\sqrt{\frac{2\hbar\sqrt{\frac{2e^2}{4\pi\varepsilon_o(2a_H)^3}}}{m_e c^2}}\right]-\frac{1}{2}\hbar\sqrt{\frac{k}{\mu}}\right\} \tag{4}$$

$$=-p^2 16.13392\ eV-p^3 0.118755\ eV$$

where p is an integer, $\hbar$ is Planck's constant bar, m_e is the mass of the electron, c is the speed of light in vacuum, μ is the reduced nuclear mass, and k is the harmonic force constant solved previously [9]. The total energy of the hydrogen molecule having a central field of $+pe$ at each focus of the prolate spheroid molecular orbital is

$$E_T=-p^2\left\{\frac{e^2}{8\pi\varepsilon_o a_0}\left[\left(2\sqrt{2}-\sqrt{2}+\frac{\sqrt{2}}{2}\right)\ln\frac{\sqrt{2}+1}{\sqrt{2}-1}-\sqrt{2}\right]\left[1+p\sqrt{\frac{2\hbar\sqrt{\frac{e^2}{4\pi\varepsilon_o a_0^3}}}{m_e c^2}}\right]-\frac{1}{2}\hbar\sqrt{\frac{k}{\mu}}\right\} \tag{5}$$

$$=-p^2 31.351\ eV-p^3 0.326469\ eV$$

where a_o is the Bohr radius.

The bond dissociation energy E_D of hydrogen molecular ion $H_2(1/p)^+$ is the difference between the total energy of the corresponding hydrogen atom $H(1/p)$ and E_T:

$$E_D=E(H(1/p))-E_T \tag{6}$$

where [31]

$$E(H(1/p))=-p^2 13.59844\ eV \tag{7}$$

E_D is given by Eqs. (6-7) and Eq. (4):

$$\begin{aligned}E_D&=-p^2 13.59844-E_T\\&=-p^2 13.59844-\left(-p^2 16.13392\ eV-p^3 0.118755\ eV\right)\\&=p^2 2.535\ eV+p^3 0.118755\ eV\end{aligned} \tag{8}$$

The bond dissociation energy E_D of hydrogen molecule $H_2(1/p)$ is the difference

between the total energy of the corresponding hydrogen atoms and E_T

$$E_D = E(2H(1/p)) - E_T \tag{9}$$

where [31]

$$E(2H(1/p)) = -p^2 27.20\ eV \tag{10}$$

E_D is given by Eqs. (9-10) and (5):

$$\begin{aligned} E_D &= -p^2 27.20\ eV - E_T \\ &= -p^2 27.20\ eV - \left(-p^2 31.351\ eV - p^3 0.326469\ eV\right) \\ &= p^2 4.151\ eV + p^3 0.326469\ eV \end{aligned} \tag{11}$$

The calculated and experimental parameters of H_2, D_2, H_2^+, and D_2^+ from Ref. [9] are given in Table 1.

The vibrational and rotational energies of fractional-Rydberg-state hydrogen molecular ion $H_2(1/p)^+$ and molecular hydrogen $H_2(1/p)$ are p^2 those of H_2^+ and H_2, respectively. Thus, the vibrational energies E_{vib} for the $\upsilon = 0$ to $\upsilon = 1$ transition of hydrogen-type molecular ions $H_2(1/p)^+$ are [9]

$$E_{vib} = p^2 0.271\ eV \tag{12}$$

where p is an integer and the experimental vibrational energy for the $\upsilon = 0$ to $\upsilon = 1$ transition of H_2^+ $E_{H_2^+(\upsilon=0\to\upsilon=1)}$ is given by Karplus and. Porter [32] and NIST [33]. Similarly, the rotational energies E_{rot} for the J to $J+1$ transition of hydrogen-type molecular ions $H_2(1/p)^+$ are [9]

$$E_{rot} = E_{J+1} - E_J = \frac{\hbar^2}{I}[J+1] = p^2(J+1)0.00739\ eV \tag{13}$$

where p is an integer, I is the moment of inertia, and the experimental rotational energy for the $J = 0$ to $J = 1$ transition of H_2 is given by Atkins [34].

The vibrational energies E_{vib} for the $\upsilon = 0$ to $\upsilon = 1$ transition of hydrogen-type molecules $H_2(1/p)$ are [9]

$$E_{vib} = p^2 0.515902\ eV \tag{14}$$

where p is an integer and the experimental vibrational energy for the $\upsilon = 0$ to $\upsilon = 1$ transition of H_2 $E_{H_2(\upsilon=0\to\upsilon=1)}$ is given by Beutler [35] and Herzberg [36].

The harmonic oscillator potential energy function can be expanded about the internuclear distance and expressed as a Maclaurin series corresponding to a Morse potential after Karplus and Porter (K&P) [32] and after Eq. (96) of Ref. [9]. Treating the Maclaurin series terms as anharmonic perturbation terms of the harmonic states, the energy corrections can be found by perturbation methods. The energy $\tilde{\nu}_{\upsilon+1}$ of state $\upsilon = \upsilon' + 1$ is

$$\tilde{\nu}_{\upsilon'+1} = (\upsilon'+1)\omega_0 - \upsilon'(\upsilon'+1)\omega_0 x_0, \quad \upsilon' = 0,1,2,3... \tag{15}$$

where

$$\omega_0 x_0 = \frac{hc\omega_0^2}{4D_0} \tag{16}$$

From Eqs. (11), (14), and (16)

$$\omega_0 x_0 = \frac{hc\omega_0^2}{4D_0} = \frac{100hc\left(8.06573X10^3 \frac{cm^{-1}}{eV} p^2 0.5159\ eV\right)^2}{4e\left(p^2 4.151\ eV + p^3 0.326469\ eV\right)} cm^{-1} \quad (17)$$

Using Eqs. (14-17) with $p = 1$ and $p = 4$, gives

$$\tilde{\nu}_{\upsilon+1} = (\upsilon'+1)4161\ cm^{-1} - \upsilon'(\upsilon'+1)119.9\ cm^{-1}$$
$$E_{vib\,\upsilon'+1} = (\upsilon'+1)0.5159\ eV - \upsilon'(\upsilon'+1)0.01486\ eV, \quad \upsilon' = 0,1,2,3... \quad (18)$$

and

$$\tilde{\nu}_{\upsilon+1} = (\upsilon'+1)66,578\ cm^{-1} - \upsilon'(\upsilon'+1)1574\ cm^{-1}$$
$$E_{vib\,\upsilon+1} = (\upsilon'+1)8.254\ eV - \upsilon'(\upsilon'+1)0.1951\ eV, \quad \upsilon' = 0,1,2,3... \quad (19)$$

respectively, where the calculated $\omega_0 x_0 = 119.9\ cm^{-1}$ for H_2 is in agreement with the literature values of $117.91\ cm^{-1}$ from K&P [32] and $121.34\ cm^{-1}$ from Lide [37].

Similarly to $H_2(1/p)^+$, the rotational energies E_{rot} for the for the J to $J+1$ transition of hydrogen-type molecules $H_2(1/p)$ are [9]

$$E_{rot} = E_{J+1} - E_J = \frac{\hbar^2}{I}[J+1] = p^2(J+1)0.01509\ eV \quad (20)$$

where p is an integer, I is the moment of inertia, and the experimental rotational energy for the $J = 0$ to $J = 1$ transition of H_2 is given by Atkins [34].

The p^2 dependence of the rotational energies results from an inverse p dependence of the internuclear distance and the corresponding impact on I. The predicted internuclear distances $2c'$ for $H_2(1/p)^+$ and $H_2(1/p)$ are

$$2c' = \frac{2a_o}{p} \quad (21)$$

and

$$\frac{a_o\sqrt{2}}{p} 2c' = \frac{a_o\sqrt{2}}{p} \quad (22)$$

respectively.

B. Experiments to Test the Theoretical Predictions

The reaction Ar^+ to Ar^{2+} has a net enthalpy of reaction of $27.63\ eV$; thus, it may serve as a catalyst to form $H(1/2)$. The product of the catalysis reaction $H(1/2)$ may further serve as both a catalyst and a reactant to form $H(1/4)$ [2-3]. Also, the second ionization energy of helium is $54.4\ eV$; thus, the ionization reaction of He^+ to He^{2+} has a net enthalpy of reaction of $54.4\ eV$ which is equivalent to $2 \cdot 27.2\ eV$. The product of the catalysis reaction $H(1/3)$ may further serve as both a catalyst and a reactant to form $H(1/4)$ and $H(1/2)$ [2-3].

Since $H_2(1/2)^+$ is a resonant state of $H_2(1/4)^+$, the reaction designated

$$H(1/4)+H^+ \rightarrow H_2(1/4)^+ \tag{23}$$

wherein $H(1/4)$ reacts with a proton to form $H_2(1/4)^+$ is possible with strong emission through vibronic coupling with the resonant state $H_2(1/2)^+$. The frequencies of resonant states of a time harmonic oscillator are an integer of the fundamental frequency corresponding to integer energy separation. The bond energy may be emitted with the energies of vibrational transitions in the transition state that superimpose to give emission to longer wavelengths of that corresponding to the bond energy.

As given previously [9], during bond formation, the electrons undergo a reentrant oscillatory orbit with vibration of the protons. The corresponding energy $\overline{E}_{osc}$ is the difference between the Doppler $\overline{E}_D$ and average vibrational kinetic energies $\overline{E}_{Kvib}$. The latter term from Eq. (4) is given by $\frac{1}{2}\hbar\sqrt{\frac{k}{\mu}}$. Transitions are possible involving the formation of $H_2(1/4)^+$ in an excited vibrational state of the transition state with the emission of the bond energy minus this additional vibrational energy where the vibrational energy of the transition state given by Eq. (108) of Ref. [9] is

$$E_{vib} = \hbar\omega = \hbar p^2 4.44865\, X\, 10^{14}\ rad/s = p^2 0.2928\ eV \tag{24}$$

Thus, with the resonant state of $p=2$, an energy of an integer times the vibrational energy of $H_2(1/2)^+$ plus $\overline{E}_{Kvib}$ goes to vibrational excitation. The energies E_{D+vib} of this series due to vibration in the transition state are given by

$$\begin{aligned} E_{D+vib} &= E_D\left(H_2(1/4)^+\right) - \left(\upsilon^* + \frac{1}{2}\right)2^2 E_{vib\,H_2^+} \\ &= 48.16 - \left(\upsilon^* + \frac{1}{2}\right)1.172\ eV \end{aligned}, \quad \upsilon^* = 0,1,2,3... \tag{25}$$

where $E_D\left(H_2(1/4)^+\right)$ is the bond energy of $H_2(1/4)^+$ given by Eq. (8) and $E_{vib\,H_2^+}$ is the vibrational energy of H_2^+ in the transition state given by Eq. (24). In Eq. (25), υ^* refers to vibrational energies of the transition state which must have equal energy separation as a requirement for resonant emission [9]. Thus, anharmonicity is not predicted. The series is predicted to end at 25.74 nm corresponding to the predicted $H_2(1/4)^+$ bond energy of 48.16 eV given by Eq. (8).

It was described previously that the reaction of $H(1/p)$ with a proton may also involve an excited electronic state and a series of corresponding vibrational and rotational state emission lines [5]. In the reaction designated

$$H(1/2)+H^+ \rightarrow H_2^*[n=1/4;n^*=2]^+ \tag{26}$$

$H(1/2)$ reacts with a proton to form an excited electronic state of the molecular ion $H_2(1/4)^+$ wherein the central field in elliptic coordinates is one half that of ground state (nonradiative

state) of $H_2(1/4)^+$. This state is analogous to the $n=2$ state of atomic hydrogen and is designated as $H_2^+[n=1/4;n^*=2]^+$, except that electronic relaxation may involve a radiationless process with a radiative component involving the oscillating and rotating nuclei which transition to the $\upsilon=0$ state of $H_2(1/4)^+$. The nonradiative energy transfer corresponding to $H(1/2)\rightarrow H(1/4)$ may occur from highest vibrational state (bond-continuum state) of $H_2(1/2)^+$. The absence of anharmonicity favors the proposed mechanism given by Eq. (25) over one given previously [5] corresponding to Eq. (26).

The present paper tests theoretical predictions [1-5, 8-13] that atomic and molecular hydrogen form stable states of lower energy than traditionally thought possible. Substantial spectroscopic and physical differences are anticipated. For example, novel EUV atomic, molecular ion, and molecular spectral emission lines from transitions corresponding to energy levels given by Eqs. (2a) and (2c), Eq. (4), and Eq. (5), respectively, are predicted. The atomic lines have been shown previously [1-4, 26] as well as a series of unique EUV lines assigned to $H_2(1/2)$ [4]. To test further predictions, EUV spectroscopy was performed to search for emission that was characteristic of and identified $H_2(1/4)^+$ and $H_2(1/4)$. Low pressure plasmas are more highly ionized. Thus, we further investigated the emission of the $H_2(1/4)^+$ vibrational series given by Eq. (25) from microwave discharges of helium-hydrogen and argon-hydrogen mixtures. The resolution of the spectra was improved compared to those recorded previously [5] by reducing each of the slits 1.5 to 7.5 times. Also, exact, closed-form solutions of hydrogen molecular ions and molecules are available for testing [9].

The rotational energies provide a very precise measure of I and the internuclear distance using well established theory [32]. Neutral molecular emission was anticipated for high pressure argon-hydrogen plasmas excited by a 15 keV electron beam. Rotational lines for $H_2(1/4)$ were anticipated and sought in the 150-250 nm region. The spectral lines were compared to those predicted by Eqs. (19-20) corresponding to the internuclear distance of 1/4 that of H_2 given by Eq. (22). The predicted energies for the $\upsilon=1\rightarrow\upsilon=0$ vibration-rotational series of $H_2(1/4)$ (Eqs. (19-20)) are

$$\begin{aligned} E_{vib-rot} &= p^2 E_{vib\,H_2(\upsilon=0\rightarrow\upsilon=1)} \pm p^2(J+1)E_{rot\,H_2} \\ &= 4^2 E_{vib\,H_2(\upsilon=0\rightarrow\upsilon=1)} \pm 4^2(J+1)E_{rot\,H_2}\,, \quad J=0,1,2,3... \\ &= 8.254432\ eV \pm (J+1)0.24144\ eV \end{aligned} \tag{27}$$

for $p=4$.

The product $H_2(1/p)$ gas was isolated by liquefaction at liquid nitrogen temperature. The boiling point of the novel molecular hydrogen product is predicted to be different from that of H_2. The ℓ quantum number of $H_2(1/p)$ may be different from zero [8-9] which would give rise to a dipole moment with a corresponding significant increase in the liquefaction temperature

relative to H_2 with no dipole moment. Furthermore, as shown previously [5, 8-9], the parameter of $H_2(1/p)$ corresponding to the radius in elliptic coordinates is $1/p$ times that of H_2 with a corresponding charge density of a factor p^2 times greater than that of H_2. Thus, $H_2(1/p)$ gas may condense at a higher temperature than H_2 due to greater corresponding van der Waals effects as given by the van der Waals equation:

$$P = \frac{RT}{\bar{V} - b} - \frac{a}{\bar{V}^2} \tag{28}$$

In Eq. (28), P is pressure of the gas at a given temperature T and volume per mole $\bar{V}$, and a and b are constants that depend on the particular gas. The term $\frac{a}{\bar{V}^2}$ is meant to correct for the effect of attractive intramolecular forces that lower the pressure. This effect is predicted to be larger for $H_2(1/p)$ compared to H_2. In addition, the nonzero volume of the molecules themselves decreases the volume available for them to move; so, some volume b is subtracted from $\bar{V}$. Again, the smaller volume of $H_2(1/p)$ compared to H_2 favors a lower pressure at a given temperature, or equivalently, favors liquefaction at a higher temperature.

Helium-hydrogen (90/10%) plasma gases were flowed through a high-vacuum (10^{-6} Torr) capable, liquid nitrogen (LN) cryotrap, and the condensed gas was characterized by ^1H nuclear magnetic resonance (NMR) of the LN-condensable gas dissolved in $CDCl_3$. Other sources of hydrogen such as hydrocarbons were eliminated by mass spectroscopy (MS) and Fourier transform infrared spectroscopy (FTIR). The ^1H NMR resonance of $H_2(1/p)$ is predicted to be upfield from that of H_2 due to the fractional radius in elliptic coordinates [8-9] wherein the electrons are significantly closer to the nuclei. The predicted shift $\frac{\Delta B_T}{B}$ for $H_2(1/p)$ derived previously [8-9] is given by the sum of that of H_2 and a relativistic term that depends on $p > 1$:

$$\frac{\Delta B_T}{B} = -\mu_0 \left(4 - \sqrt{2} \ln \frac{\sqrt{2}+1}{\sqrt{2}-1} \right) \frac{e^2}{36 a_0 m_e} (1 + \pi \alpha p) \tag{29}$$

$$\frac{\Delta B_T}{B} = -(28.01 + 0.64p) ppm \tag{30}$$

where $p = 0$ for H_2 since there is no relativistic effect and $p = \text{integer} > 1$ for $H_2(1/p)$ where $p = \text{integer} > 1$.

In addition to liquefaction at liquid nitrogen temperature, $H_2(1/p)$ gas was also isolated by decomposition of compounds found to contain the corresponding hydride ions $H^-(1/p)$. The total shift $\frac{\Delta B_T}{B}$ was calculated previously [8, 20] for the hydride ions $H^-(1/p)$ having a fractional principal quantum number. The shift was given by the sum of that of ordinary hydride ion H^- and a component due to a relativistic effect:

$$\frac{\Delta B_T}{B} = -\mu_0 \frac{e^2}{12 m_e a_0 \left(1+\sqrt{s(s+1)}\right)} (1 + \alpha 2\pi p) = -(29.9 + 1.37p) ppm \qquad (31)$$

where $p = 0$ for H^- since there is no relativistic effect and $p = \text{integer} > 1$ for $H^-(1/p)$ where $p = \text{integer} > 1$. The experimental absolute resonance shift of tetramethylsilane (TMS) is -31.5 ppm relative to the proton's gyromagnetic frequency [38-39]. The results of ^1H MAS NMR spectroscopy were given previously [20, 28-30] on control and novel hydrides synthesized using atomic potassium as a hydrogen catalyst wherein the triple ionization reaction of K to K^{3+}, has a net enthalpy of reaction of $81.7766\,eV$, which is equivalent to $3 \cdot 27.2\,eV$. The KH experimental shift of +1.3 ppm relative to TMS corresponding to absolute resonance shift of -30.2 ppm matched very well the predicted shift of H^- of -30 ppm given by Eq. (31). The ^1H MAS NMR spectrum of novel compound $KH*Cl$ relative to external tetramethylsilane (TMS) showed a large distinct upfield resonance at -4.4 ppm corresponding to an absolute resonance shift of -35.9 ppm that matched the theoretical prediction of $p = 4$. A novel peak of $KH*I$ at -1.5 ppm relative to TMS corresponding to an absolute resonance shift of -33.0 ppm matched the theoretical prediction of $p = 2$. The predicted catalyst reactions, position of the upfield-shifted NMR peaks, and spectroscopic data for $H^-(1/2)$ and $H^-(1/4)$ were found to be in agreement [9, 20].

The decomposition reaction of $H^-(1/p)$ is

$$2M^+H^-(1/p) \xrightarrow{\Delta} H_2(1/p) + 2M \qquad (32)$$

where M^+ is a metal ion. NMR peaks of $H_2(1/p)$ given by Eqs. (29-30) provide a direct test of whether compounds such as $KH*I$ contain hydride ions in the same fractional quantum state p. Furthermore, the observation of a series of singlet peaks upfield of H_2 with a predicted integer spacing of 0.64 ppm provides a powerful means to confirm the existence of $H_2(1/p)$.

The exothermic helium plasma catalysis of atomic hydrogen was shown previously [14-15] by the observation of an average hydrogen atom temperature of $180-210\,eV$ for helium-hydrogen mixed plasmas versus $\approx 3\,eV$ for hydrogen alone. Since the electronic transitions are very energetic power balances of helium-hydrogen plasmas compared to control krypton plasmas were measured using water bath calorimetry to determine whether this reaction has sufficient kinetics to merit its consideration as a practical power source.

II. Experimental

To investigate the vibrational series of $H_2(1/4)^+$, EUV spectra (20-65 nm) were recorded on light emitted from microwave discharge plasmas of helium, argon, krypton, or xenon or a mixture of 10% hydrogen with each noble gas. Each ultrapure test gas or mixture was flowed

through a half inch diameter quartz tube at 100 mTorr maintained with a total gas flow rate of 10 sccm. The tube was fitted with an Opthos coaxial microwave cavity (Evenson cavity). The microwave generator was an Opthos model MPG-4M generator (Frequency: 2450 MHz). The input power to the plasma was set at 40 W.

The spectrometer was a McPherson 4° grazing incidence EUV spectrometer (Model 248/310G) equipped with a grating having 600 G/mm with a radius of curvature of $\approx 1\,m$ that covered the region $5-65\,nm$. The angle of incidence was 87°. The wavelength resolution was about 0.1 nm (FWHM) with an entrance and exit slit width of 40 μm. A CEM was used to detect the EUV light. The increment was 0.01 nm and the dwell time was 1 s.

Vibration-rotational emission of $H_2(1/4)$ was investigated using an electron gun provided by Rutgers University and described previously [40-41] to initiate argon plasmas with 1% hydrogen and oxygen or nitrogen in the pressure range of 450-1000 Torr. Krypton replaced argon in the controls. The electrons were accelerated with a high voltage of 12.5 keV at a beam current of 10 μA. The electron gun was sealed with a thin (300 nm thickness) SiN_x foil that served as a 1 mm^2 electron window to the cell at high gas pressure (760 torr). The beam energy was deposited by hitting the target gases, and the light emitted by beam excitation exited the cell thorough a MgF_2 window mounted at the entrance of a normal incidence McPherson 0.2 meter monochromator (Model 302) equipped with a 1200 lines/mm holographic grating with a platinum coating. The wavelength region covered by the monochromator was $5-560\,nm$. The EUV spectrum was recorded with a photomultiplier tube (PMT). The wavelength resolution was about 0.8 nm (FWHM) with an entrance and exit slit width of 200 μm. The increment was 0.1 nm and the dwell time was 1 s. The PMT (Model R8486, Hamamatsu) used has a spectral response in the range of 115-320 nm with a peak efficiency at about 225 nm. The emission was essentially flat for $200 < \lambda > 275\,nm$, but a notch in the response existed in the short wavelength range with a minimum at 150 nm. Peak assignments were based on an external calibration against standard line emissions.

Condensable gas from helium-hydrogen (90/10%) microwave plasmas maintained in the Evenson cavity was collected in a high-vacuum (10^{-6} Torr) capable, LN cryotrap shown in Figure 1 as described previously [27]. After each plasma run the cryotrap was pumped down to 10^{-5} Torr to remove any non-condensable gases in the system. The pressure was recorded as a function of time as the cryotrap was warmed to room temperature. Typically, about 3 Torr of condensed gas was collected in a 2 hr plasma run. Controls were hydrogen and helium alone.

The mass spectra ($m/e = 1$ to $m/e = 200$) of ultrahigh purity hydrogen (Praxair) control samples and samples of the condensable gas from the helium-hydrogen microwave plasmas were recorded with a residual gas analyzer.

Gases from a 700 mTorr He/H_2 (90/10%) Evenson microwave plasma were flowed

through a long capillary tube which was maintained in the temperature range ~12-17 K by a cryo-cooler. Residual gas was pumped from the capillary, condensable gas was collected over a period of several hours, and the system was evacuated to 10^{-5} Torr to remove any non-condensable gases in the system. Controls were hydrogen and helium alone. Two capillary valves were closed to trap any vaporizing gas as the cryo-cooler was stopped, and the tube was warmed to room temperature. Typically about 100 mTorr of gas was collected over a 24 to 48 hour period and then analyzed by mass spectroscopy and compared with the results for a control sample collected in the same way, except without plasma.

The system comprised welded stainless steel tubing with metal gasket and rubber o-ring connections as shown in Figure 2. Premixed He/H_2 (90/10%) was flowed from a supply bottle through a metering valve and a LN trap just upstream of the plasma tube. A second LN trap downstream of the plasma tube was used to remove any water vapor generated by the plasma. The process gas pressure was monitored by a Baratron absolute pressure gauge upstream of the cryo-head. The cryo-cooler comprised a compressor (CTI Model SC) and cryo-head (CTI Cryogenics Model 22). The principle component of the cryo-head was an evacuated cylindrical chamber of approximately one liter volume through which the cryogenic refrigerant was circulated in a closed system. A stainless steel cold stage extended from the base of the chamber on the chamber axis. A fabricated cylindrical copper spindle was attached to the existing cold stage by screws. Thermal contact resistance between the spindle and cold stage was minimized by an intervening layer of conducting grease. Approximately 1.7 m of copper capillary tubing, 1.56 mm OD and 0.88 mm ID, was wound onto a spiral groove with 5.5 grooves per cm pitch machined onto the spindle. The capillary tube was fused to the spindle along its span with tin/lead solder. A cryogenic silicon diode temperature sensor was also attached to the spindle just beneath the capillary winding. The sensor output was monitored with a readout (TRI Research Cryo-Controller Model T-2000). The sensor accuracy was better than ± 0.1 K in the range 10-300 K.

The system was connected to either a Dycor Model DM200MS or Model D200MP mass spectrometer through a sampling tube. A background scan ($m/e = 1$ to $m/e = 200$) was acquired for reference before introducing the collected gas to the mass spectrometer. Then, the valve just downstream of the cryo-head was opened, allowing gas to flow into the sample tube and spectrometer. Several scans were taken over a period of about 10 minutes while gas was slowly drawn out of the capillary tube into the spectrometer.

Sealed ^1H NMR samples were prepared by collecting the condensed gas from the cryotrap in $CDCl_3$ solvent (99.99% Cambridge isotopes) in an NMR tube (5 mm OD, 23 cm length, Wilmad) maintained at LN-temperature which was then sealed as described previously [27]. Control NMR samples comprised ultrahigh purity hydrogen (Praxair) and the helium-

hydrogen (90/10%) mixture with $CDCl_3$ solvent. The NMR spectra were recorded with a 300 MHz Bruker NMR spectrometer that was deuterium locked. The chemical shifts were referenced to the frequency of tetramethylsilane (TMS) at 0.00 ppm.

*KH*I* that was prepared under long duration (two weeks) synthesis according to methods given previously [28-30], and one gram samples were placed in a thermal decomposition reactor under an argon atmosphere. The reactor comprised a 1/4" OD by 3" long quartz tube that was sealed at one end and connected at the open end with Swagelock™ fittings to a T. One end of the T was connected to the NMR tube containing $CDCl_3$ solvent, and the other end was attached to a turbo pump. The apparatus was evacuated to less than 1 milliTorr with the $CDCl_3$ maintained at LN temperature. The sample was heated to 200 °C under vacuum. A valve to the pump was closed, and the sample was heated in the evacuated quartz chamber containing the sample to above 600 °C until the sample melted. Gas released from the sample was collected in the $CDCl_3$ solvent, the NMR tube was sealed and warmed to room temperature, and the NMR spectrum was recorded. Using identical samples, the NMR-tube end of the collection apparatus was connected directly to the sampling port of a quadrupole mass spectrometer to test for hydrocarbon contamination. FTIR was also performed on the released gas for this purpose.

An NMR sample from *KH*I* provided by BlackLight Power, Inc. was also prepared and analyzed at the Naval Air Warfare Center Weapons Division, Naval Air Warfare Center, China Lake, CA under the same procedure except that the $CDCl_3$ solvent was maintained at ice temperature during hydrogen gas collection, and the NMR spectrum was recorded with a 400 MHz instrument at China Lake. Control NMR samples of ultrapure hydrogen dissolved in $CDCl_3$ solvent were also prepared, and NMR spectra were obtained under conditions matching those of the *KH*I*-derived samples.

The excess power was measured by water bath calorimetry on helium-hydrogen (95/5%) plasmas maintained in a microwave discharge cell compared to control plasmas with the same input power as described previously [26]. The system is shown in Figure 3. The water bath was calibrated by a high precision heater and power supply. A high precision linear response thermistor probe (Omega OL-703) recorded the temperature of the 45 L water bath as a function of time for the stirrer alone to establish the baseline. The heat capacity was determined for several input powers, 30, 40, and 50 W ± 0.01 W, and was found to be independent of input power over this power range within ± 0.05%. The temperature rise of the reservoir as a function of time gave a slope in °C/s. This slope was baseline corrected for the negligible stirrer power and loss to ambient. The constant known input power (J/s), was divided by this slope to give the heat capacity in J/°C. Then, in general, the total power output from the cell to the reservoir was determined by multiplying the heat capacity by the rate of temperature rise (°C/s) to give J/s.

Since the cell and water bath system were adiabatic, the general form of the power balance equation with the possibility of excess power is:

$$P_{in} + P_{ex} - P_{out} = 0 \tag{33}$$

where P_{in} is the microwave input power, P_{ex} is the excess power generated from the hydrogen catalysis reaction, and P_{out} is the thermal power loss from the cell to the water bath. Since the cell was surrounded by water that was contained in an insulated reservoir with negligible thermal losses, the temperature response of the thermistor T as a function of time t was determined to be

$$\dot{T}(t) = \left(1.940\,X\,10^5\ J/°C\right)^{-1} \times P_{out} \tag{34}$$

where $1.940\,X\,10^5\ J/°C$ is the heat capacity for the least square curve fit of the response to power input for the control experiments ($P_{ex} = 0$). The slope was recorded for about 2 hours after the cell had reached a thermal steady state, to achieve an accuracy of ± 1%.

III. Results and Discussion

A. EUV spectroscopy of Helium-Hydrogen and Argon-Hydrogen Plasmas

a. Detection of Fractional Rydberg State Hydrogen Molecular Ion $H_2(1/4)^+$

In the case of the EUV spectra of helium, krypton, xenon, krypton-hydrogen (90/10%), or xenon-hydrogen (90/10%), no peaks were observed below 65 nm, and no spurious peaks or artifacts due to the grating or the spectrometer were observed. No changes in the emission spectra were observed by the addition of hydrogen to noncatalysts krypton or xenon. Only known atom and ion peaks were observed in the EUV spectrum of the helium and argon microwave discharge emission.

The EUV spectra (20-65 nm) of the microwave plasmas of xenon and 10% hydrogen mixed with helium, krypton, and xenon are shown in Figure 4. No emission was observed from the noncatalyst controls, krypton and xenon. A characteristic vibrational series was observed for helium-hydrogen (90/10%), but at higher energies than any known molecule by about an order of magnitude. The series was not observed with helium alone as shown in Figure 5. The energies of the peaks observed in Figures 4 and 5 are plotted in Figure 6 as a function of peak number or integer υ^*. The slope of the linear curve fit in Figure 6 is 1.18 eV, and the intercept is 47.6 eV which matches the predicted series given by Eq. (25) to within the spectrometer resolution of 1%. This energy separation matches the vibrational energy of the resonant state $H_2(1/2)^+$, and the series terminates at about 25.7 nm corresponding to the predicted bond energy of $H_2(1/4)^+$ of 48.16 eV given by Eq. (8). The absence of anharmonicity identifies the mechanism given by Eq. (25) over that given by Eq. (26). Thus, emission in this region is due to the reaction

$H(1/4)+H^{+}\rightarrow H_2(1/4)^{+}$ with vibronic coupling with the resonant state $H_2(1/2)^{+}$ within the transition state. The predicted emission at $E_{D+vib}=E_D\left(H_2(1/4)^{+}\right)-\left(\upsilon^{*}+\frac{1}{2}\right)2^2E_{vib\,H_2^{+}}$ was observed for $\upsilon^{*}=0,1,2,3...24$. All other peaks in the spectra were assigned to He I and He II.

The EUV spectra (20-65 nm) of microwave plasmas of argon-hydrogen (90/10%) compared with argon alone are shown in Figure 7. The vibrational series of peaks with an energy spacing of 1.18 eV was observed from the argon-hydrogen plasma having Ar^{+} catalyst with hydrogen. In contrast, the series was not observed without hydrogen. The peaks matched Eq. (25) for $\upsilon^{*}=0,1,2,3...24$.

b. Detection of Fractional Rydberg State Molecular Hydrogen $H_2(1/4)$

The observation of emission due to the reaction $H(1/4)+H^{+}\rightarrow H_2(1/4)^{+}$ at low pressure (< 1 Torr) shown in Figures 4 and 5 indicates that $H(1/4)$ formed in the argon-hydrogen plasma. Molecular formation was anticipated under high-pressure conditions (~760 Torr). Thus, EUV spectroscopy of argon-hydrogen plasmas was performed to search for $H_2(1/4)$ from $H(1/4)$ formed by Ar^{+} as a catalyst. Rather than using the 4° grazing incidence EUV spectrometer, the normal incidence spectrometer was used at high pressure which required a window and a electron beam to maintain a plasma. Since the 15 keV beam rapidly transfers energy to the target gas and produces a large population of species with energies of a few 10's of eVs of kinetic energy, it was anticipated that the beam could directly or indirectly collisionally excite vibration-rotational states of $H_2(1/4)$. The corresponding emission provides a direct measure of the internuclear distance; thus, this method provides the possibility of direct confirmation of $H_2(1/4)$.

The atmospheric-pressure argon plasma formed with the 15 keV electron beam contains a high population of excimers such as Ar_2^{*} [40-41]. Ar_2^{*} has an excited state energy of about 9-10 eV; thus, the ionization reaction

$$Ar_2^{*}+O^{+}\rightarrow Ar+Ar^{+}+O \qquad (35)$$

is energetically favorable wherein the first ionization energies of Ar and O are 15.75962 and 13.61806 eV, respectively. Ar^{+} serves as a catalyst when H is present. Thus, spectra were recorded on argon-hydrogen-oxygen plasmas maintained with a 15 keV electron beam. The 100-350 nm spectrum of a 783 Torr plasma of argon containing about 1% hydrogen and oxygen is shown in Figure 8. Lyman α was observed at 121.6 nm with an adjoining H_2 band, the third continuum of Ar was observed at 210 nm [41], and the $OH(A-X)$ bands were observed at 282.7 and 308.6 nm [24, 42-43]. A series of sharp, evenly-spaced lines was observed in the region 145-185 nm. The only possibilities for the source of the sharp peaks are rotational, atomic, or ion transitions. None of the strong O I and O II lines match any of the lines [33]. No

combination of O species matches the evenly spaced lines. The series was not observed with argon alone, and only Ar VII and Ar VIII are possible in this region which is not possible at this pressure. Furthermore, no argon species match the observed lines [33].

The series matched the P branch of $H_2(1/4)$ for the vibrational transition $\upsilon = 1 \rightarrow \upsilon = 0$. P(1), P(2), P(3), P(4), P(5), and P(6) were observed. The sharp peak at 146.84 nm may be the first member of the R branch, R(1). The PMT has a response-notch in the region of the R branch, but the R-branch lines may correspond to forbidden transitions. Selection rules for $H_2(1/p)$ may be $\Delta\upsilon = -1$ $\Delta J = +1$ in order for a net state change with vibration-rotation coupling. Alternatively, the emission could be suppressed by the argon second continuum, or the vibrational energy may favor partial internal conversion rather than emission. Similarly, as shown in Sec. IIIAa, the $H_2(1/4)^+$ series was only observed for wavelengths longer than the bond energy corresponding to the result that only the P branch of $H_2(1/4)$ was allowed.

The plot of the energies of the peaks shown in Figure 8 is shown in Figure 9. The slope of the linear curve fit is 0.245 eV with an intercept of 8.224 eV which matches Eq. (27) very well for $p = 4$. The series matches the predicted $\upsilon = 1 \rightarrow \upsilon = 0$ vibrational energy of $H_2(1/4)$ of 8.2544 eV (Eq. (14)) and its predicted rotational energy spacing of 0.241 eV (Eq. (20)) with $\Delta J = +1$; $J = 0,1,2,3,4,5$.

The vibration-rotational series was observed only when oxygen was also present with hydrogen. For oxygen, there are several chemical reactions that fulfill the catalyst criterion. The bond energy of the oxygen molecule is 5.165 eV, and the first, second, and third ionization energies of an oxygen atom are 13.61806 eV, 35.11730 eV, and 54.9355 eV, respectively [31]. The reactions $O_2 \rightarrow O + O^{2+}$, $O_2 \rightarrow O + O^{3+}$, and $2O \rightarrow 2O^+$ provide a net enthalpy of about 2, 4, and 1 times E_h, respectively. It was previously reported that H lines were selectively broadened and that both the Lyman and the Balmer α lines were observed to be inverted in certain plasmas with oxygen catalyst [24-25]. However, oxygen may serve a role other than as a catalyst to give rise to the vibration-rotational series. Emission of the $H_2(1/4)$ vibration-rotational series may occur via electron-collisional excitation of O_2 followed by vibration-rotational activation of $H_2(1/4)$ through a collisional energy exchange with the excited O_2:

$$O_2^* + H_2(1/4) \rightarrow O_2 + H_2(1/4)^* \qquad (36)$$

where * denotes an energetic state. This mechanism is favored at the high operating pressure. Furthermore, the role of argon as the source of the catalyst was shown by the absence of the vibration-rotational series when krypton replaced argon. Thus, the activation role of a molecule is implicated.

It was anticipated that if selection rules or kinetics require that the $H_2(1/4)$ be vibration-rotationally excited by a collisional energy exchange with a molecule, then nitrogen may be effective as well. It was also anticipated that lower pressure could result in higher kinetic

energies and result in the excitation of $H_2(1/4)$ to higher vibration-rotational energies. The 100-350 nm spectrum of a 456 Torr plasma of argon containing about 1% hydrogen and nitrogen is shown in Figure 10. Lyman α was observed at 121.6 nm, the third continuum of Ar was observed at 190 nm [41], and background molecular emission was observed including $N_2\ C^3\Pi_u - B^3\Pi_g$ emission in the 270-350 region [44-46]. The series of sharp, evenly-spaced lines observed for trace oxygen addition was observed for nitrogen but in the region 200-275 nm. Again, the only possibilities for the source of the sharp peaks are rotational, atomic, or ion transitions. None of the strong N I and N II lines match any of the lines [33]. No combination of N I and N II lines matches the evenly spaced lines. Rather than nitrogen line emission, molecular emission was observed as previously recorded on air-plasma discharges [44-46].

The series matched the P branch of $H_2(1/4)$ for the vibrational transition $\upsilon = 5 \rightarrow \upsilon = 4$. P(1), P(2), P(3), P(4), P(5), P(6), and P(7) were observed. In this case, the R-branch lines also appeared to correspond to forbidden transitions. Alternatively, the emission could be suppressed by the argon third continuum. The plot of the energies of the peaks shown in Figure 10 is shown in Figure 11. The slope of the linear curve fit is 0.245 eV with an intercept at 6.25 eV which matches Eqs. (19) and (27) very well for $p = 4$. The series matched the predicted $\upsilon = 5 \rightarrow \upsilon = 4$ vibrational energy of $H_2(1/4)$ of 6.30 eV (Eq. (19)) and its predicted rotational energy spacing of 0.241 eV (Eq. (20)) with $\Delta J = +1$; $J = 0,1,2,3,4,5,6$. Using Eqs. (20) and (22) with the measured rotational energy spacing of 0.24 eV establishes an internuclear distance of 1/4 that of the ordinary hydrogen species for $H_2(1/4)$. This technique which is the best measure of the bond distance of any diatomic molecule identifies and unequivocally confirms $H_2(1/4)$.

A possible confirmation of the novelty of the lines identified in this study or similar lines has been published previously. The comparison of the third continuum of argon gas as recorded by Ulrich, Wieser, and Murnick [41] with a very pure gas (upper spectrum) and a spectrum in which the gas was slightly contaminated by oxygen as evidenced by the second order of the 130 nm resonance lines at 160 nm is shown in Figure 12. A series of narrow, evenly-spaced lines that appear similar to those in Figures 8 and 10 were observed that could not be assigned by Ulrich et al. to known species. The series was not observed in krypton and xenon plasmas. The determination of the presence of hydrogen in the argon plasmas is warranted in future studies.

B. Isolation and Characterization of $H_2(1/p)$

a. Cryotrap Pressure

Helium-hydrogen (90/10%) gas was flowed through the microwave tube and the cryosystem for 2 hours with the trap cooled to LN temperature. No change in pressure over time was observed when the dewar was removed, and the system was warmed to room temperature as

shown in Figure 13. The experiment was repeated under the same conditions but with a plasma maintained with 60 W forward microwave power and 10 W reflected. In contrast to the control case, a liquid-nitrogen-condensable gas was generated in the helium-hydrogen plasma reaction since the pressure due to the reaction product rose from 10^{-5} Torr to 3 Torr as the cryotrap warmed to room temperature.

b. Mass Spectroscopy

The mass spectrum for the gases collected in the cryotrap from the He/H_2 (90/10%) plasma over the range $m/e = 1$ to $m/e = 200$ showed that the LN-condensable gas was highly pure hydrogen. The mass spectrum for the ($m/e = 1$ to $m/e = 50$) region is shown in Figure 14a. The mass spectrum ($m/e = 1$ to $m/e = 200$) for the gases collected in the cryo-cooler from the He/H_2 (90/10%) plasma only showed peaks in the ($m/e = 1$ to $m/e = 50$) region. The $m/e = 2$ peak shown in Figure 14b was 40-50 times more intense than the $m/e = 28$ (nitrogen), $m/e = 32$ (oxygen), and $m/e = 40$ (argon) peaks that were assigned to very trace residual air contamination. Whereas, without the plasma, the mass $m/e = 2$ peak was present in only trace concentration (~10^{-10} Torr) compared with the air contaminant gases that were also present in low abundance (~10^{-9} Torr). Von Engel [47] gives the efficiency of production of various common ions at 70 eV and shows that the cross section for the formation of H_2^+ is 10% of that of air contaminants at the same partial pressure. Thus, hydrogen was ~500 times more abundant in the collected gas than air contaminants which may have originated through back-streaming in the mass spectrometer.

The phase diagram of helium and hydrogen is shown in Figure 15 that was plotted from data given by Lide [48] and extended to lower pressures and temperatures using the Clausius-Clapeyron equation [49]. It is not possible to condense ordinary hydrogen below ~50 Torr at 12-17 K as shown by its phase diagram. The condensation of a $m/e = 2$ gas in the temperature range of 12-17 K at 700 mTorr that was not removed at 10^{-5} Torr indicates that a novel hydrogen gas formed in the plasma reaction between hydrogen and helium. The results are even more dramatic in the case of the condensation of a $m/e = 2$ gas in the temperature range of 77 K using the LN cryotrap.

c. ^1H NMR

The ^1H NMR on $CDCl_3$ showed only a singlet solvent ($CHCl_3$) peak at 7.26 ppm relative to tetramethylsilane (TMS) with small ^{13}C side bands. The ^1H NMR on ultrahigh purity hydrogen dissolved in $CDCl_3$ relative to tetramethylsilane (TMS) showed only singlet peaks at 7.26, 4.63, and 1.57 ppm corresponding to $CHCl_3$, H_2, and H_2O, respectively. The chemical shifts of the $CHCl_3$ and H_2O peaks matched the literature values of 1.56 and 7.26 ppm,

respectively [50]. The error in the observed peaks was determined to be ±0.01 ppm. The ^1H NMR spectroscopic results of the control prepared from the reagent helium-hydrogen mixture was the same as that of the high purity hydrogen control.

H_2 has been characterized by gas phase ^1H NMR. The experimental absolute resonance shift of gas-phase TMS relative to the proton's gyromagnetic frequency is -28.5 ppm [51]. H_2 was observed at 0.48 ppm compared to gas phase TMS set at 0.00 ppm [52]. Thus, the corresponding absolute H_2 gas-phase resonance shift of -28.0 ppm (-28.5 + 0.48) ppm was in excellent agreement with the predicted absolute gas-phase shift of -28.01 ppm given by Eq. (30).

The absolute H_2 gas-phase shift can be used to determine the solvent shift for H_2 dissolved in $CDCl_3$. The correction for the solvent shift can then be applied to other peaks to determine the gas-phase absolute shifts to compare to Eq. (30). The shifts of all of the peaks were relative to liquid-phase TMS which has an experimental absolute resonance shift of -31.5 ppm relative to the proton's gyromagnetic frequency [38-39]. Thus, the experimental shift of H_2 in $CDCl_3$ of 4.63 ppm relative to liquid-phase TMS corresponds to an absolute resonance shift of -26.87 ppm (-31.5 ppm + 4.63 ppm). Using the absolute H_2 gas-phase resonance shift of -28.0 ppm corresponding to 3.5 ppm (-28.0 ppm - 31.5 ppm) relative to liquid TMS, the $CDCl_3$ solvent effect is 1.13 ppm (4.63 ppm - 3.5 ppm) which is comparable to that of hydrocarbons [50].

^1H NMR spectra on sealed samples of condensable helium-hydrogen plasma gases dissolved in $CDCl_3$ relative to tetramethylsilane (TMS) are shown in Figure 16 (a)-(f). The solvent peak was observed at 7.26 ppm, the H_2 peak was observed at 4.63 ppm, and a singlet at 3.22 ppm matched silane. Small ^{29}Si side bands were observed for the latter. The source was determined to be hydrogen-plasma reduction of the quartz tube. The peak was unchanged after three weeks at room temperature. No other silanes, silane decomposition species, or solvent decomposition species were observed after one month of repeat NMR analysis. Since the plasma gases were first passed through an LN trap before the plasma cell, and the cryotrap was high-vacuum (10^{-6} Torr) capable, no hydrocarbons were anticipated. This was confirmed by mass spectroscopic and FTIR analysis that showed only water vapor as a contaminant. Again, the source was determined to be hydrogen-plasma reduction of the quartz tube.

As further shown in Figures 16 (a)-(f), singlet peaks upfield of H_2 were observed at 3.47, 2.18, 1.47, 0.85, 0.21, and -1.8 ppm relative to TMS corresponding to solvent-corrected absolute resonance shifts of -29.16, -30.45, -31.16, -31.78, -32.42, and -34.43 ppm, respectively. Using Eq. (30), the data indicates that p = 2, 4, 5, 6, 7, and 10, respectively. The data matched the series $H_2(1/2)$, $H_2(1/4)$, $H_2(1/5)$, $H_2(1/6)$, $H_2(1/7)$, and $H_2(1/10)$.

The observed series and the absence of $H_2(1/3)$ has implications for the catalysis reactions and the corresponding rates. The second ionization energy of helium is 54.4 eV; thus,

the ionization reaction of He^+ to He^{2+} has a net enthalpy of reaction of $54.4\ eV$ which is equivalent to $2 \cdot 27.2\ eV$. Since the products of the catalysis reaction have binding energies of $m \cdot 27.2\ eV$, they may further serve as catalysts by so called exothermic disproportionation reactions where one atom goes to a lower state while another goes to a higher state [2-3]. Extreme ultraviolet (EUV) spectroscopy was recorded on microwave discharges of helium with 2% hydrogen. Novel emission lines were observed with energies of $q \cdot 13.6\ eV$, $q = 1,2,3,7,9,11$ or $q \cdot 13.6\ eV$, $q = 4,6,8$ less $21.2\ eV$ corresponding to inelastic scattering of these photons by helium atoms due to excitation of $He(1s^2)$ to $He(1s^1 2p^1)$. Alternatively, the photon emission of the intermediate formed by resonant nonradiative energy transfer to the catalyst He^+ is partially quenched by the strong $He(1s^2)$ to $He(1s^1 2p^1)$ transition [40-41]. As given previously [40-41], the quenching reaction is selection rule dependent and results in the emission of a photon less energetic by $21.2\ eV$. Thus, helium ion catalyzes $H\left[a_H\right]$ to $H\left[\frac{a_H}{3}\right]$ as shown in Eqs. (5-7) of Ref. [3]. Further disproportionation reactions may then proceed:

$$H\left[\frac{a_H}{3}\right] + H\left[\frac{a_H}{3}\right] \rightarrow H\left[\frac{a_H}{4}\right] + H\left[\frac{a_H}{2}\right] + 27.2\ eV \tag{37}$$

The observed, strong 45.6 nm emission [1-4, 26] indicates that the reaction rate for Eq. (37) is very high. Thus, species corresponding to the product atoms such as $H_2(1/2)$ and $H_2(1/4)$ with products from further transitions having $p > 4$ as given in Refs. [2-3] may dominate the reaction products.

The results of the ^1H NMR spectra recorded at China Lake on ultrahigh purity hydrogen and gases from the thermal decomposition of $KH*I$ dissolved in $CDCl_3$ relative to tetramethylsilane (TMS) are shown in Figures 17 and 18, respectively. Results matching those shown in Figures 17 and 18 were obtained at BlackLight Power, Inc. In addition, these samples were determined not to contain hydrocarbons by mass spectroscopy and FTIR analysis. The closest possible peak to H_2O in Figure 18 is at 1.41 ppm; however, the assignment has some difficulty since the control (Figure 17) and literature [50] values put the H_2O peak at 1.57 ppm rather than 1.41 ppm and the peak is expected to be much broader as shown in the control (Figure 17). Excessive H_2O contamination may form a separate phase in $CDCl_3$, but the shift is downfield and the peak further broadens. In controls of 1% D_2O in $CDCl_3$, a very broad H_2O peak was observed at 4.79 ppm which matches the literature value [50].

Considering solvent effects, singlet peaks upfield of H_2 were observed from the $KH*I$-derived sample at 3.03, 2.18, 1.47, 0.85, and 0.22 ppm. From Eq. (30), the series matched the consecutive series $H_2(1/3)$, $H_2(1/4)$, $H_2(1/5)$, $H_2(1/6)$, and $H_2(1/7)$, respectively. The observed products were consistent with those anticipated with the catalysis of H by K to form $H(1/4)$ and subsequent disproportionation reactions [2-3, 18, 20, 9].

As shown in Figures 16 and 18, the observation of the combined series of singlet peaks upfield of H_2 with a predicted integer spacing of 0.64 ppm at 3.47, 3.03, 2.18, 1.47, 0.85, and 0.22 ppm identified as the consecutive series $H_2(1/2)$, $H_2(1/3)$, $H_2(1/4)$, $H_2(1/5)$, $H_2(1/6)$, and $H_2(1/7)$ and $H_2(1/10)$ at -1.8 ppm provides powerful confirmation of the existence of $H_2(1/p)$. Furthermore, the ^1H NMR spectra of gases from the thermal decomposition of $KH*I$ matched those of LN-condensable hydrogen. This provides strong support that compounds such as $KH*I$ contain hydride ions $H^-(1/p)$ in the same fractional quantum state p as the corresponding observed $H_2(1/p)$. Observational agreement with predicted positions of upfield-shifted ^1H MAS NMR peaks (Eq. (31)) of the compounds [9, 20, 28-30], catalyst reactions [18, 20, 22-23], and spectroscopic data [18] supports this conclusion. On this basis, possibilities for advanced technologies are discussed in Sec. IIIBe.

d. Power Balance of the Helium-Hydrogen Microwave Plasma

The water bath calorimeter is an absolute standard and indicated $P_{in} = 41.9 \pm 1\ W$ input power at the selected diode settings for all control plasmas. From these results, power input to the helium-hydrogen plasma was confidently known as the diode readings were identically matched for the controls. For example, the $T(t)$ water bath response to stirring and then with selected panel meter readings of the constant forward and reflected microwave input power to krypton was recorded as shown in Figure 19. Using the corresponding $\dot{T}(t)$ in Eq. (34), the microwave input power was determined to be 41.9 ± 1 W. The $T(t)$ response was significantly increased for helium-hydrogen (95/5%) as shown in Figure 19. From the difference in the $T(t)$ water bath response, the output and excess power of the helium-hydrogen plasma reaction was determined to be 62.1 ± 1 W and 20.2 ± 1 W using Eq. (34) and Eq. (33) with the measured $P_{in} = 41.9 \pm 1\ W$. The sources of error were the error in the calibration curve (± 0.05 W) and the measured microwave input power (± 1 W). The propagated error of the calibration and power measurements was ± 1 W. Given an excess power of 20.2 W in 3 cm^3 and a helium-hydrogen (95/5%) flow rate of 10.0 sccm, the excess power density and energy balance were high, 6.7 W/cm^3 and $-5.4\ X10^4\ kJ/mole\ H_2$ (280 $eV/H\ atom$), respectively.

In addition to high energy spectral emission as shown in Sec. IIIA and previously [1-5], other indications of very energetic reactions are observed. For example, population inversion has been observed from plasmas which contain atomic hydrogen with the presence of a catalyst [22-25], and selective H broadening with a microwave plasma having no high DC field present was reported previously [14-16]. Microwave He/H_2 and Ar/H_2 plasmas showed extraordinary broadening corresponding to an average hydrogen atom temperature of 180 - 210 eV and 110 - 130 eV, respectively. Whereas, pure hydrogen and Xe/H_2 microwave plasmas showed no excessive broadening corresponding to an average hydrogen atom temperature of < 2 eV [14-

16]. Only the H lines were Doppler broadened, and this result was shown to be inexplicable by any mechanism based on electric field acceleration of charged species. The observation of excessive Balmer line broadening in microwave driven plasmas as well as other hydrogen-mixed plasmas maintained in glow discharge [11-15] and RF discharge cells [15, 17] as well as unique chemically driven plasmas called resonant-transfer or rt-plasmas [18, 20, 22-23] requires a source of energy other than that provided by the electric field. The formation of fast H only in specific predicted plasmas was explained by a resonant energy transfer between hydrogen atoms and catalysts such as Ar^+ or He^+ of an integer multiple of the potential energy of atomic hydrogen, 27.2 eV [14-16]. Consistent with predictions, noncatalyst plasma mixtures such as Kr/H_2 and Xe/H_2 show no unique features. The observation of the $H_2(1/4)$ rotational lines reported in Sec. IIIAb from Ar/H_2 plasmas but not from Kr/H_2 and Xe/H_2 plasmas also matches predictions.

e. Applications

The existence of novel alkaline and alkaline earth hydride and halido-hydrides were previously identified by large distinct upfield ^1H NMR resonances compared to the NMR peaks of the corresponding ordinary hydrides [20, 28-30]. Using a number of analytical techniques such as XPS and time-of-flight-secondary-mass-spectroscopy (ToF-SIMS) as well as NMR, the hydrogen content was assigned to $H^-(1/p)$, novel high-binding-energy hydride ions in stable fractional principal quantum states [9, 20, 28-30]. The upfield shifts of the novel hydride compounds matched those predicted for $H^-(1/2)$ and $H^-(1/4)$ (Eq. (31)). Novel spectral emission from $H^-(1/2)$ and $H^-(1/4)$, the predicted products from the potassium catalyst reaction and the supporting results of 1.) the formation of an intense hydrogen plasma chemically without an electric field or power input other than thermal [21], 2.) a high positive net enthalpy of reaction [20], 3.) characteristic predicted catalyst emission [18, 22-23], 4.) ~15 eV Doppler broadening of the Balmer lines [18, 22-23], and 5.) inversion of the Lyman lines [22-23] have also been reported previously.

Hydride ions with increased binding energies form novel compounds with potential for future applications in many industries including chemical, electronics, computer, military, energy, and aerospace in the form of products such as battery materials, propellants, solid fuels, surface coatings, structural materials, and chemical processes. The previously derived equation [8, 18] for the hydride binding energies E_B is

$$E_B = \frac{\hbar^2\sqrt{s(s+1)}}{8\mu_e a_0^2\left[\frac{1+\sqrt{s(s+1)}}{p}\right]^2} - \frac{\pi\mu_0 e^2\hbar^2}{m_e^2}\left(\frac{1}{a_H^3} + \frac{2^2}{a_0^3\left[\frac{1+\sqrt{s(s+1)}}{p}\right]^3}\right) \quad (38)$$

where p is an integer greater than one, $s = 1/2$, μ_o is the permeability of vacuum, and μ_e is the reduced electron mass given by $\mu_e = \frac{m_e m_p}{\frac{m_e}{\sqrt{\frac{3}{4}}} + m_p}$ where m_p is the mass of the proton. The ionic radius is

$$r_1 = \frac{a_0}{p}\left(1+\sqrt{s(s+1)}\right) \; s = \frac{1}{2} \quad (39)$$

From Eq. (38), the calculated ionization energy of the hydride ion is $0.75418\,eV$. The experimental value given by Lykke [53] is $6082.99 \pm 0.15\,cm^{-1}$ (0.75418 eV). From Eq. (39), the radius of the hydride ion $H^-(1/p)$, p = integer is $\frac{1}{p}$ that of ordinary hydride ion, H^-. As shown in Table 2, the binding energies go through a maximum stability at $p = 16$ and decrease in stability such that $p = 24$ corresponds to the last stable ion of the series. Applications are anticipated based on this range of stability. Significant applications also exist for the corresponding molecular species $H_2(1/p)$.

i. High Voltage Battery

Hydride ions having extraordinary binding energies may stabilize a cation M^{x+} in an extraordinarily high oxidation state such as +2 in the case of lithium. Thus, these hydride ions may be used as the basis of a high voltage battery of a rocking chair design wherein the hydride ion moves back and forth between the cathode and anode half cells during discharge and charge cycles. Exemplary reactions for a cation M^{x+} are:

Cathode reaction:

$$MH_x + e^- \rightarrow MH_{x-1} + H^- \quad (40)$$

Anode reaction:

$$MH_{x-2} + H^- \rightarrow MH_{x-1} + e^- \quad (41)$$

Overall reaction:

$$MH_x + MH_{x-2} \rightarrow 2MH_{x-1} \quad (42)$$

ii. Energetic Propellant

The reaction to form $H_2(1/p)$ from a hydride compound $M^+H^-(1/p)$ containing $H^-(1/p)$ where M^+ is a metal ion such as Li^+ and $p \approx 24$ represents a potentially very energetic reaction. In the application of $M^+H^-(1/p)$ as a solid, liquid, or gaseous rocket fuel, rocket propellant power may be provided by reaction of $M^+H^-(1/p)$ with a proton to form $H_2(1/p)$ or by the thermal decomposition of $M^+H^-(1/p)$ to form $H_2(1/p)$[1]. The total energy of $H_2(1/p)$ and $H^-(1/p)$ are given by Eqs. (5) and (38), respectively. Using $32p^2\ eV$ as an estimate of the total energy of $H_2(1/p)$ and the total energy of $H(1/p)$ given by Eqs. (2a) and (2c) as an estimate of total energy of $H^-(1/p)$, the energy balance of the proton reaction is

$$M^+H^-(1/p) + H^+X^- \rightarrow H_2(1/p) + MX + p^2(32 - 13.6)\ eV \tag{43}$$

The energy of the decomposition reaction is

$$2M^+H^-(1/p) \xrightarrow{\Delta} H_2(1/p) + 2M + p^2(32 - 2 \cdot 13.6)\ eV \tag{44}$$

Very high energy balances are possible as p approaches the limit for a stable hydride ion at 24. In the case of $H^-(1/24)$, the energy balances for Eqs. (43) and (44) are truly unconventional, 10 keV and 2.7 keV, respectively. The mass of the reactants of Eqs. (43) and (44) may be comparable to those of hydrogen combustion that releases 1.48 eV per hydrogen atom; thus, energies of about 7000 and 2000 times that of the conventional hydrogen-oxygen reaction, respectively, are expected. Thus, a $H^-(1/24)$-based propellant may be transformational especially given the logarithmic dependence on fuel-weight to lift in the rocketry equation [54].

iii. UV Laser

The existence of excited vibration-rotational levels of $H_2(1/p)$ presents the possibility of a laser using transitions between levels other than one to a state with both υ. and $J = 0$ A laser may be realized using standard cavities and mirrors that are appropriate for the desired wavelength similar to those of current lasers based on molecular vibration-rotational levels such as the CO_2 laser. However, an advantage exists to produce laser light at much shorter wavelengths. Based on the current results, a laser based on vibration-rotational levels of $H_2(1/4)$ could lase in the UV which has a significant application in photolithography.

IV. Conclusion

In this study we make specific theoretical predictions and test them with standard, easily interpretable experiments. The results show that the possibility that a novel reaction of atomic

---

[1] The helium-hydrogen microwave plasma contains H^+ which favors the reaction product $H_2(1/p)$ over $H^-(1/p)$ due to the highly exothermic reaction of Eq. (43) wherein X^- is a plasma electron or ordinary hydride ion. $HeH(1/2)$ is also not favored due to the highly exothermic reaction to form $H_2(1/2)$.

hydrogen that uses certain catalysts such as He^+, Ar^+, and K may be a clean new energy source is supported by spectroscopic, chemical, and thermal data. For example, we report the discovery of new states of hydrogen formed in a catalytic plasma reaction. The atomic states $H(1/p)$ were identified previously [1-4] by the spectroscopic observation of emission lines occurring at energies that are an extension of the Rydberg series to lower states. A corresponding molecular ion $H_2(1/4)^+$ and molecule $H_2(1/4)$ were identified by vibrational-rotational series that established an internuclear distance of 1/4 that of the ordinary hydrogen species. The molecular hydrogen gas product was isolated by liquefaction at liquid nitrogen temperature and by decomposition of compounds previously found to contain the corresponding hydride ions $H^-(1/p)$ [9, 20, 28-30]. Singlet peaks upfield of H_2 with a predicted integer spacing of 0.64 ppm at 3.47, 3.03, 2.18, 1.47, 0.85, and 0.22 ppm identified as the consecutive series $H_2(1/2)$, $H_2(1/3)$, $H_2(1/4)$, $H_2(1/5)$, $H_2(1/6)$, and $H_2(1/7)$ and $H_2(1/10)$ at -1.8 ppm provides powerful confirmation of the existence of $H_2(1/p)$. Furthermore, the ^1H NMR spectra of gases from the thermal decomposition of $KH*I$ matched those of LN-condensable hydrogen which provides strong support that compounds such as $KH*I$ contain hydride ions $H^-(1/p)$ in the same fractional quantum state p as the observed $H_2(1/p)$. Observational agreement with predicted positions of upfield-shifted ^1H MAS NMR peaks (Eq. (31)) of the compounds, catalyst reactions, and spectroscopic data supports this conclusion. On this basis, possibilities for advanced technologies are considered.

It was reported previously that stationary H populations were formed by using certain catalysts in hydrogen plasmas, and novel processes and hydride products with significant commercial potential were characterized by EUV and visible spectroscopy, NMR, ToF-SIMS, and XPS. Very high (>100 eV) H energies and substantial excess thermal energy were observed [14-16, 4, 26]. Using water bath calorimetry in this study, excess power was observed from the helium-hydrogen plasma compared to control krypton plasma. For example, for an input of 41.9 W, the total plasma power of the helium-hydrogen plasma measured by water bath calorimetry was 62.1 W corresponding to 20.2 W of excess power in 3 cm^3. The excess power density and energy balance were high, $6.7\ W/cm^3$ and $-5.4\ X10^4\ kJ/mole\ H_2$ ($280\ eV/H\ atom$), respectively. The reaction of hydrogen to form water which releases $-241.8\ kJ/mole\ H_2$ ($1.48\ eV/H\ atom$) is about 200 times less than that observed. The results indicate that a new power source based on the catalysis of atomic hydrogen is not only possible, but it may be competitive with gas turbine combustion.

Based on their stability characteristics, advanced hydride technologies are indicated. Hydride ions $H^-(1/p)$ having extraordinary binding energies may stabilize a cation M^{x+} in an extraordinarily high oxidation state as the basis of a high voltage battery. And, a rocketry propellant based on $H^-(1/24)$ to $H_2(1/24)$ may be possible with an energy release so large that

it may be transformational. Significant applications also exist for the corresponding molecular species $H_2(1/p)$. The results of this study indicate that excited vibration-rotational levels of $H_2(1/4)$ could be the basis of a UV laser that could significantly advance photolithography.

Acknowledgments

Special thanks to D. E. Murnick and M. Salvermoser of Rutgers University for providing the 15 keV electron gun. D. C. Harris, Naval Air Warfare Center Weapons Division, Naval Air Warfare Center, China Lake, CA, is acknowledged for suggesting the method of identifying $H_2(1/p)$ by ^1H NMR using $CDCl_3$ solvent. D. C. Harris and L. Merwin are acknowledged for preparing and analyzing a $KH*I$ NMR sample.

References

1. R. L. Mills, P. Ray, "Extreme Ultraviolet Spectroscopy of Helium-Hydrogen Plasma", J. Phys. D, Applied Physics, Vol. 36, (2003), pp. 1535-1542.
2. R. L. Mills, P. Ray, B. Dhandapani, M. Nansteel, X. Chen, J. He, "New Power Source from Fractional Quantum Energy Levels of Atomic Hydrogen that Surpasses Internal Combustion", J Mol. Struct., Vol. 643, No. 1-3, (2002), pp. 43-54.
3. R. Mills, P. Ray, "Spectral Emission of Fractional Quantum Energy Levels of Atomic Hydrogen from a Helium-Hydrogen Plasma and the Implications for Dark Matter", Int. J. Hydrogen Energy, Vol. 27, No. 3, pp. 301-322.
4. R. L. Mills, P. Ray, J. Dong, M. Nansteel, B. Dhandapani, J. He, "Spectral Emission of Fractional-Principal-Quantum-Energy-Level Atomic and Molecular Hydrogen", Vibrational Spectroscopy, Vol. 31, No. 2, (2003), pp. 195-213.
5. R. Mills, P. Ray, "Vibrational Spectral Emission of Fractional-Principal-Quantum-Energy-Level Hydrogen Molecular Ion", Int. J. Hydrogen Energy, Vol. 27, No. 5, (2002), pp. 533-564.
6. N. V. Sidgwick, *The Chemical Elements and Their Compounds*, Volume I, Oxford, Clarendon Press, (1950), p.17.
7. M. D. Lamb, *Luminescence Spectroscopy*, Academic Press, London, (1978), p. 68.
8. R. Mills, *The Grand Unified Theory of Classical Quantum Mechanics*, September 2001 Edition, BlackLight Power, Inc., Cranbury, New Jersey, Distributed by Amazon.com; January (2003) Edition posted at www.blacklightpower.com.
9. R. L. Mills, "The Nature of the Chemical Bond Revisited and an Alternative Maxwellian Approach", submitted.

10. R. Mills, J. Dong, Y. Lu, "Observation of Extreme Ultraviolet Hydrogen Emission from Incandescently Heated Hydrogen Gas with Certain Catalysts", Int. J. Hydrogen Energy, Vol. 25, (2000), pp. 919-943.
11. R. Mills and M. Nansteel, P. Ray, "Argon-Hydrogen-Strontium Discharge Light Source", IEEE Transactions on Plasma Science, Vol. 30, No. 2, (2002), pp. 639-653.
12. R. Mills and M. Nansteel, P. Ray, "Bright Hydrogen-Light Source due to a Resonant Energy Transfer with Strontium and Argon Ions", New Journal of Physics, Vol. 4, (2002), pp. 70.1-70.28.
13. R. Mills, M. Nansteel, and P. Ray, "Excessively Bright Hydrogen-Strontium Plasma Light Source Due to Energy Resonance of Strontium with Hydrogen", J. of Plasma Physics, Vol. 69, (2003), pp. 131-158.
14. R. L. Mills, P. Ray, B. Dhandapani, R. M. Mayo, J. He, "Comparison of Excessive Balmer α Line Broadening of Glow Discharge and Microwave Hydrogen Plasmas with Certain Catalysts", J. of Applied Physics, Vol. 92, No. 12, (2002), pp. 7008-7022.
15. R. L. Mills, P. Ray, B. Dhandapani, J. He, "Comparison of Excessive Balmer α Line Broadening of Inductively and Capacitively Coupled RF, Microwave, and Glow Discharge Hydrogen Plasmas with Certain Catalysts", IEEE Transactions on Plasma Science, Vol. 31, No. (2003), pp. 338-355.
16. R. L. Mills, P. Ray, "Substantial Changes in the Characteristics of a Microwave Plasma Due to Combining Argon and Hydrogen", New Journal of Physics, www.njp.org, Vol. 4, (2002), pp. 22.1-22.17.
17. J. Phillips, C. Chen, "Evidence of Energetic Reaction Between Helium and Hydrogen Species in RF Generated Plasmas", submitted.
18. R. L. Mills, P. Ray, "A Comprehensive Study of Spectra of the Bound-Free Hyperfine Levels of Novel Hydride Ion $H^-(1/2)$, Hydrogen, Nitrogen, and Air", Int. J. Hydrogen Energy, Vol. 28, No. 8, (2003), pp. 825-871.
19. R. Mills, "Spectroscopic Identification of a Novel Catalytic Reaction of Atomic Hydrogen and the Hydride Ion Product", Int. J. Hydrogen Energy, Vol. 26, No. 10, (2001), pp. 1041-1058.
20. R. Mills, P. Ray, B. Dhandapani, W. Good, P. Jansson, M. Nansteel, J. He, A. Voigt, "Spectroscopic and NMR Identification of Novel Hydride Ions in Fractional Quantum Energy States Formed by an Exothermic Reaction of Atomic Hydrogen with Certain Catalysts", submitted.
21. H. Conrads, R. Mills, Th. Wrubel, "Emission in the Deep Vacuum Ultraviolet from a Plasma Formed by Incandescently Heating Hydrogen Gas with Trace Amounts of Potassium Carbonate", Plasma Sources Science and Technology, Vol. 12, (3003), pp. 389-395.

22. R. Mills, P. Ray, R. M. Mayo, "CW HI Laser Based on a Stationary Inverted Lyman Population Formed from Incandescently Heated Hydrogen Gas with Certain Group I Catalysts", IEEE Transactions on Plasma Science, Vol. 31, No. 2, (2003), pp. 236-247.
23. R. L. Mills, P. Ray, "Stationary Inverted Lyman Population Formed from Incandescently Heated Hydrogen Gas with Certain Catalysts", J. Phys. D, Applied Physics, Vol. 36, (2003), pp. 1504-1509.
24. R. Mills, P. Ray, R. M. Mayo, "The Potential for a Hydrogen Water-Plasma Laser", Applied Physics Letters, Vol. 82, No. 11, (2003), pp. 1679-1681.
25. R. L. Mills, P. C. Ray, R. M. Mayo, M. Nansteel, B. Dhandapani, J. Phillips, "Spectroscopic Study of Unique Line Broadening and Inversion in Low Pressure Microwave Generated Water Plasmas", submitted.
26. R. L. Mills, X. Chen, P. Ray, J. He, B. Dhandapani, "Plasma Power Source Based on a Catalytic Reaction of Atomic Hydrogen Measured by Water Bath Calorimetry", in press.
27. R. Mills, B. Dhandapani, M. Nansteel, J. He, P. Ray, "Liquid-Nitrogen-Condensable Molecular Hydrogen Gas Isolated from a Catalytic Plasma Reaction", submitted.
28. R. Mills, B. Dhandapani, M. Nansteel, J. He, T. Shannon, A. Echezuria, "Synthesis and Characterization of Novel Hydride Compounds", Int. J. of Hydrogen Energy, Vol. 26, No. 4, (2001), pp. 339-367.
29. R. Mills, B. Dhandapani, N. Greenig, J. He, "Synthesis and Characterization of Potassium Iodo Hydride", Int. J. of Hydrogen Energy, Vol. 25, Issue 12, December, (2000), pp. 1185-1203.
30. R. Mills, B. Dhandapani, M. Nansteel, J. He, A. Voigt, "Identification of Compounds Containing Novel Hydride Ions by Nuclear Magnetic Resonance Spectroscopy", Int. J. Hydrogen Energy, Vol. 26, No. 9, (2001), pp. 965-979.
31. D. R. Lide, *CRC Handbook of Chemistry and Physics*, 79 th Edition, CRC Press, Boca Raton, Florida, (1998-9), p. 10-175.
32. M. Karplus, R. N. Porter, *Atoms and Molecules an Introduction for Students of Physical Chemistry*, The Benjamin/Cummings Publishing Company, Menlo Park, California, (1970), pp. 447-484.
33. NIST Atomic Spectra Database, www.physics.nist.gov/cgi-bin/AtData/display.ksh.
34. P. W. Atkins, *Physical Chemistry*, Second Edition, W. H. Freeman, San Francisco, (1982), p. 589.
35. H. Beutler, Z. Physical Chem., "Die dissoziationswarme des wasserstoffmolekuls H_2, aus einem neuen ultravioletten resonanzbandenzug bestimmt", Vol. 27B, (1934), pp. 287-302.
36. G. Herzberg, L. L. Howe, "The Lyman bands of molecular hydrogen", Can. J. Phys., Vol. 37, (1959), pp. 636-659.

37. D. R. Lide, *CRC Handbook of Chemistry and Physics*, 79 th Edition, CRC Press, Boca Raton, Florida, (1998-9), p. 9-82.
38. K. K. Baldridge, J. S. Siegel, "Correlation of empirical δ(TMS) and absolute NMR chemical shifts predicted by ab initio computations", J. Phys. Chem. A, Vol. 103, (1999), pp. 4038-4042.
39. J. Mason, Editor, *Multinuclear NMR*, Plenum Press, New York, (1987), Chp. 3.
40. J. Wieser, D. E. Murnick, A. Ulrich, H. A Higgins, A. Liddle, W. L. Brown, "Vacuum ultraviolet rare gas excimer light source", Rev. Sci. Instrum., Vol. 68, No. 3, (1997), pp. 1360-1364.
41. A. Ulrich, J. Wieser, D. E. Murnick, "Excimer Formation Using Low Energy Electron Beam Excitation", Second International Conference on Atomic and Molecular Pulsed Lasers, Proceedings of SPIE, Vol. 3403, (1998), pp. 300-307.
42. A. K. Shuaibov, A. I. Dashchenko, I. V. Shevera, "Stationary radiator in the 130-190 nm range based on water vapour plasma", Quantum Electronics, Vol. 31, No. 6, (2001), pp. 547-548.
43. A. K. Shuaibov, L. L. Shimon, A. I. Dashchenko, I. V. Shevera, "Optical characteristics of a glow discharge in a He/H_2O mixture", Plasma Physics Reports, Vol. 27, No. 10, (2001), pp. 897-900.
44. C. O. Laux, R. J. Gessman, C. H. Kruger, "Measurements and modeling of the absolute spectral emission of air plasmas between 185 and 800 nm", Journal of Quantitative Spectroscopy and Radiative Transfer", (2001), submitted.
45. C. O. Laux, C. H. Kruger, R. N. Zare, "Diagnostics of atmospheric pressure air plasmas", www-krg.stanford.edu/kruger.html.
46. A. Lofthus, P. H. Krupenie, "The spectrum of molecular nitrogen", J. Phys. Chem. Ref. Data, Vol. 6, No. 1, (1977), pp. 113-312.
47. A. von Engel, *Ionized Gases*, American Institute of Physics Press, New York, (1965), pp. 62-64.
48. D. R. Lide, *CRC Handbook of Chemistry and Physics*, 76 th Edition, CRC Press, Boca Raton, Florida, (1995-6), p. 6-66 and p. 6-140.
49. I. N. Levine, *Physical Chemistry*, McGraw-Hill Book Company, New York, (1978), pp. 174-175.
50. H. E. Gottlieb, V. Kotlyar, A. Nudelman, "NMR chemical shifts of common laboratory solvents as trace impurities", J. Org. Chem., Vol. 62, (1997), pp. 7512-7515.
51. C. Suarez, E. J. Nicholas, M. R. Bowman, "Gas-phase dynamic NMR study of the internal rotation in N-trifluoroacetlypyrrolidine", J. Phys. Chem. A, Vol. 107, (2003), pp. 3024-3029.
52. C. Suarez, "Gas-phase NMR spectroscopy", The Chemical Educator, Vol. 3, No. 2, (1998).

53. K. R. Lykke, K. K. Murray, W. C. Lineberger, "Threshold photodetachment of H^-", Phys. Rev. A, Vol. 43, No. 11, (1991), pp. 6104-6107.
54. G. R. Fowles, *Analytical Mechanics*, Third Edition, Holt, Rinehart, and Winston, New York, (1977), pp. 182-184.

Table 1. The Maxwellian closed-form calculated and experimental parameters of H_2, D_2, H_2^+ and D_2^+.

Parameter	Calculated	Experimental	Eqs.[a]
H_2 Bond Energy	4.478 eV	4.478 eV	248
D_2 Bond Energy	4.556 eV	4.556 eV	250
H_2^+ Bond Energy	2.654 eV	2.651 eV	221
D_2^+ Bond Energy	2.696 eV	2.691 eV	223
H_2 Total Energy	31.677 eV	31.675 eV	244
D_2 Total Energy	31.760 eV	31.760 eV	245
H_2 Ionization Energy	15.425 eV	15.426 eV	246
D_2 Ionization Energy	15.463 eV	15.466 eV	247
H_2^+ Ionization Energy	16.253 eV	16.250 eV	219
D_2^+ Ionization Energy	16.299 eV	16.294 eV	220
H_2^+ Magnetic Moment	$9.274\ X\ 10^{-24}\ JT^{-1}$ μ_B	$9.274\ X\ 10^{-24}\ JT^{-1}$ μ_B	311-317
Absolute H_2 Gas-Phase NMR Shift	-28.0 ppm	-28.0 ppm	328
H_2 Internuclear Distance[c]	0.748 A $\sqrt{2}a_o$	0.741 Å	235
D_2 Internuclear Distance[c]	0.748 Å $\sqrt{2}a_o$	0.741 Å	235
H_2^+ Internuclear Distance[b]	1.058 Å $2a_o$	1.06 Å	208
D_2^+ Internuclear Distance[c]	1.058 Å $2a_o$	1.0559 Å	208
H_2 Vibrational Energy	0.517 eV	0.516 eV	256
D_2 Vibrational Energy	0.371 eV	0.371 eV	258
H_2^+ Vibrational Energy	0.270 eV	0.271 eV	229
D_2^+ Vibrational Energy	0.193 eV	0.196 eV	231
H_2 J=1 to J=0 Rotational Energy[c]	0.0148 eV	0.01509 eV	273
D_2 J=1 to J=0 Rotational Energy[c]	0.00741 eV	0.00755 eV	261-266, 273
H_2^+ J=1 to J=0 Rotational Energy[b]	0.00740 eV	0.00739 eV	269
D_2^+ J=1 to J=0 Rotational Energy[c]	0.00370 eV	0.003723 eV	261-269

[a] Ref. [9].

[b] The internuclear distances are not corrected for the reduction due to $\overline{E}_{osc}$.

[c] The internuclear distances are not corrected for the increase due to $\overline{E}_{osc}$.

Table 2. The ionization energy of the hydride ion $H^-(1/p)$ as a function of p.

Hydride Ion	r_1 (a_o)[a]	Calculated Ionization Energy[b] (eV)	Calculated Wavelength (nm)
$H^-(n=1)$	1.8660	0.7542	1644
$H^-(n=1/2)$	0.9330	3.047	406.9
$H^-(n=1/3)$	0.6220	6.610	187.6
$H^-(n=1/4)$	0.4665	11.23	110.4
$H^-(n=1/5)$	0.3732	16.70	74.23
$H^-(n=1/6)$	0.3110	22.81	54.35
$H^-(n=1/7)$	0.2666	29.34	42.25
$H^-(n=1/8)$	0.2333	36.09	34.46
$H^-(n=1/9)$	0.2073	42.84	28.94
$H^-(n=1/10)$	0.1866	49.38	25.11
$H^-(n=1/11)$	0.1696	55.50	22.34
$H^-(n=1/12)$	0.1555	60.98	20.33
$H^-(n=1/13)$	0.1435	65.63	18.89
$H^-(n=1/14)$	0.1333	69.22	17.91
$H^-(n=1/15)$	0.1244	71.55	17.33
$H^-(n=1/16)$	0.1166	72.40	17.12
$H^-(n=1/17)$	0.1098	71.56	17.33
$H^-(n=1/18)$	0.1037	68.83	18.01
$H^-(n=1/19)$	0.0982	63.98	19.38
$H^-(n=1/20)$	0.0933	56.81	21.82
$H^-(n=1/21)$	0.0889	47.11	26.32
$H^-(n=1/22)$	0.0848	34.66	35.76
$H^-(n=1/23)$	0.0811	19.26	64.36
$H^-(n=1/24)$	0.0778	0.6945	1785
$H^-(n=1/25)$		not stable	

[a] from Eq. (39) where a_o is the Bohr radius

[b] from Eq. (38)

Figure 1. Microwave plasma system and liquid nitrogen trap system for condensing gases from helium-hydrogen microwave plasmas maintained in an Evenson cavity. The experimental setup comprised a welded-joint stainless steel tubing system (1.27 cm OD X 165 cm length), two mass-flow controllers, two cryotraps, the quartz plasma cell (1.27 cm OD x 31 cm length), ion and TC vacuum gauges (SenTorr, Varian), six bellows valves (welded construction, Nupro U-series, helium leak tested to $4 X 10^{-9}$ sccm), and a turbo-molecular pump.

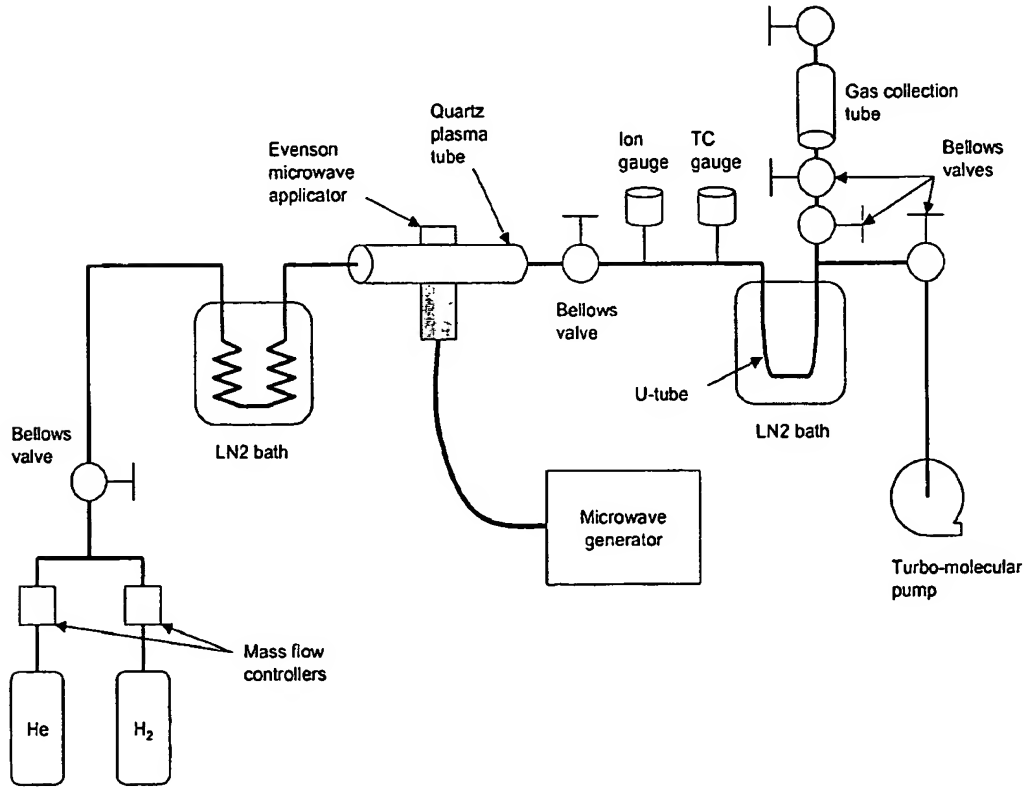

Figure 2. Microwave plasma system and cryo-cooler trap system maintained at ~12-17 K for condensing gases from helium-hydrogen microwave plasmas maintained in an Evenson cavity. The experimental setup comprised a welded-joint stainless steel tubing system, a metering valve, two LN cryotraps, the quartz plasma cell (1.27 cm OD x 31 cm length), a Baratron vacuum gauge, four bellows valves (Nupro B-series, helium leak tested to 4×10^{-9} sccm), a cryo-cooler compressor, a cryohead, a copper capillary tube (0.88 mm ID X 1.7 m length) spiraled on the cold stage of the cryo-head in an evacuated cylindrical chamber, a cryogenic silicon diode temperature sensor, and a turbo-molecular pump.

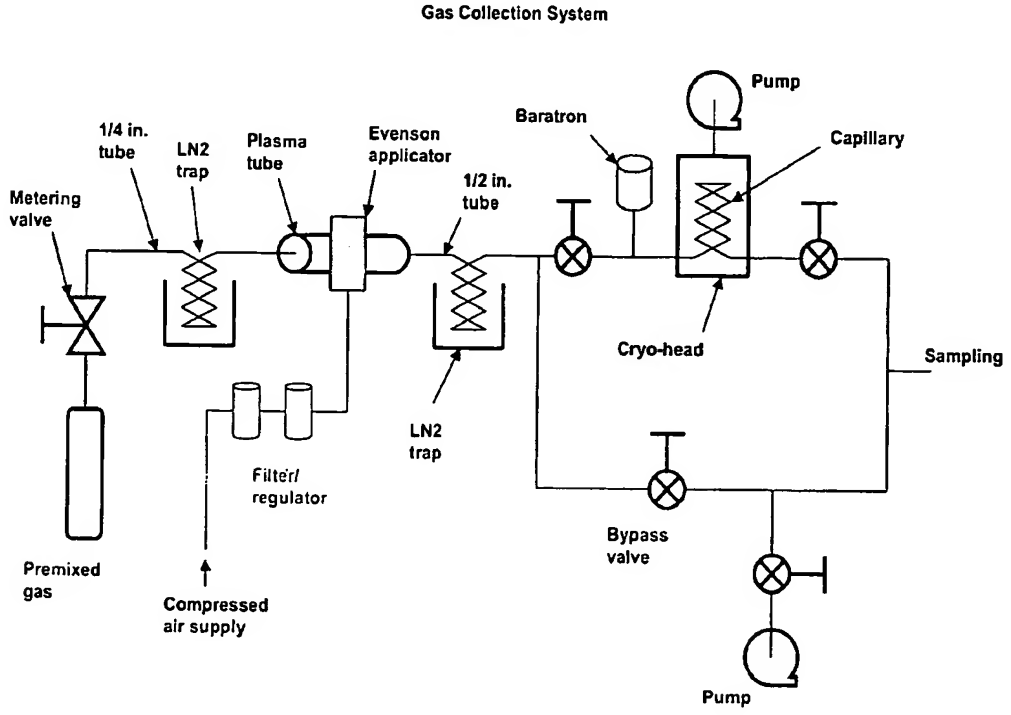

Figure 3. Schematic of the water bath calorimeter. The Evenson cavity and a plasma-containing section of the quartz tube were fitted with a water-tight stainless steel housing, and the housing and cell assembly were suspended by 4 support rods from an acrylic plate which held the cell vertically from the top of a water bath calorimeter.

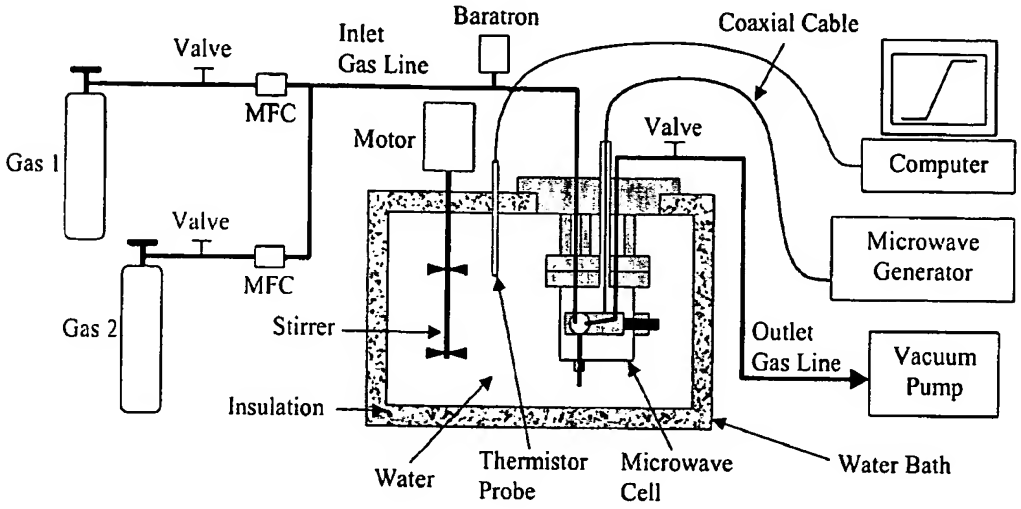

Figure 4. The EUV spectra (20-65 nm) of microwave plasmas of xenon and 10% hydrogen mixed with helium, krypton, and xenon. A vibrational pattern of peaks with an energy spacing of 1.18 eV was observed from the helium-hydrogen plasma having He^+ catalyst. The peaks matched Eq. (25) for $\upsilon^* = 0,1,2,3...24$. The series terminates at about 25.7 nm corresponding to the predicted bond energy of $H_2(1/4)^+$ of 48.16 eV given by Eq. (8). No emission was observed from the noncatalyst controls, krypton and xenon alone or with hydrogen. The sharp peaks in the spectrum were assigned to He I and He II.

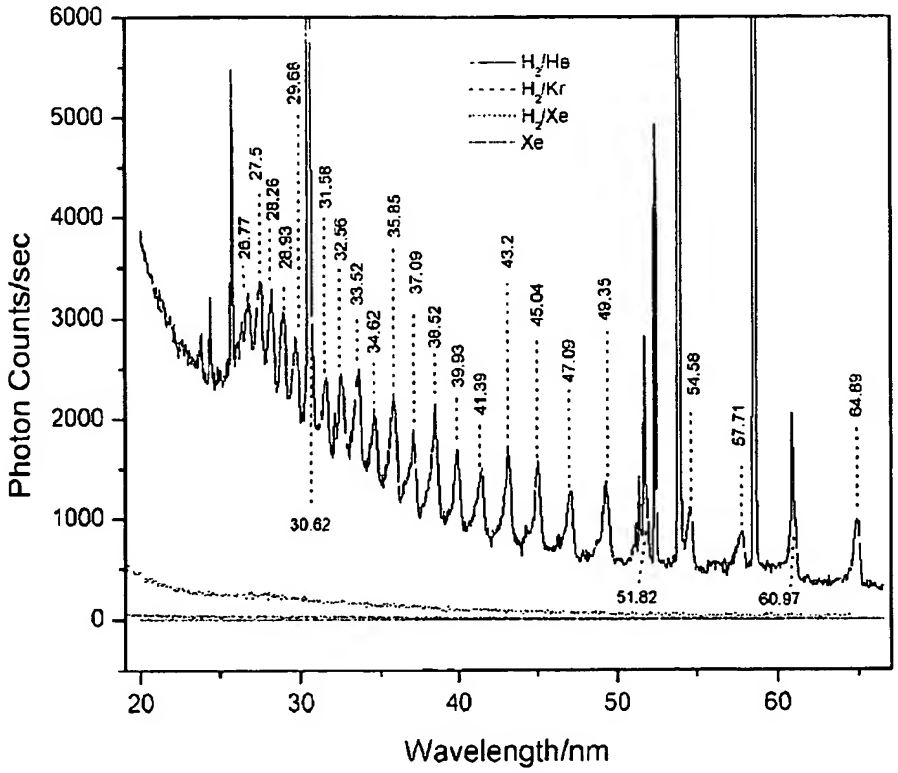

Figure 5. The EUV spectra (20-65 nm) of microwave plasmas of helium-hydrogen (90/10%) (solid) and helium alone (dashed). The vibrational series of peaks assigned to the reaction $H(1/4)+H^{+} \rightarrow H_2(1/4)^{+}$ was observed from the helium-hydrogen plasma having He^{+} catalyst and hydrogen, but not from helium alone. The sharp peaks in the spectrum were assigned to He I and He II.

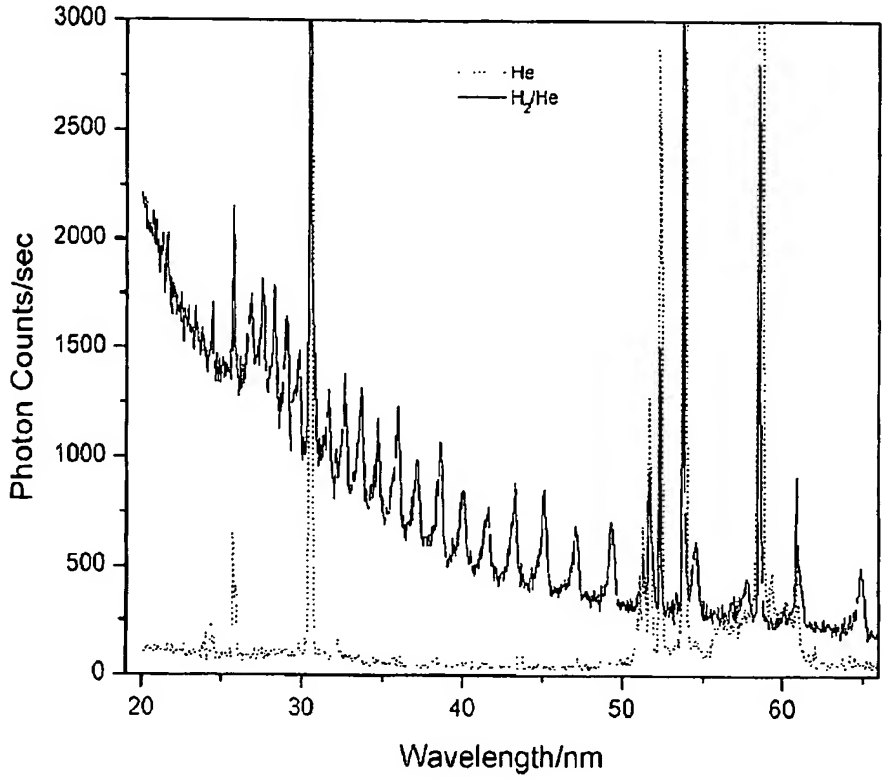

Figure 6. The plot of the energies of the peaks shown in Figures 4 and 5. The slope of the linear curve fit is 1.18 eV, and the intercept is 47.6 eV which matches the predicted emission given by Eq. (25) to within the spectrometer resolution of about 1%.

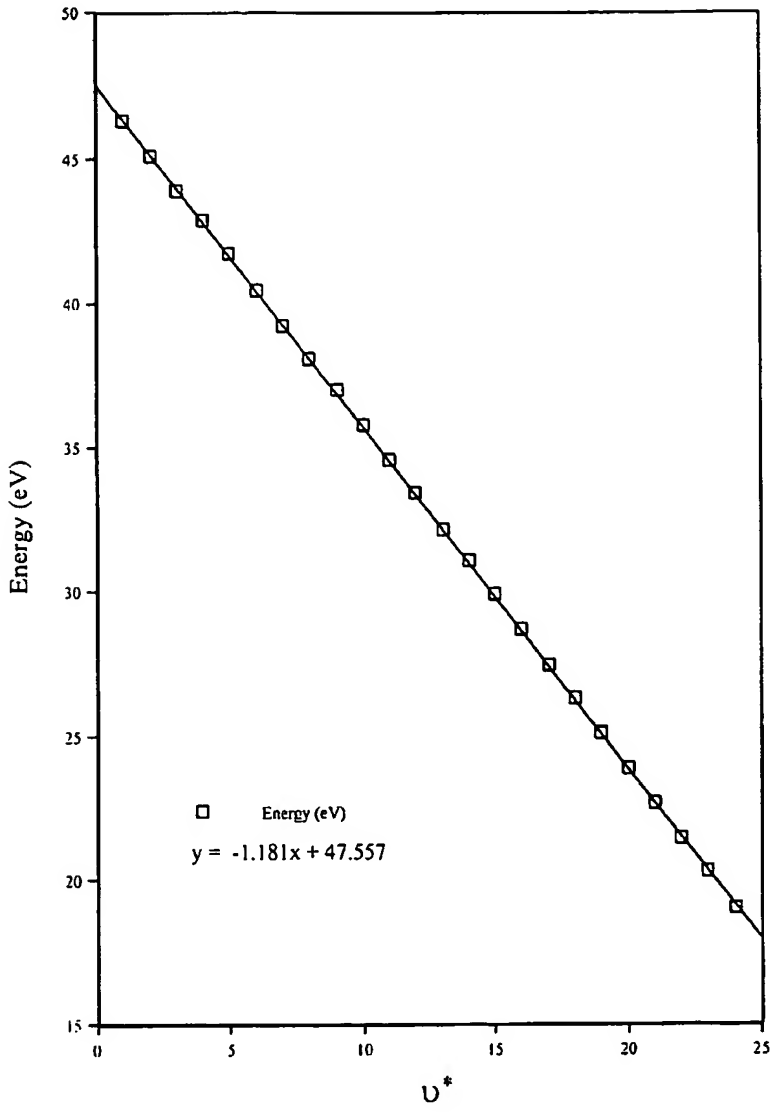

Figure 7. The EUV spectra (20-65 nm) of microwave plasmas of argon-hydrogen (90/10%) (solid) and argon alone (dashed). The vibrational series of peaks assigned to the reaction $H(1/4)+H^{+} \rightarrow H_2(1/4)^{+}$ was observed from the argon-hydrogen plasma having Ar^{+} catalyst and hydrogen, but not from argon alone. The sharp peaks in the spectrum were assigned to Ar I and Ar II.

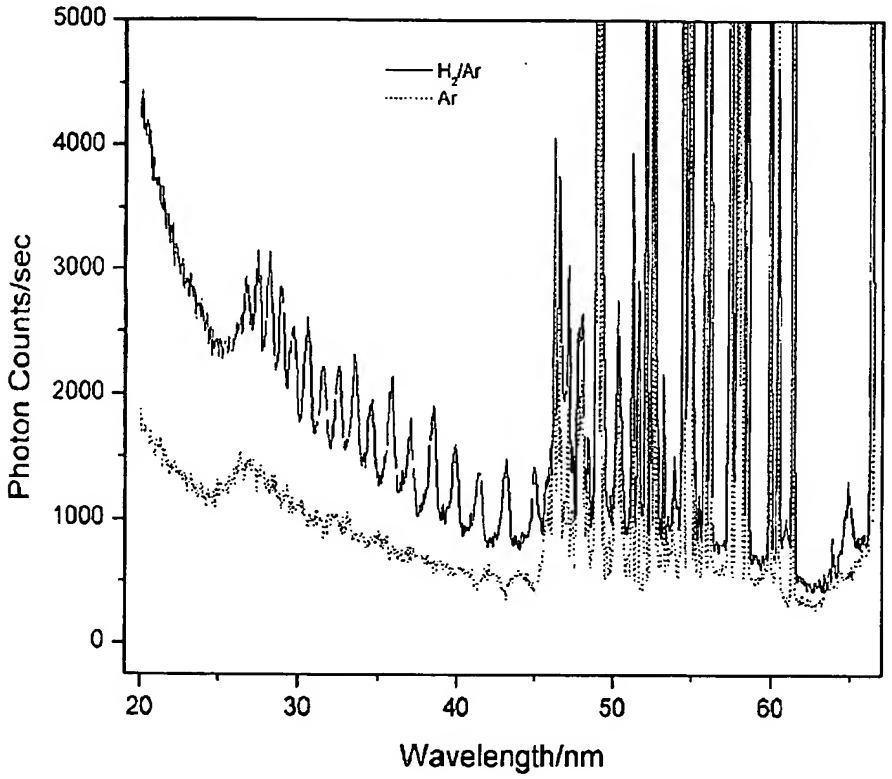

Figure 8. The 100-350 nm spectrum of a 783 Torr plasma of argon containing about 1% hydrogen and oxygen. Lyman α was observed at 121.6 nm with an adjoining H_2 band, the third continuum of Ar was observed at 210 nm, and the $OH(A-X)$ bands were observed at 282.7 and 308.6 nm. A series of sharp, evenly-spaced lines was observed in the region 145-185 nm. The series matched the P branch of $H_2(1/4)$ for the vibrational transition $\upsilon = 1 \rightarrow \upsilon = 0$. P(1), P(2), P(3), P(4), P(5), and P(6) were observed at 154.94 nm, 159.74 nm, 165.54 nm, 171.24 nm, 178.14 nm, and 183.14 nm, respectively. The sharp peak at 146.84 nm may be the first member of the R branch, R(1). The R-branch lines appeared to correspond to forbidden transitions, or the emission was suppressed by the argon second continuum.

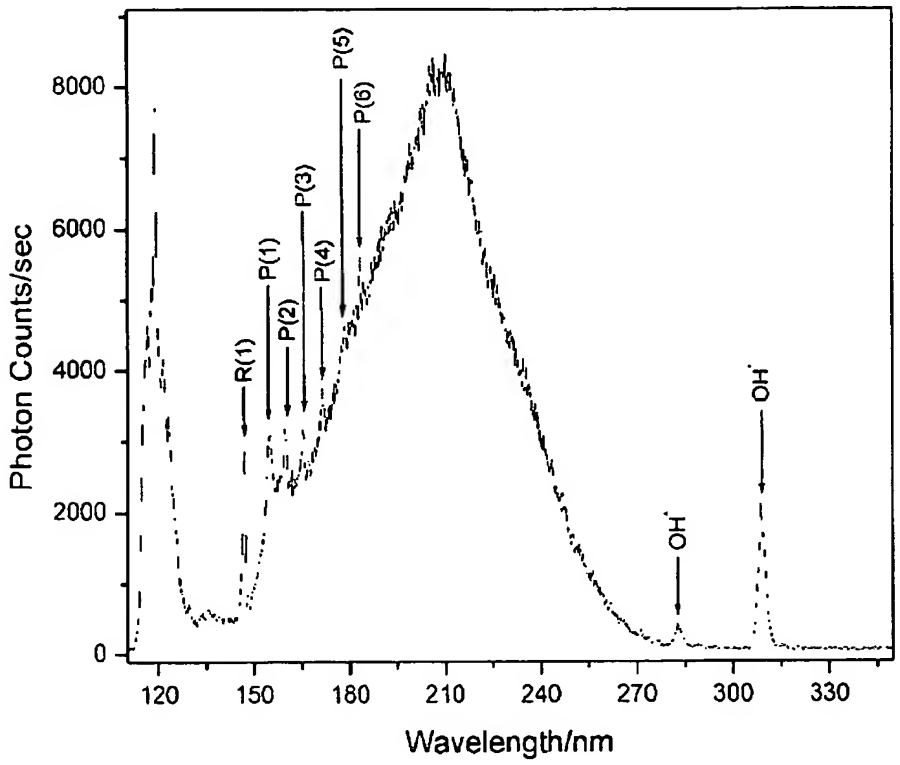

Figure 9. The plot of the energies of the peaks shown in Figure 8. The slope of the linear curve fit is 0.245 eV with an intercept of 8.25 eV which matches Eq. (27) very well for $p = 4$. The series matches the predicted $\upsilon = 1 \rightarrow \upsilon = 0$ vibrational energy of $H_2(1/4)$ of 8.224 eV (Eq. (14)) and its predicted rotational energy spacing of 0.241 eV (Eq. (20)) with $\Delta J = +1$; $J = 0,1,2,3,4,5$.

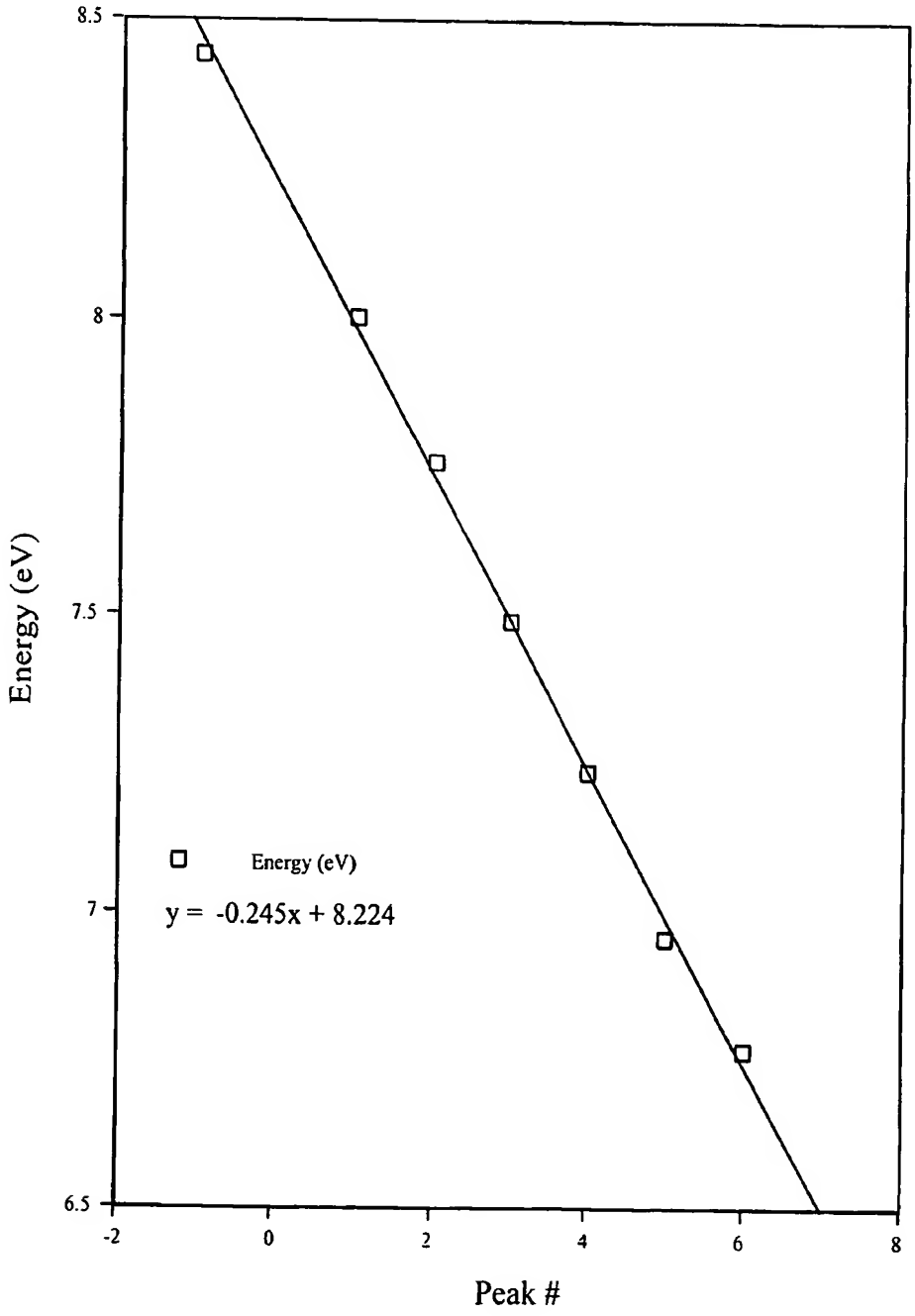

Figure 10. The 100-350 nm spectrum of a 456 Torr plasma of argon containing about 1% hydrogen and nitrogen. Lyman α was observed at 121.6 nm, the third continuum of Ar was observed at 190 nm, and background molecular emission was observed including $N_2\, C^3\Pi_u - B^3\Pi_g$ emission in the 270-350 region. A series of sharp, evenly-spaced lines was observed in the region 200-275 nm. The series matched the P branch of $H_2(1/4)$ for the vibrational transition $\upsilon = 5 \rightarrow \upsilon = 4$. P(1), P(2), P(3), P(4), P(5), P(6), and P(7) were observed at 204.94 nm, 215.04 nm, 226.44 nm, 236.44 nm, 247.14 nm, 258.74, and 271.34 nm, respectively. The R-branch lines appeared to correspond to forbidden transitions, or the emission was suppressed by the argon third continuum.

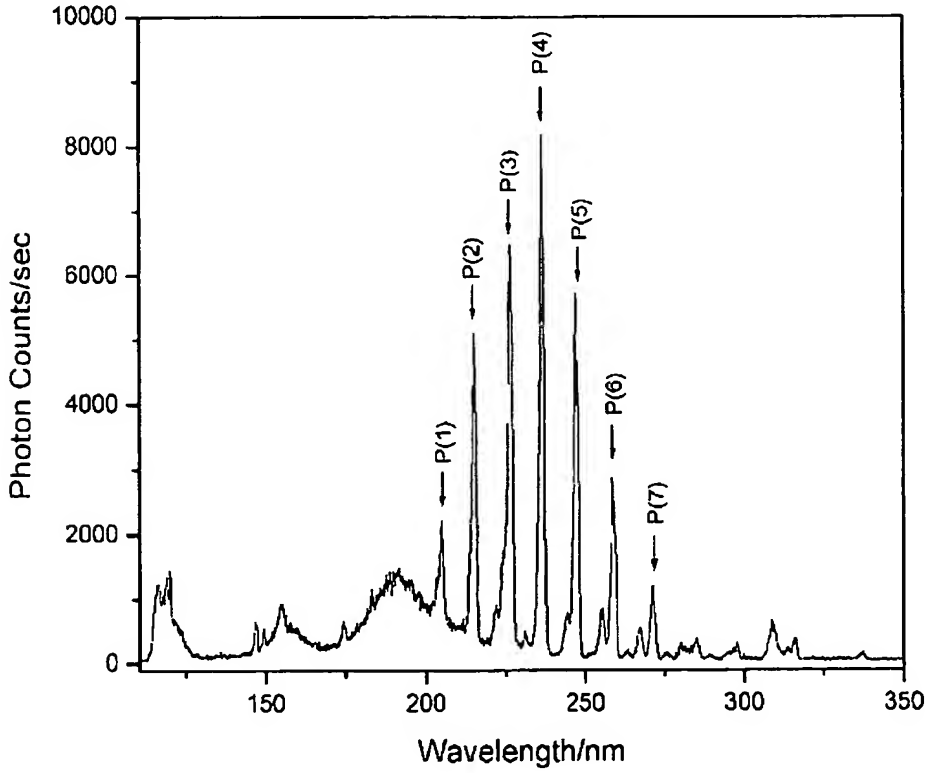

Figure 11. The plot of the energies of the peaks shown in Figure 10. The slope of the linear curve fit is 0.245 eV with an intercept at 6.25 eV which matches Eq. (27) very well for $p = 4$. The series matches the predicted $\upsilon = 5 \rightarrow \upsilon = 4$ vibrational energy of $H_2(1/4)$ of 6.30 eV (Eq. (14)) and its predicted rotational energy spacing of 0.241 eV (Eq. (20)) with $\Delta J = +1$; $J = 0,1,2,3,4,5,6$.

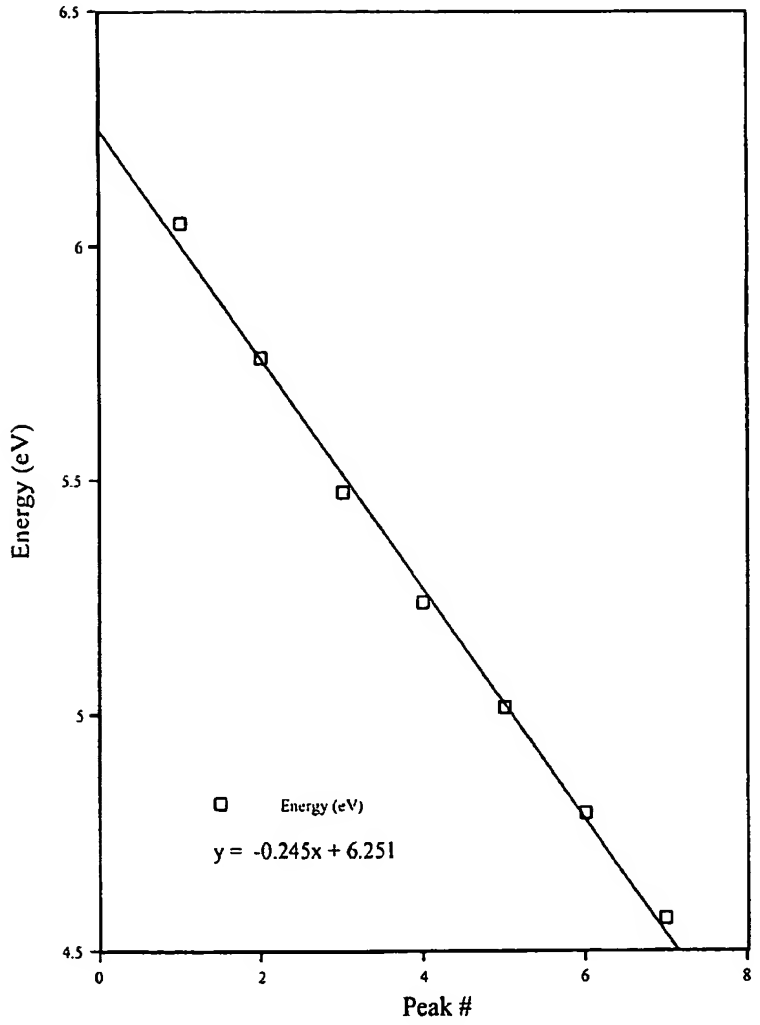

Figure 12. Comparison of the third continuum of argon gas as recorded by Ulrich, Wieser, and Murnick [41] with a very pure gas (upper spectrum) and a spectrum in which the gas was slightly contaminated by oxygen as evidenced by the second order of the 130 nm resonance lines at 160 nm. A series of narrow, evenly-spaced lines that appear similar to those in Figures 8 and 10 were observed that could not be assigned by Ulrich et al. to known species. The determination of the presence of hydrogen is warranted in future studies.

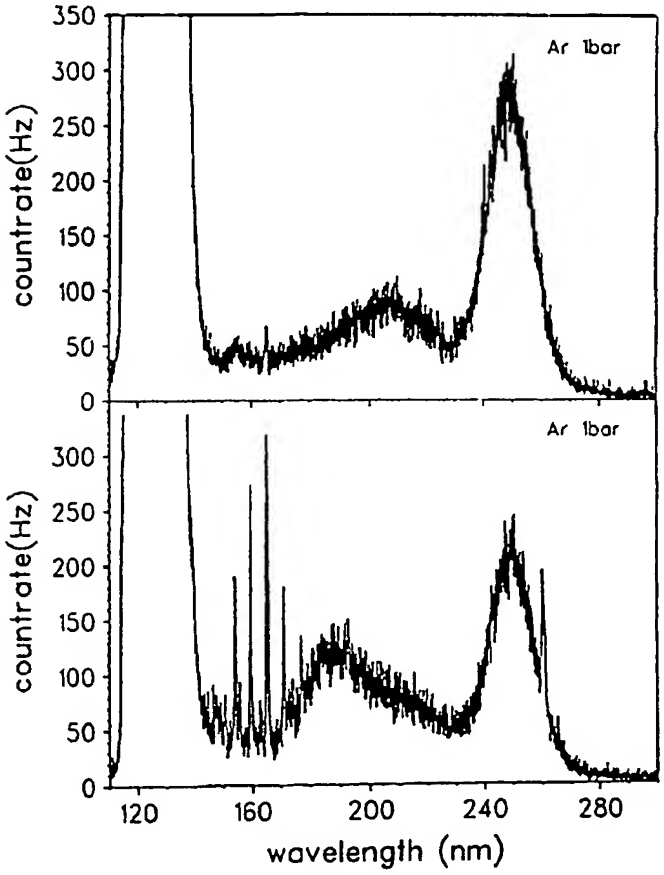

Figure 13. The pressure as a function of time after the liquid nitrogen dewar was removed from the U-tube cryotrap following 2 hours of helium-hydrogen (90/10%) gas flow through the microwave tube and the cryosystem shown in Figure 1 without plasma (dotted) and with a plasma maintained with 60 W forward microwave power and 10 W reflected (solid). A liquid-nitrogen condensable gas product was only observed for the plasma reaction run.

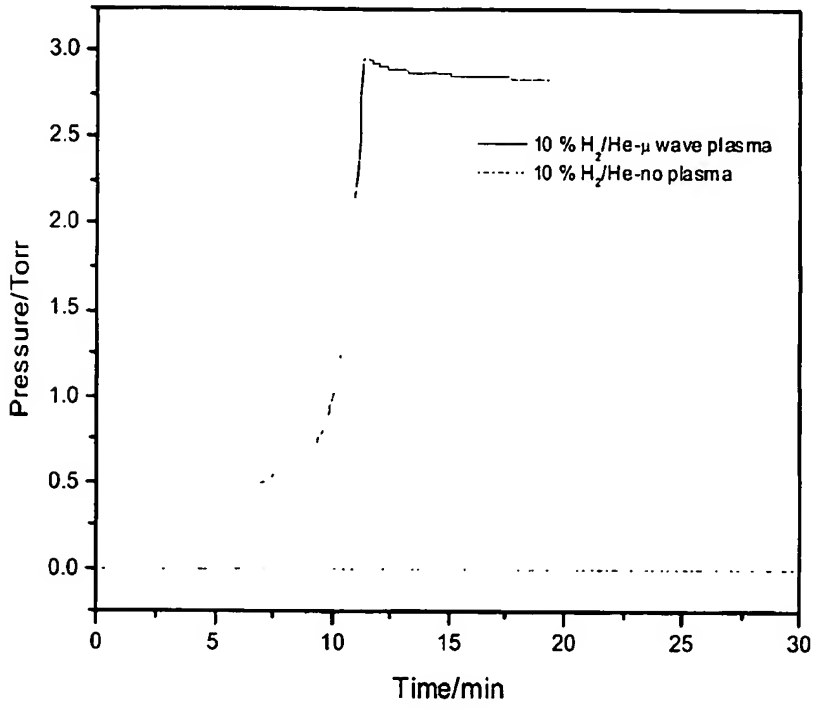

Figure 14. The mass spectra ($m/e = 1$ to $m/e = 50$) for the gases collected from He/H_2 (90/10%) microwave plasmas (IP =70 eV). (a) The mass spectrum of the gas condensed by the LN cryotrap over 2 hours. Only hydrogen peaks were observed which identified the liquid-nitrogen-condensable gas as hydrogen. (b) The mass spectrum of plasma gas collected by the cryo-cooler. The $m/e = 2$ peak was 40-50 times more intense than the $m/e = 28$ and $m/e = 32$ peaks that were assigned to very trace residual air contamination. When corrected for ionization efficiency, H_2 ($m/e = 2$) was determined to be ~500 times more abundant than the background.

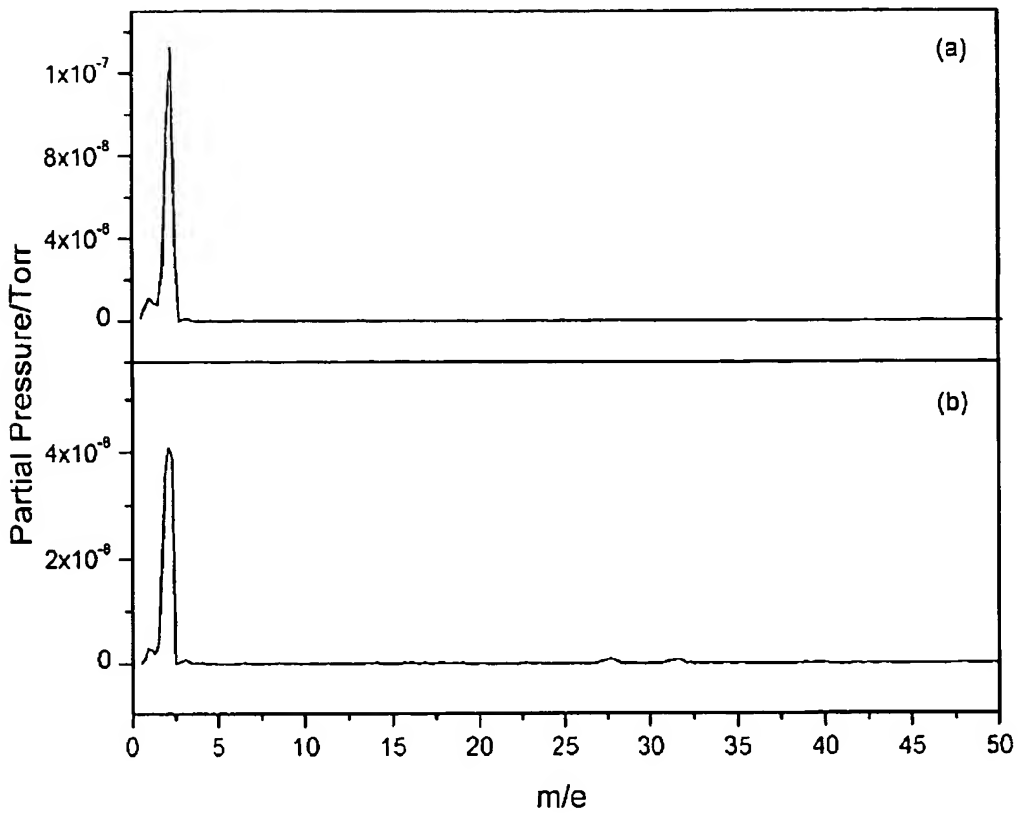

Figure 15. The phase diagram of hydrogen and helium. Since it is not possible to condense ordinary hydrogen below ~50 Torr at 12-17 K, the $m/e = 2$ peak of the mass spectrum (Figure 14) of plasma gas collected by the cryo-cooler at 700 mTorr that was not removed at 10^{-5} Torr indicates that a novel hydrogen gas formed in the plasma reaction between hydrogen and helium.

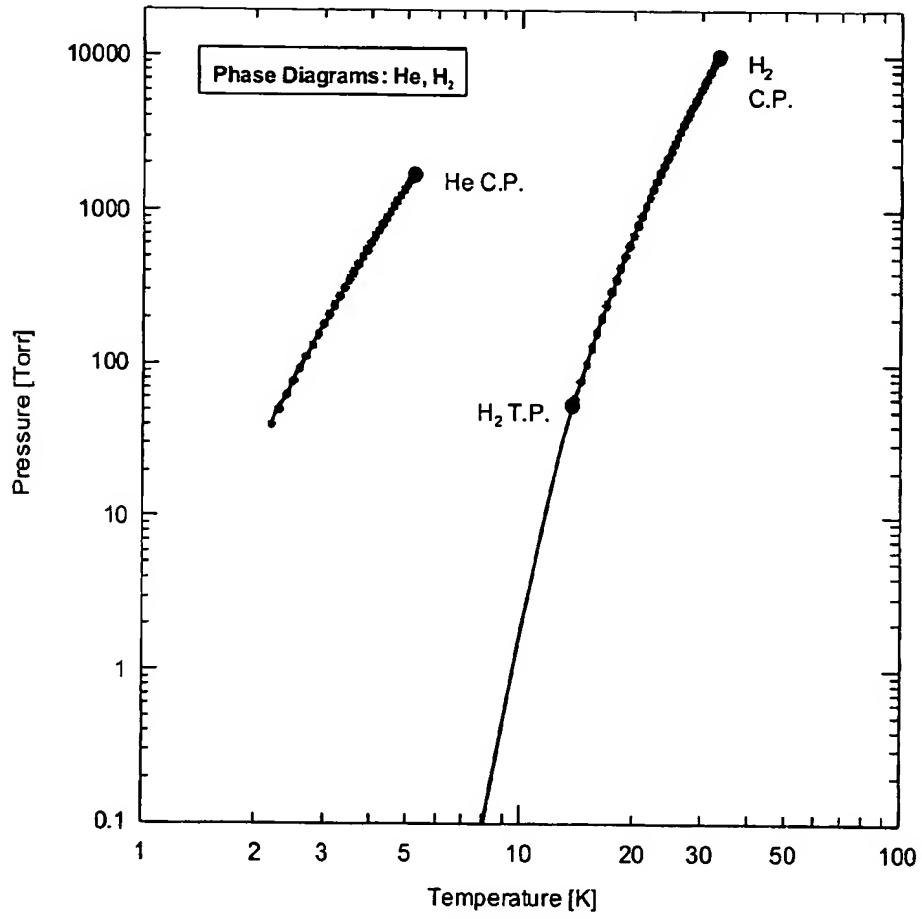

Figure 16 (a)-(f). ^1H NMR spectra on sealed samples of liquid-nitrogen-condensable helium-hydrogen plasma gases dissolved in $CDCl_3$ relative to tetramethylsilane (TMS). The solvent peak was observed at 7.26 ppm, the H_2 was observed at 4.63 ppm, and a singlet at 3.22 ppm matched silane. Singlet peaks upfield of H_2 were observed at 3.47, 2.18, 1.47, 0.85, 0.21, and -1.8 ppm relative to TMS corresponding to solvent-corrected absolute resonance shifts of -29.16, -30.45, -31.16, -31.78, -32.42, and -34.43 ppm, respectively. Using Eq. (30), the data indicates that p = 2, 4, 5, 6, 7, and 10, respectively. The data matched the series $H_2(1/2)$, $H_2(1/4)$, $H_2(1/5)$, $H_2(1/6)$, $H_2(1/7)$, and $H_2(1/10)$.

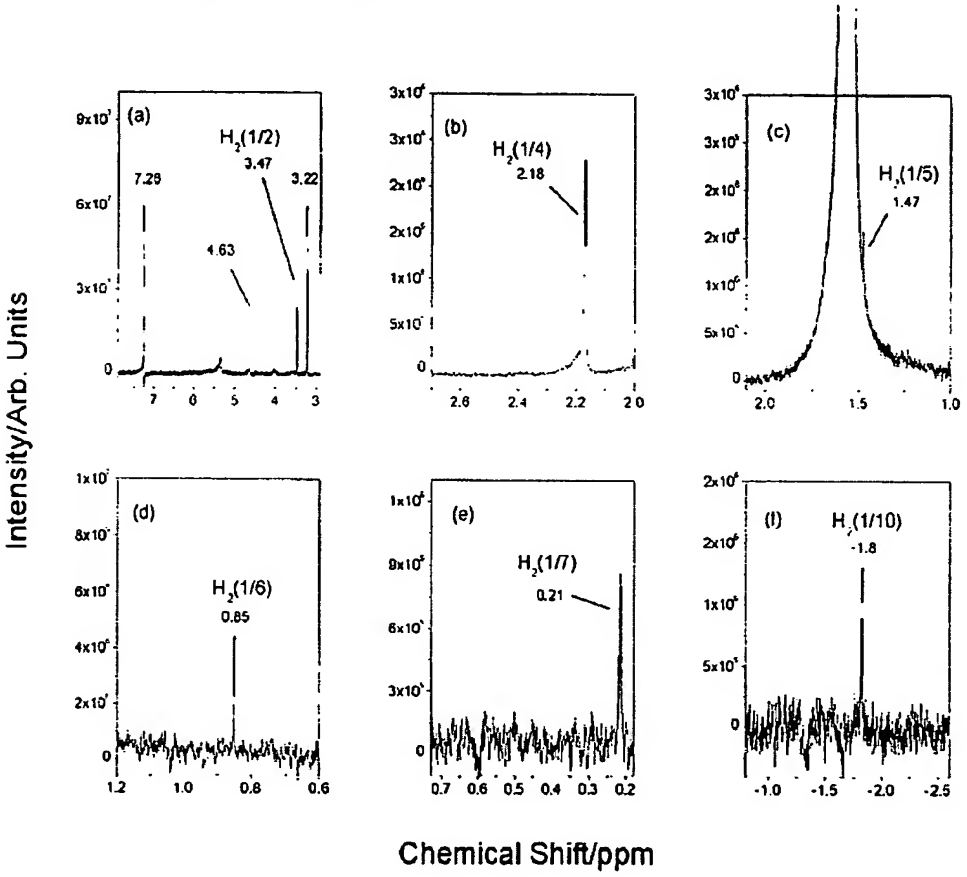

Figure 17. The ^1H NMR spectrum recorded at China Lake on a sealed sample of ultrahigh purity hydrogen dissolved in $CDCl_3$ relative to external tetramethylsilane (TMS). Singlet peaks were observed at 7.27, 4.63, and 1.56 ppm corresponding to $CHCl_3$, H_2, and H_2O, respectively.

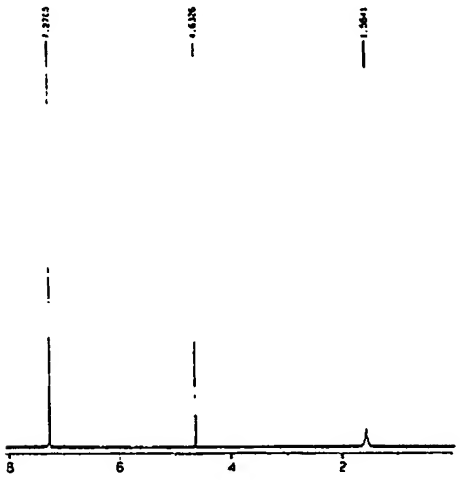

Figure 18. The ^1H NMR spectrum recorded at China Lake on gases from the thermal decomposition of $KH*1$ dissolved in $CDCl_3$ relative to tetramethylsilane (TMS). H_2 was observed at 4.63 ppm. Considering solvent effects, singlet peaks upfield of H_2 were observed with a predicted integer spacing of 0.64 ppm at 3.03, 2.18, 1.47, 0.85, and 0.22 ppm which matched the consecutive series $H_2(1/3)$, $H_2(1/4)$, $H_2(1/5)$, $H_2(1/6)$, and $H_2(1/7)$, respectively.

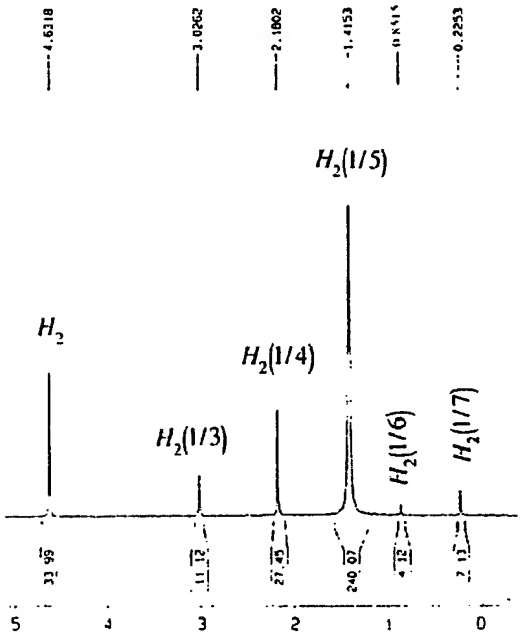

Figure 19. The $T(t)$ water bath response to stirring and then with selected panel meter readings of the constant forward and reflected microwave input power to helium-hydrogen (95/5%) mixture was recorded. Krypton control was run at identical microwave input power readings, and the microwave input power was determined to be 41.9 ± 1 W. From the difference in the $T(t)$ water bath response, the excess power of the helium-hydrogen plasma reaction was determined to be 20.2 ± 1 W.

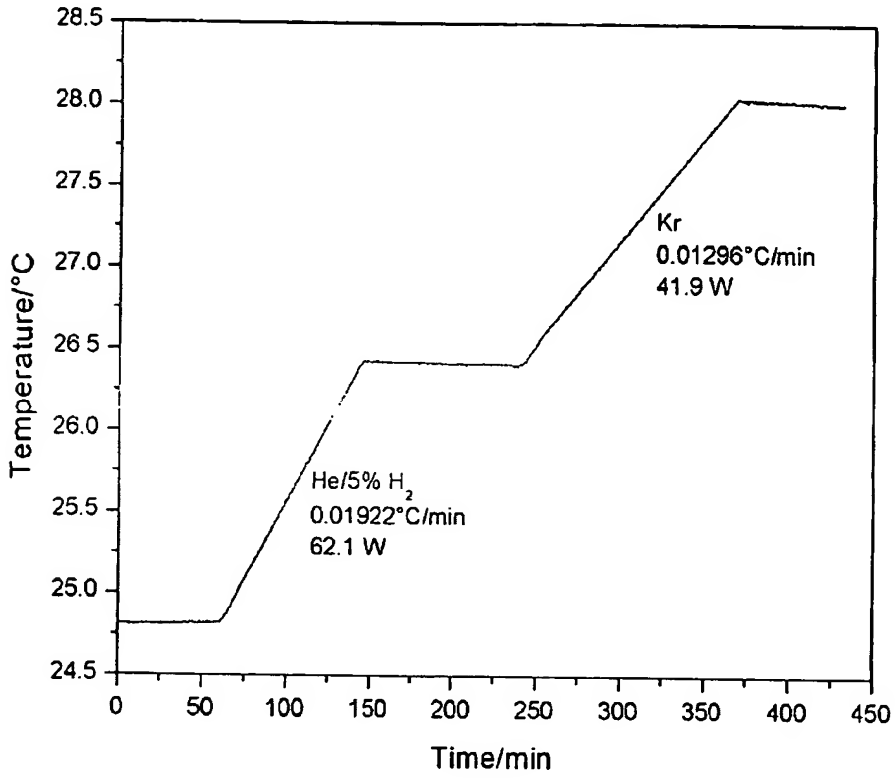

In the case that the object to be imaged has a small spatial variation in the magnetic susceptibility, a contrast agent may be added to increase the variation in magnetic susceptibility. For example, an ion containing contrast agent may be added to the vascular system including the coronary arterial system by methods such as intravenous or infusion. The variation in magnetic susceptibility may be imaged over time. High contrast of the spatial variation of magnetic susceptibility may be obtained. A preferred agent is ferromagnetic such as iron oxide nickel micro particles.

Continued on Page

Read and Understood By

Signed	Date	Signed	Date
[signature]	12/15/99	Nelson F Greene	12/16/99

The present invention of a high frequency electromagnetic wave generator and a power converter comprises a power cell which reacts atomic hydrogen with a catalyst having a net enthalpy of about m 27.2 eV where m is an integer. The hydrogen undergoes an electronic transition to form increased binding energy hydrogen having a binding energy given by

$$\frac{13.6}{\left(\frac{1}{p}\right)^2}$$

The electromagnetic wave generator and power converter further comprises a magnet or a source of a magnetic field preferably a uniform magnetic field longitudinal ~~to the~~ relative to a cylindrical ~~vessel~~ vessel of a ~~gas~~ power cell. The energy of the catalysis of hydrogen produces a plasma, ~~which~~

Continued on Page

Read and Understood By

Signed [signature] Date 12/30/99

Signed Date

The electron and proton of the plasma travel in an orbit in a plane transverse to the applied B field. The cyclotron frequency is given by

$\omega = \frac{eB}{m}$ where e is the fundamental charge B is the field strength, and m is the mass of the charged particle such as an electron, a proton or an ion of ~~a~~ the catalyst or product from the catalyst.

The orbiting charged particle emits electromagnetic radiation at this frequency which is received by an antenna such as a microwave antenna. The power P, emitted & collected by the cell which may be received by the

Continued on Page

Read and Understood By

Signed	Date	Signed	Date
[signature]	11/30/95		

antenna or used directly is
given by the equation for the time
dipole antenna

$$P = \frac{4\pi}{3}\sqrt{\frac{\mu_0}{\epsilon_0}}\left|\frac{\omega}{c} I p z\right|^2$$

where $\omega = \frac{2\pi}{T}$

the current $I = Ne\omega$

$$\frac{Ne\omega}{2\pi}$$

where N is the number of charged
particles pz is the dimension
of the orbit

The radius is given by

$$\frac{mv^2}{r} = eVxB$$

$$r = \frac{mv}{eB}$$

For the case of an electron
at 100,000 K

$$v = 4 \times 10^6 \text{ m/s}$$

where $\frac{1}{2}mv^2 = kT$ was used

Continued on Page

Read and Understood By

Signed _____ Date 12/30/84 Signed _____ Date _____

The radius for [illegible]

$$r = \frac{1.2 \times 10^{-5}}{B}\ m$$

In the case of protons at a temperature of 10,000 K the radius is

$$r = \frac{3 \times 10^{-4}\ m}{B}\ m$$

The electron cyclotron frequency for a 1.0 G field is

$$f = \frac{eB}{2\pi m} = \frac{1.8 \times 10^{10}}{2\pi} = 2.9 \times 10^{9}\ Hz$$

2.9 GHz

The proton cyclotron frequency is

$$f = \frac{eB}{2\pi m} = \frac{[illegible] \times 10^{[illegible]}}{2\pi} = 1.4\ MHz$$

The ratio of ionized to unionized hydrogen atoms is given by the Boltzmann equation

$$N/N_0 = e^{-\frac{\Delta E}{kT}}$$

In the case of an ionization energy of 13.6 eV and a temperature of

Continued on Page

100,000 K, 20% of the atoms are ionized.

The N of charged particles N is given by the product of ~~the~~ N, ~~charged~~ the density of ~~charge particles~~ atoms, given by V, the volume, times f the ionization fraction.

$$N = \rho V f$$

At one torr and a wall temperature of ~~300~~ 1000 K, the atom density is

$$PV = nRT$$

$$\frac{P}{RT} = \frac{n}{V}$$

$$\frac{1.3 \times 10^{-3}\ \text{atm}}{0.0821\ \frac{\text{liter-atm}}{\text{mole-°K}}(1000)} = \frac{n}{V} = 1.6 \times 10^{-5}\ \frac{\text{moles}}{\text{liter}} \times \frac{6 \times 10^{23}}{\text{mole}}$$

Continued on Page

Read and Understood By

Signed [signature] Date 12/30/99

Signed ______ Date ______

PROJECT ____ Notebook No. ____

Continued From Page ____

$$\frac{9.6\times10^{18}\ \text{ions}}{\text{l-km}}$$

For a 1 km wire

$$N = \frac{9.6\times10^{18}\ \text{ions}}{\text{l-km}}\,(1\ \text{km})(0.20) =$$

$$N = (9.6\times10^{18}\ \text{ions})(.2) = 1.9\times10^{18}\ \text{ions}$$

The current is

$$I = \frac{(1.9\times10^{18})(1.6\times10^{-19})}{2\pi}\left(\frac{1.1\times10^{10}}{2\pi}\right)$$

$$I = 1.4\times10^{8}\ \frac{C}{sec}$$

The length of the antenna, ΔZ, is equivalent to the diameter of the orbit. For a 10 T field and a temp of 100,000 K, the diameter is

$$\Delta Z = d = 2.4\times10^{-4}\ m$$

the power is

$$P = \frac{4}{3}\pi\sqrt{\frac{\mu_0}{\epsilon_0}}\left|\frac{2.9\times10^{9}}{4\pi}\ \frac{1.4\times10^{8}\ 2.4\times10^{-4}}{3\times10^{8}}\right|^2$$

$$P = 1\times10^{12}\ \text{watts}$$

Continued on Page ____

Read and Understood By

[signature] 12/30/95

Signed ____ Date ____ Signed ____ Date ____

a contrast agent to produce a variable magnetic susceptibility of a tissue of blood. Superparamagnetic iron oxide particles 2-4 nm commercially available from Sigma-Aldrich Corporation

[redacted]

17643 (2-8°C)
AMINE-TERMINATED Magnetic Particles 1 ml 18.95 / 5 ml 74.25
Matrix: superparamagnetic iron oxide particles, approx. 1 µm in size
Concentration: 50 mg per ml
Extent of activation: approx 12 µmoles per ml
Coupling capacity: typically 10 mg protein per ml
Form: suspension in 1 mM EDTA, pH 7.0.
Magnetic separators for a variety of vessels, from microcentrifuge tubes to flasks, are listed on Page 2276
[105808-72-8]

17518 (2-8°C)
CARBOXY-TERMINATED Magnetic Particles 1 ml 28.05 / 5 ml 93.35
Matrix: superparamagnetic iron oxide particles, approx. 1 µm in size
Concentration: 20 mg per ml
Extent of activation: approx 4.8 µmoles per ml
Form: suspension in distilled water
Magnetic separators for a variety of vessels, from microcentrifuge tubes to flasks, are listed on Page 2276
[105808-72-8]

To place an order call 800-325-3010

Continued on Page

Read and Understood By

Signed _____ Date 2/1/2000

Signed _____ Date 2/1/00

A prodrug of the present invention comprises a photochromic dye of my US patent 5,773,592 or similar type dye that is bonded to a biologically active agent such as those disclosed in my US patent Application 5,773,592. The prodrug comprises the dye and biologically active agent penetrating into one or more biological compartments of interest and releases the drug in free form due to the reversibility of the bond between the dye and the biologically active agent. In an embodiment, attached drug delivery is achieved based on the stability of this bond which permits the prodrug to penetrate the compartment before the drug is released.

Continued on Page

Read and Understood By

Signed 4/7/2000 Date

Signed 3-10-2000 Date

In another embodiment, the mechanism considered an equilibrium between drug and dye or carrier such that a steady state concentration of prodrug is formed which delivers the drug into the compartment such as intracellularly where it is released. The drug may be trapped inside the compartment, thus, over time effective drug delivery is achieved.

Continued on Page

Read and Understood By

Signed	Date	Signed	Date
	4/7/2000		3-10-2000

In an embodiment of the gyrotron plasma to electric power utility the magnetic field is provided by the Earth's magnetic field. In another embodiment, the Earth's field ~~provide~~ is ~~~~ applied in a z direction, ~~~~ the long axis or axis of the electromagnetic wave of the wave guide which satisfies the relationship

$$w \neq -k_z v_z = s w_c$$

where k_z is the electromagnetic wave in the z direction and v_z is the electron velocity in the z direction and s is an integer.

Continued on Page

Read and Understood By

Signed: [signature] Date: 3/30/00 Signed: Nelson J. Gorenz Date

PROJECT ReMSI
Notebook No. ______
Continued From Page ______

In an embodiment of my ReMSI imager, a contrast agent that is an electron paramagnetic resonance (EPR) active is added. In a preferred embodiment the EPR signal is preferably of narrow line width.

In an embodiment, the local magnetic susceptibility of the imaged object shifts the EPR signal such that each voxel emits a characteristic frequency. The EPR signal as a function of time is recorded with a 3D detector. A fourier transform gives the spectrum. The spatial variation of the signal at each frequency is used to reconstruct the position of each corresponding emitting voxel. A magnetic susceptibility map is plotted.

Continued on Page

Read and Understood By

Signed [signature] Date 5/26/00

Signed Nelson L Gorenig Date 6/20/00

In another embodiment of
my present invention a
magnetic field gradient is
applied along one axis and a
ultrasonic frequency gradient
is applied along another
axis so that the ultrasonic
frequency matches the
hydrogen frequency due to
the magnetic field such
that each voxel has a
unique frequency which may
be detected to reconstruct
an image.

Continued on Page

Read and Understood By

Signed _____ Date 5/11/00

Signed Nelson L Greene Date 6/20/00

PROJECT RMST

Notebook No. _____

Continued From Page _____

In an embodiment of my RMST sequence an RF gradient is applied in the Ky phase that encodes each voxel in the 2 directions according to the larmor frequency. After a time to another RF pulse is applied in the transverse plane to recall the phase of the voxels due to the dispersion based on the local magnetic field which corresponds to the local magnetic susceptibility. The RF signal as a function of time is recorded over the 3-D distance or over 3D space. A Fourier transform is performed with respect to frequency and phase. For a particular sequence, each voxel produces a unique frequency and phase. The Larmor frequency determines the position of a line at a

Continued on Page

Read and Understood By

6/4/00		Nelson F Greene	6/20/00
Signed	Date	Signed	Date

position z corresponding to the applied RF gradient in z.

This value of z is substituted into the Fourier transform algorithm. Thus the spatial variations of the intensity of the RF signal ~~at~~ at a given frequency and phase over the 3 D detection space is used to reconstruct the image which represents T_2 according to by variations of the magnetic susceptibility and molecular ~~dephase~~ processes which shift the phase angle of ~~phase~~ nuclear magnetic precession at each voxel.

Different RF pulse sequences known to those skilled in the art may be used to produce different phase angles of nuclear precession to give a desired image.

Continued on Page

Read and Understood By

Signed: [illegible signature] Date: 6/7/00

Signed: [illegible signature] Date: 6/20/00

PROJECT RAMSI

Notebook No. _____

Continued From Page _____

In an embodiment of my RAMSI scanner a magnetic field gradient along the Z axis selects a slice to be imaged. A second gradient is applied in the XY plane to create a frequency gradient in the transverse or XY plane, then an RF phase gradient is applied in the direction of the gradient so that each voxel in the plane may have a distinct harmonic frequency and phase. The ~~harmonic~~ RF signal is recorded over the three dimensional detector array.

Continued on Page

Read and Understood By

Signed	Date	Signed	Date
[signature]	6/20/00	Nelson F Greene	6/20/00

and the FID at each detector is fourier transformed into the frequency and phase spectrum. The intensity variations at each distinct frequency and phase are the 3-D detector array is used to reconstruct the position of each voxel. ~~a~~

Since a 3D array and time is used ~~used~~ (corresponding to phase) the method and system of the present invention may be referred to a four dimensional magnetic resonance imaging or (4D MRI).

Another method of encoding voxels with unique spatial tags to permit their reconstruction according to the present invention ~~is~~ use of phase gradients in two orthogonal directions,

Continued on Page

Read and Understood By

Signed	Date	Signed	Date
[illegible signature]	6/20/00	6/20/00 [illegible signature]	6/20/00

Notebook No.
Continued From Page

Standard T_2 and T_2^* imaging methods, techniques, and systems may be used with the 40 MRE system. For example, a 90° pulse may be followed by a 180° pulse before the data is recorded to give a T_2 or T_2^* image.

Continued on Page

Read and Understood By

Signed [signature] Date 6/20/00 Signed [signature] Date 6/20/00

In an embodiment of my RFMSI scanner, the magnetic susceptibility of the object to be imaged is spatially varying. Thus, in the embodiment employing the application of a uniform magnetic field, the larmor frequency at each location in the object. The FID signal as a function of time is recorded at each detector and a three dimensional space, voxel. Since each detector is at a unique position relative to each detector, the phase from each voxel at a given detector varies. Thus, the three dimensional detector array provides phase modulations in each of 3 dimensions. Continued on Page

Read and Understood By

[signature]	7/11/00	Adam P Feeney	7/11/00
Signed	Date	Signed	Date

In an embodiment, the FID at each detector is recorded as a function of time. The first signal is then Fourier transformed according to a constant kernel frequency with a phase that is a function of the x,y,z position of the detector relative to each emitting voxel. The position of each detector is then used to transform the intensity and phase data of each detector to an intensity and standard relative phase so that all the detectors are related to the standard. The result is that each voxel will have a unique phase and each

Continued on Page

Read and Understood By

[signature]	7/14/00	Nelson L Greene	7/14/00
Signed	Date	Signed	Date

[illegible], These intensity variations over the detector array at a given phase is then used to reconstruct the position of the voxel. This procedure is applied to reconstruct all of the voxels of the image.

The intensity map can be T_2 map or a T_1 map for standard, wherein the data is recorded following the ~~[illegible]~~ corresponding T_2 or T_1 encoding pulse sequency that is standard to those in the art; except that the phase and frequency of all of the voxels is made the same. In the case that a frequency or phase gradient is applied, this is deconvolved when

Continued on Page

Read and Understood By

[illegible] 7/11/00 — Nelson L. Greening 7/11/00

Signed Date Signed Date

Notebook No. ______
Continued From Page ______

processing the data by the method given previously.

Example of phase separation: in the case that the Larmor frequency is 42 MHz, the wavelength is 7 m. If each detector is separated by 2 mm then the corresponding percentage is 0.3 ppt.

Typical NMR separation required to distinguish two peaks are about 2-3 ppm. Thus, significant voxel separation in phase space is possible. The total phase range is 0.3 ppt times the # of detectors

number of detectors in each direction.

For 100 detectors the relative phase range is 30 ppt.

Continued on Page

Read and Understood By

Signed [signature] Date 7/11/00 Signed Nelson L Saenz Date 7/11/00

In an embodiment the phases of the signals at each detector is transformed into standard phases which are relative to the position in the detector array and ~~corresponding~~ provide ~~the~~ a corresponding phase for any given voxel at each detector. In order to achieve a standard phase, the variation of the phase of each Fourier component as function of z is determined. The consistent with the maximum change or ~~of~~ the predicted change based on the ~~differ~~ distance in z between detectors is selected. In this case, the ~~[illegible]~~ voxel

Continued on Page

Read and Understood By

Signed ______ Date 7/15/00 Signed ______ Date 7/24/00

which gives rise to the Fourier component at the given detector is aligned with the detector along the Z axis. From the ~~this~~ phase of this component, the phases at ~~all other~~ each corresponding ~~[illegible]~~ components at each detector due to the voxel may be calculated using vector addition ~~in~~ of phases corresponding to vector addition in space ~~which~~. For example, a component is selected that is vertical with respect to a voxel (i.e. $\Delta X, \Delta Y = 0$ with respect to the voxel and detector). The phase corresponds to ΔZ only. The phase for the component a detector $\Delta X, \Delta Y$ from this detector is

Continued on Page

Read and Understood By

Signed: [signature] Date: 7/15/00

Signed: Nelson L. Greening Date: 7/24/00

B* proportional to

$\sqrt{\Delta z^2 + \Delta x^2 + \Delta y^2}$.

For an embodiment, the correction phase for the Fourier components added in is given by $\sqrt{\phi_1^2 + (\Delta x)^2 + \Delta z^2}$ + k

$\phi_2 = k \sqrt{\phi_1^2 + (k\Delta x)^2 + (k\Delta y)^2}$

where k is the wave number of the NMR signal.

For an embodiment a phase relative to the RF excitation field may be determined by synchronous detection with the RF excitation pulse.

Continued on Page

Read and Understood By

Signed	Date	Signed	Date
	7/15/00	7/24/00	7/24/00

In addition to the phase angle due to the distance from the ~~the~~ voxel to the detector a phase angle component due to the solid angle (SP) ~~between~~ the ~~[illegible]~~ detecting 2 crossed RF ~~[illegible]~~ dipole and the 2 ends of the detector, the solid ~~[illegible]~~ angle θ is ~~[illegible]~~ shown in Fig 1 given by

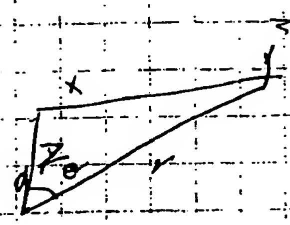

Fig 1

$$\theta = \sin^{-1}\frac{x}{r} = \sin^{-1}\frac{x}{\sqrt{x^2+z^2}}$$

This solid angle ~~is added~~ superimposes φ that due to the ~~[illegible]~~ distance between the voxel and the detector where

Continued on Page

Read and Understood By

Signed [signature] Date 7/20/00

Signed Nelson L Greenis Date 7/24/00

$\Phi = \frac{2\pi}{\lambda}\sqrt{x^2+y^2+z^2}$

The solid angle is zero in the case that a voxel is aligned with a given detector. The phase angle of each Fourier component at a given detector is calculated for all other detectors for the aligned voxels by adding the contributions there of each solid angle Θ and ϕ. The phase due to solid angle does not change as a function of z for voxels aligned with the detector. The phase of the corresponding Fourier component at a second detector is given by

$\Phi_1 + \Phi = \left(\sin\frac{x}{(x^2+z^2)}\right)^2 + \sqrt{\Phi_1 + (k\alpha)^2 + (k\beta)^2}$

Continued on Page

Read and Understood By

Signed Date Signed Date

7/29/00

PROJECT Bems1 Notebook No. ______

Continued From Page ______

where x, y, z are the distances ~~from~~ of ~~the~~ second detector from the first.

The corresponding Fourier components ~~of all~~ of a given detector are determined at each of n detectors to form n sets of n Fourier components with the same phase. The ~~p~~ intensity variations of the n Fourier components of each set is used to reconstruct the position of a voxel. This is repeated for all sets of n Fourier components of the same phase.

In an embodiment the phase angle of the signal ~~at each any~~ from each voxel at each detector is unique.

Continued on Page

Read and Understood By

[signature] 7/20/00 Signed Date

Nelson L Greene 7/24/[illegible] Signed Date

Consider a voxel with $\Delta x = 0$ cm

$\Delta z = 0.1$ cm in relation to a

detector, for this case the solid

angle is zero, but the

spherical delay angle is $\phi = \frac{2\pi}{\lambda} \Delta z$.

Next consider the phase angle

due to voxels at

Case 1 $\Delta x = 0.1$ cm $\Delta z = $ ~~20~~ 0.1 cm

Case 2 $\Delta x = 0.1$ cm $\Delta z = 20$ cm

Case 3 $\Delta x = 20$ cm $\Delta z = 0.1$ cm

Case 4 $\Delta x = 20$ cm $\Delta z = 20$ cm

$\lambda = 15m = 1500$ cm

$\theta = \sin^{-1} \frac{.1}{\sqrt{.1^2 + .1^2}}$ $\quad \phi = \frac{2\pi}{\lambda} \sqrt{(0.1)^2 + (0.1)^2}$

$\theta = .78$ rad $\quad \phi = 5.9 \times 10^{-4}$ rad

Case 1 $\quad \theta_T = 0.7806$

Case 2 $\quad \theta = \sin^{-1} \frac{0.1}{\sqrt{(0.1)^2 + (20)^2}}$ $\quad \phi = \frac{2\pi}{\lambda} \sqrt{(0.1)^2 + (20)^2}$

$\theta = 5 \times 10^{-3}$ $\quad \phi = $ ~~[illegible]~~ 8.377×10^{-2}

$\phi_T = 8.88 \times 10^{-2}$

Continued on Page

Read and Understood By

[signature] Signed 7/24/00 Date

[signature] Signed 7/24/00 Date

Case 3

$\theta = \sin^{-1} \frac{20}{\sqrt{(20)^2 + (0.1)^2}}$ $\phi = \frac{2\pi}{\lambda} \sqrt{(20)^2 + (0.1)^2}$

$\theta = 1.56$ $\phi = 0.0834$

$\phi_T = 1.643$

Case 4

$\theta = \sin^{-1} \frac{20}{\sqrt{(20)^2 + (20)^2}}$ $\phi = \frac{2\pi}{\lambda} \sqrt{(20)^2 + (20)^2}$

$\theta = 0.785$ $\phi = 0.1184$

$\phi_T = \theta + \phi = 0.9034$

~~In the case that~~
~~$kr < \theta$ ...~~

~~voxel will have a unique~~

$\phi = kr$ is the same for a family of voxels along an ~~arch~~ circular arch a distance r from the voxel. However each voxel will

Continued on Page

Read and Understood By: [signature] 7/24/00

[signature] 7/24/00
Signed Date Signed Date

have a unique solid angle, thus each voxel will have a unique phase with the antenna thus

$\Theta_{max} > \phi_{max}$ for any r,

$\sin^{-1} \frac{x_{min}}{\sqrt{x^2_{min}+z^2_{min}}} > \frac{2\pi}{\delta} \sqrt{x^2_{min}+z^2_{max}}$

$\frac{x_{min}}{\sqrt{x^2_{min}+z^2_{min}}} > \sin \frac{2\pi}{\delta} \sqrt{x^2_{min}+z^2_{max}}$

for $z >> x$

$\frac{x_{min}}{\sqrt{x^2_{min}+z^2_{min}}} > \frac{2\pi}{\delta} z_{max}$

~~$\delta > \frac{2\pi z_{max} x_{min}}{\sqrt{x^2_{min}+z^2_{min}}}$~~

for $x_{min} = z_{min}$

$\delta > 2\pi \sqrt{2}\ z_{max}$

$\delta > 8.9\ z_{max}$

$f < \frac{c}{8.9\ z_{max}}$ for $z_{max} = 20\text{cm}$

$f < 168$ MHz

Continued on Page

Read and Understood By

Signed [signature] Date 7/22/00 Signed [signature] Date 7/24/00

Plasma Electric Power Converter

In an embodiment of the plasma-electric power converter, the microwave plasma discharge power cell comprises a microwave transparent cell enclosure such as an alumina enclosure, and the cell is located in a large microwave cavity. The plasma may be magnetized to generate microwaves in the ionized gas caused by the catalysis reactions. The catalyst may be He^{+} or Ar^{+} generated from He or Ar by the plasma. The microwaves also dissociate molecular hydrogen to atomic hydrogen. The cavity and/or the cell may comprise a MASER active medium which absorbs microwaves from the hydrogen catalysis powered plasma and emit coherent microwaves which are collected by

Continued on Page

Read and Understood By

[signature] 8/3/01 — Signed / Date

Nelson L. [signature] 8/07/01 — Signed / Date

PROJECT ______

Continued From Page ______

means such a waveguide
and may be retrofitted to the
electricity. Thus rather than
photon bunching electrons to achieve
~~[illegible]~~ direct conversion
Photons are "bunched" and
convertible to DC electricity.

Continued on Page

Signed [signature] Date 8/3/01

Read and Understood By

Nelson [signature] Signed Date 8/07/01

PROJECT _____ Notebook No. _____

Continued From Page _____

Continued on Page

Read and Understood By

Signed _____ Date _____ Signed _____ Date _____

PROJECT _____ Continued From Page _____

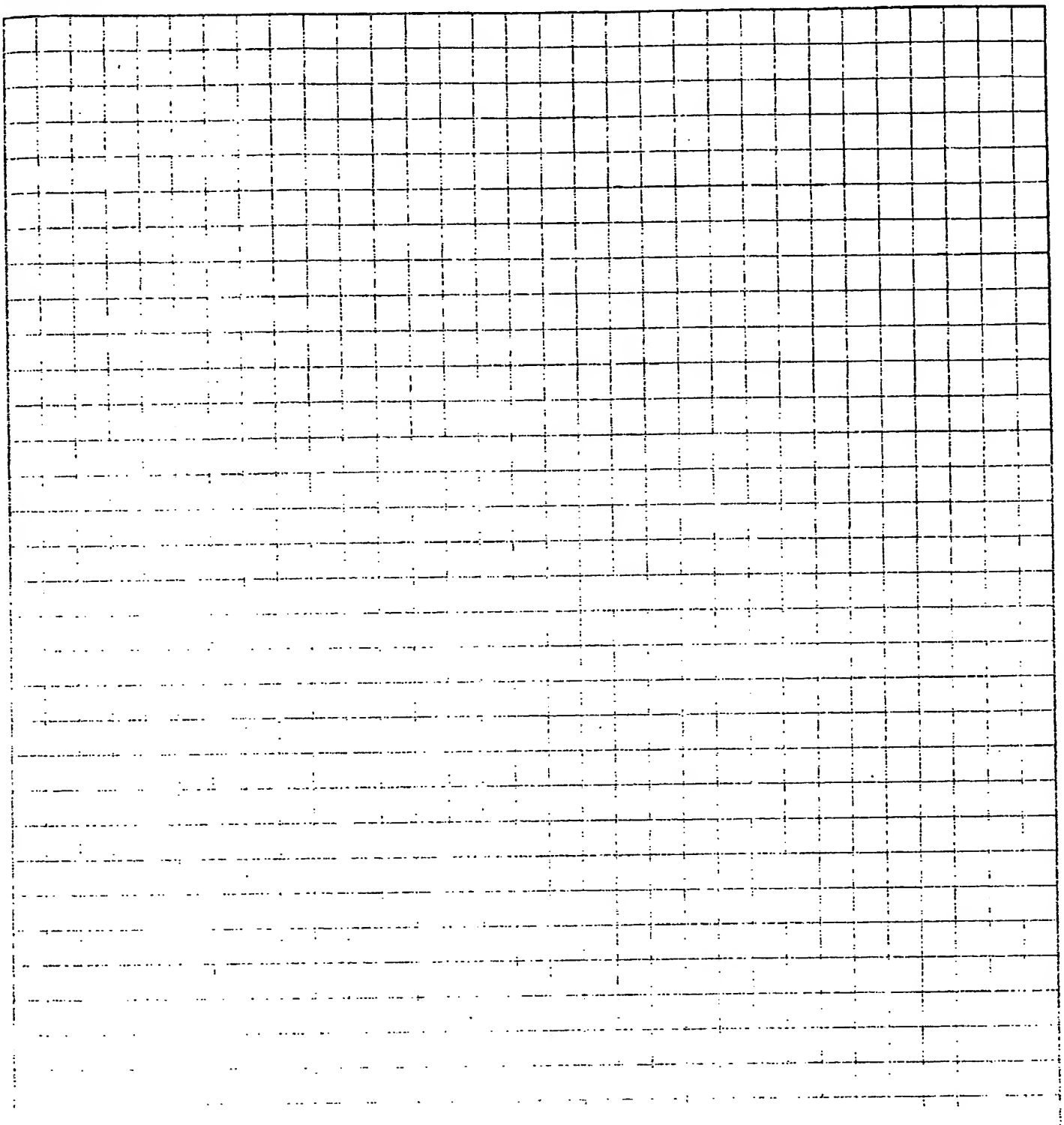

Continued on Page

Read and Understood By

Signed	Date	Signed	Date

PROJECT ______ Notebook No. ______

Continued From Page ______

Microwave Plasma to Electric Power Converter

In an embodiment of the plasma to electric power converter, a plasma is generated by the catalysis of hydrogen. The plasma is magnetized such that it emits microwaves to a receiver such as an output wave guide antenna, or rectifier which converts the microwave power to electricity. In an embodiment, self absorption of the generated microwaves is limited by providing a plasma with inhomogeneities in electron density and/or a variable rather than constant magnetization. In the latter case, the cyclotron frequency is variable and may be continuous as a function of a linear position.

Continued on Page

Read and Understood By

[signature]	8/20/01	Nelson I Greene	8/20/01
Signed	Date	Signed	Date

PROJECT ____

Continued From Page ____

A magnetic mirror designed previously may create both an inhomogeneous plasma and the continuously variable cyclotron frequency to permit the plasma to emit microwaves.

Continued on Page

Read and Understood By

Signed: [signature] Date: 8/20/01

Signed: Nelson L. Greene Date: 8/20/01

10/7/01

The mobility of free electrons in oil increased by a factor of two as indicated by the results of Kelly [Arnold J. Kelly, "Electrostatic Atomizing Device, United States Patent No. 4,581,675, April 8, 1986]. Above breakdown, the slope of the current versus electric field was discontinuous. It shifted to one half that before breakdown. This corresponds to a higher mobility of electrons to the grounded electrode of a triode, with a concomitant reduction in charging of the moving oil and the corresponding charged fluid current at the outlet of the dispersion device of Kelly. The breakdown current proves light which excites the electron transition from the n=1 to the n=1/2 state as described by Mills [R. Mills, The Nature of Free Electrons in Superfluid Helium--a Test of Quantum Mechanics and a Basis to Review its Foundations and Make a Comparison to Classical Theory, Int. J. Hydrogen Energy, Vol. 26, No. 10, (2001), pp. 1059-1096]. Excitation of electrons to fractional states is a method to increase their mobility to more effectively charge a fluid in order to form a dispersed fluid. The apparatus taught by Kelly [Arnold J. Kelly, "Electrostatic Atomizing Device, United States Patent No. 4,581,675, April 8, 1986] may be improved by a modification to include a source of light to cause the electron transitions as taught by Mills [R. Mills, The Nature of Free Electrons in Superfluid Helium--a Test of Quantum Mechanics and a Basis to Review its Foundations and Make a Comparison to Classical Theory, Int. J. Hydrogen Energy, Vol. 26, No. 10, (2001), pp. 1059-1096].

(Graphs at TIL

Continued on Page

Read and Understood By

Signed 10/7/01 Date

Signed 10/8/01 Date

In an embodiment of the micro wave power cell disclosed in my U.S. Provisional Additional patent application, "Microwave Power Cell, Chemical Reactor, and Power Converter" filed 10/4/01 incorporated herein in its entirety,

the plasma is seeded with ~~[illegible]~~ small or micro particles that are conducting or are a source of conducting small or microparticles such as Al_2O_3 particles. In an embodiment the conducting microparticles are seeded in the plasma torch of ~~the~~ the ~~disclosed~~ cited U.S. Prov. Application.

In ~~another~~ other embodiments, of the plasma torch and/or the micro wave cell ~~[illegible]~~ the cell further comprises a field amplification structure such as an antenna of a pinned conductor. ~~[illegible]~~

Continued on Page

Read and Understood By

[signature] Signed 10/8/01 Date

[signature] Signed 10/8/01 Date

AD PROJECT: Plasma Torch and Particle ~~nano~~ Hydrogen Catalysis Cell

Notebook No. ______

Continued From Page ______

The local field is intensified at the point ~~such~~ that ions are created at the plasma ~~the~~ temperatures, and a non thermal plasma is generated. In an embodiment, the nonthermal plasma comprises at least one of an argon hydrogen ~~gas~~ and a helium-hydrogen plasma.

The conducting particles ~~are~~ or source of conducting particles may be suspended by the same means as the catalyst by the methods such as agitation ~~agitated~~ and ~~core~~ flow provided by the plasma gas or hydrogen gas, or by aspiration or injection.

Continued on Page

Read and Understood By

[signature]	10/8/01	W Good	10/8/01
Signed	Date	Signed	Date

1/24/02

• The high power levels observed previously in the microwave cells [R. L. Mills, P. Ray, B. Dhandapani, M. Nansteel, X. Chen, J. He, "New Power Source from Fractional Rydberg States of Atomic Hydrogen", Chem. Phys. Letts., submitted.] may be due to the accumulation of an energetic material such as HeH or ArH* on the quartz tube wall that undergoes reaction with a plasma containing helium to produce very high power as seen with the Beenakker cavity and the red-yellow coating which appears to be ArH*. Run the microwave for an extended duration of build up these materials which may decompose to produce power and provide hydrino as a catalyst and a reactant for disproportionation reactions.

Alternatively, the helium-hydrogen microwave plasma showed very strong hydrino lines down to 8 nm with KI present in the reaction chamber. A titanium screen was also present in some experiments. Both KI and Ti act as a source of electrons to form hydrino hydride compounds. When these have accumulated to a sufficient extent, the disproportionation reaction may occur sufficiently to sustain a very high catalysis reaction rate which exceeds the rate at which hydrinos are lost by reaction or transport. This condition is akin to ignition in a fusion reaction or critical mass in fission chain reactions. Run the cell with a source of electrons such as KI, Sr, and/or Ti to form hydrino hydride compounds to generate a high power condition. In one case, the reactant may be placed directly into the cell. In another, the reactant may be volatilized from a reservoir by heating.

Continued on Page

Read and Understood By

Signed	Date	Signed	Date
[signature]	1/24/02		

In another embodiment of an apparatus, methods, and compounds terminated or comprising lower-energy hydrogen of the present invention disclosed in my Provisional U.S. Patent Applicatio entitled "Diamond Synthesis", filed on May 1, 2002, a source of carbon in replaced by a source of any Group IV element such as silicon, germanium, tin or lead. Solid, liquid, and gaseous sources of Group IV elements are given in David R. Linde, *CRC Handbook of Chemistry and Physics*, 79 th Edition, CRC Press, Boca Raton, Florida, (1998-1999), p. 4-82 to 4-83, 4-59, 4-91 to 4-92, 4-65 to 4-66 which is herein incorporated by reference. Sources of carbon of the present invention are also given by Linde at 3-3 to 3-330 and 4-49 to 4-50 which is herein incorporated by reference in its entirety.

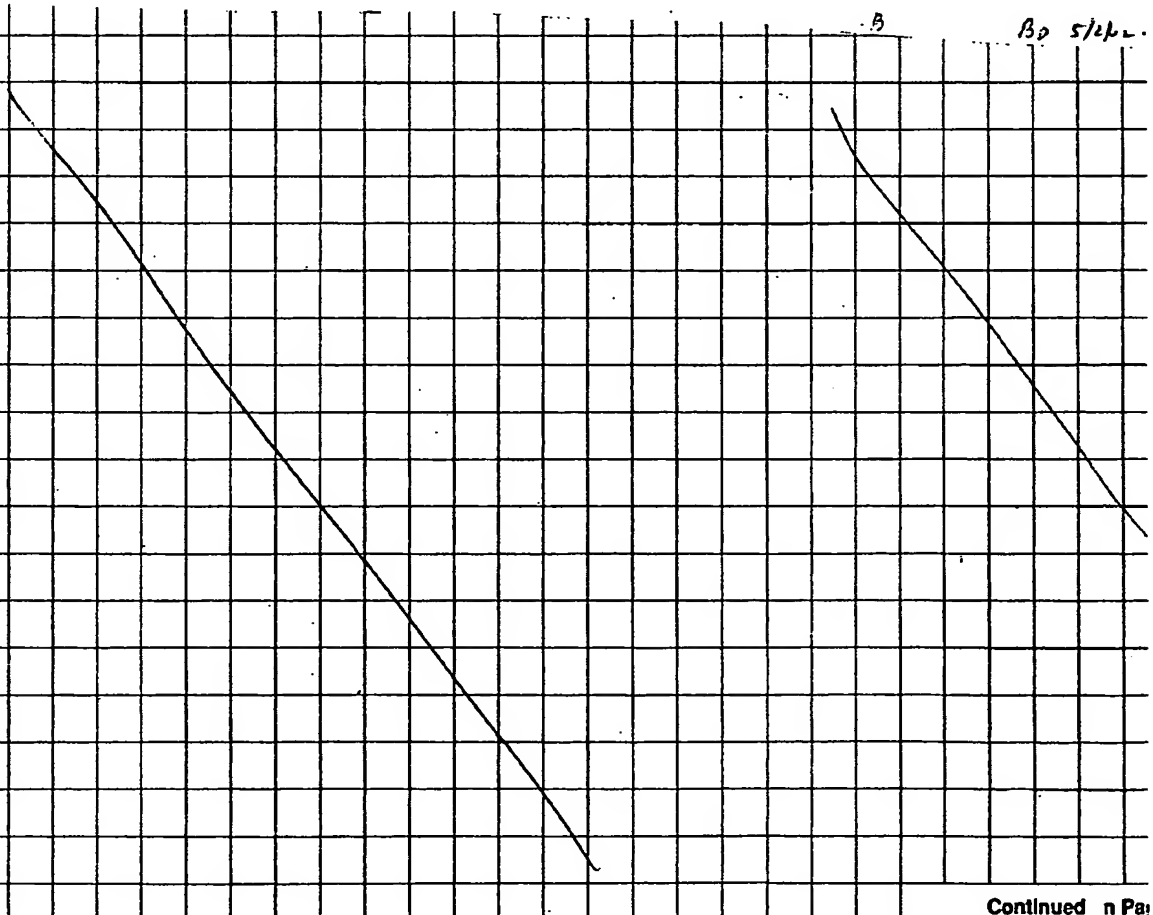

Continued on Page

Read and Understood By

Signed	Date	Signed	Date
DM	5/1/02	Bala Ramadurai	5/2/02

5/23/02
In an embodiment, of the microwave power cell and hydrino hydride reactor, the output power is optimized by using a cavity such as an Evenson cavity and tuning the cell to an optimal voltage staging wave. In an embodiment, the reflected versus input power is tuned such that a desired voltage standing wave is obtained which optimizes or controls the output power. Typically, the ratio of the maximum voltage to the minimum voltage on the transmission line determines the voltage standing wave. In another embodiment, the cell comprises a tunable microwave cavity having a desired voltage standing wave to optimize and control the output power.

5/23/02
Metal hydride films such as FeH form with a neon-hydrogen (99/1%) plasma with a stainless steel reactor and a stainless steel cathode. Preferably the cathode is made of a metal M and MH is synthesized wherein H is an increased binding energy hydrogen species. In an embodiment, the cathode is iron in the case of the synthesis of FeH. In another embodiment, the cell is operated at an elevated temperature. The cell may be operated in the temperature range of about 25-100°C. Preferably the cell is operated in the range of about 100-3500°C. More preferably the cell is operated in the range of about 200-1500°C. Most preferably the cell is operated in the range of about 400-800°C. The higher operating temperature may also cause hydrino hydride compounds to volatilize from the cathode to increase the power of the hydrogen catalysis reaction by maintaining a high voltage, hollow cathode discharge as opposed to a lower voltage discharge at a constant input power.

5/16/02
new patent claiming use of ultrasound to force motion in the tissue to achieve resonance at a specific frequency and to produce a finite recoilless fraction. Rather than thermal and body motion causing a destruction of the resonance, drive a specific motion with ultrasound that suppresses the random motion in order to achieve the Mossbauer effect. Selectivity is also achieved since the corresponding resonance frequency may be induced only in the tissue of interest.

5/15/02
The synthesis of the metal hydride films requires lining the reactor with

quartz and maintaining a plasma with a catalyst gas such as neon, argon, or helium with hydrogen. The hydrino metal hydride can be peeled from the quartz. The reaction must be run at high temperature in order to achieve a sufficient metal reactant vapor pressure such as 500°C in order to achieve a sufficient iron vapor pressure to form iron hydrino hydride.

5/13/02

Another embodiment of the hydrino hydride reactor and power cell comprises a glow discharge cell and a microwave and or RF cell of the present invention. In an embodiment, the glow discharge cell provides a catalyst for a source of catalyst such as He^+, Ar^+, and Ne^+ from helium, argon, and neon gas, respectively.

an out-of-tune microwave cavity may give excess power
match panel readings of catalyst-hydrogen gas mixture to that of control gas mixture measured in water bath calorimeter to measure the actual microwave power into the load which is the same in each case.

use the three stub coaxial cable tuner to match the load with zero reflected power, measure the input to the tuner, place the entire system, tuner and cavity onto the calorimeter, and measure the output power. a high voltage standing wave may exist between the cavity and the tuner which may enhance the catalysis reaction. the input power is not all to the cavity; thus, any excess power gives a conservative ratio

RLM
6/4/02

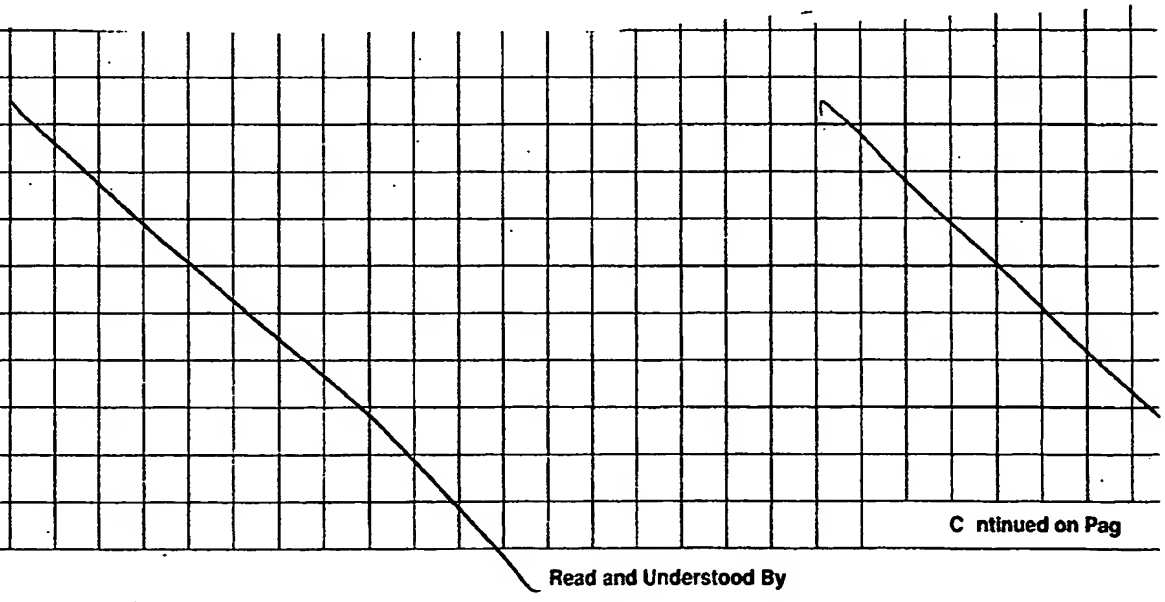

Continued on Page

Read and Understood By

Signed	Date	Signed	Date
[signature]	6/4/02	Bala Ramadapani	6/4/02

7/15/02

The present invention of a power cell and power converter comprises a hydrogen catalysis cell that produces an inverted hydrogen population such as one of those disclosed in my US Provisional Patent Applications entitled "Blue Laser" filed on May 17, 2002 and June 6, 2002 which are herein incorporated by reference in their entirety. In an embodiment, the power cell comprises a hydrogen laser as further disclosed in my US Provisional Patent Applications entitled "Blue Laser" filed on May 17, 2002 and June 6, 2002. The laser light is converted to electricity using a photon-to-electric converter of the present invention such as a photoelectric or photovoltaic cell. In the case of a photoelectric cell, the photons are incident on a photoelectric material that is responsive to the wavelength of the laser light such that electrons are ejected and collected at a grid or electrode. The photoelectric material serves as a anode (positive electrode) and the electron collector serves as a cathode (negative electrode). The electrical circuit completed between these electrodes through a load such that the voltage developed between the electrodes drives a current. Thus, electrical power is delivered to and dissipated in the load.

Continued n Page

Read and Understood By

Signed	Date	Signed	Date
	7/15/02		7/15/02

H_2O (helium hydrino hydride)

10/3/02

Helium hydrino hydride (HeH*) may be formed by a plasma reaction of helium and hydrogen as described in my previous journal articles: R. L. Mills, P. Ray, B. Dhandapani, J. He, "New Energy States of Atomic Hydrogen Formed in a Catalytic Helium-Hydrogen Plasma", IEEE Transactions on Plasma Science, submitted and R. Mills, P. Ray, "Spectral Emission of Fractional Quantum Energy Levels of Atomic Hydrogen from a Helium-Hydrogen Plasma and the Implications for Dark Matter", Int. J. Hydrogen Energy, Vol. 27, No. 3, pp. 301-322 which are incorporated herein by reference in their entirety. HeH* may be collected in a liquid nitrogen cryotrap that is connected to the plasma reactor. The reaction gases may be pumped off and the condensed HeH* may then be warmed to form the gas. HeH* may be used as an energetic material, a fuel, or a propellant as describe in my previous patent applications such as Serial No. 09/009,294 filed January 20, 1998; Serial No. 09/111,160 filed July 7, 1998; Serial No. 09/111,170 filed July 7, 1998; Serial No. 09/111,016 filed July 7, 1998; Serial No. 09/111,003 filed July 7, 1998; Serial No. 09/110,694 filed July 7, 1998; Serial No. 09/110,717 filed July 7, 1998; Serial No. 60/053378 filed July 22, 1997; which are herein incorporated by reference in their entirety.

BD 10/3/02.

Continued on Page

Read and Understood By

Signed 10/3/02 Date

Bala Dhandapani Signed 10/3/02 Date

6/3/03

In an embodiment of the power cell and hydride reactor to form atomic states of hydrogen having energies given by $\frac{13.6\ eV}{\left(\frac{1}{p}\right)^2}$ where p is an integer by reaction of atomic hydrogen with a catalyst, a catalyst is generated by ionization or excimer formation of a source of catalyst. The means to ionize or form an excimer may be an ion beam. The beam may pass through a window into a cell capable of maintaining a vacuum or pressures greater than atmospheric pressure. The beam may be an electron beam. The catalyst may be He^+, He_2^*, Ne_2^*, Ne^+, Ne^+/H^+ or Ar^+ catalysts from a source comprising helium, helium, neon, neon-hydrogen mixture, and argon gases, respectively. The beam energy may be in the range of about 0.1 to 100 MeV, preferably on the range of about 10 eV to 1 MeV, more preferably in the range of about 100 eV to 100 keV, and most preferably in the range of about 1 keV to 50 keV. The beam may maintain a plasma of hydrogen and the source of catalyst. The plasma may provide atomic hydrogen or the atomic hydrogen may be formed by a dissociator such as a filament, or metal such as platinum, palladium, titanium, or nickel.

6/2/03

The predicted vibrational energy of $H_2(1/4)$ is

p	p^2	eV	cm^-1	nm
4	16	8.729332138	70406.23518	142.0328589

The predicted rotational energy of $H_2(1/4)$ is

p	p^2	eV	cm^-1	nm
4	16	0.24144	1947.328977	5135.238569

A series of lines are predicted at

J+1 to J	eV	cm^-1	nm
0	8.729332138	70406.23518	142.0328589
1	8.487892138	68458.9062	146.0730155
2	8.246452138	66511.57722	150.3497479
3	8.005012138	64564.24825	154.8844622

BD 6/4/03

I on Pag

Signed 6/3/03 Date Signed Bala Dhandapani 6/4/03 Date

4	7.763572138	62616.91927	159.7012275
5	7.522132138	60669.59029	164.8272029
6	7.280692138	58722.26131	170.2931502
7	7.039252138	56774.93234	176.1340517
8	6.797812138	54827.60336	182.3898594
9	6.556372138	52880.27438	189.1064104
10	6.314932138	50932.94541	196.3365517

BD 6/4/03

These lines may be observed from argon-hydrogen plasma emission when oxygen was added. Run argon-hydrogen. Add oxygen or alternatively water vapor.

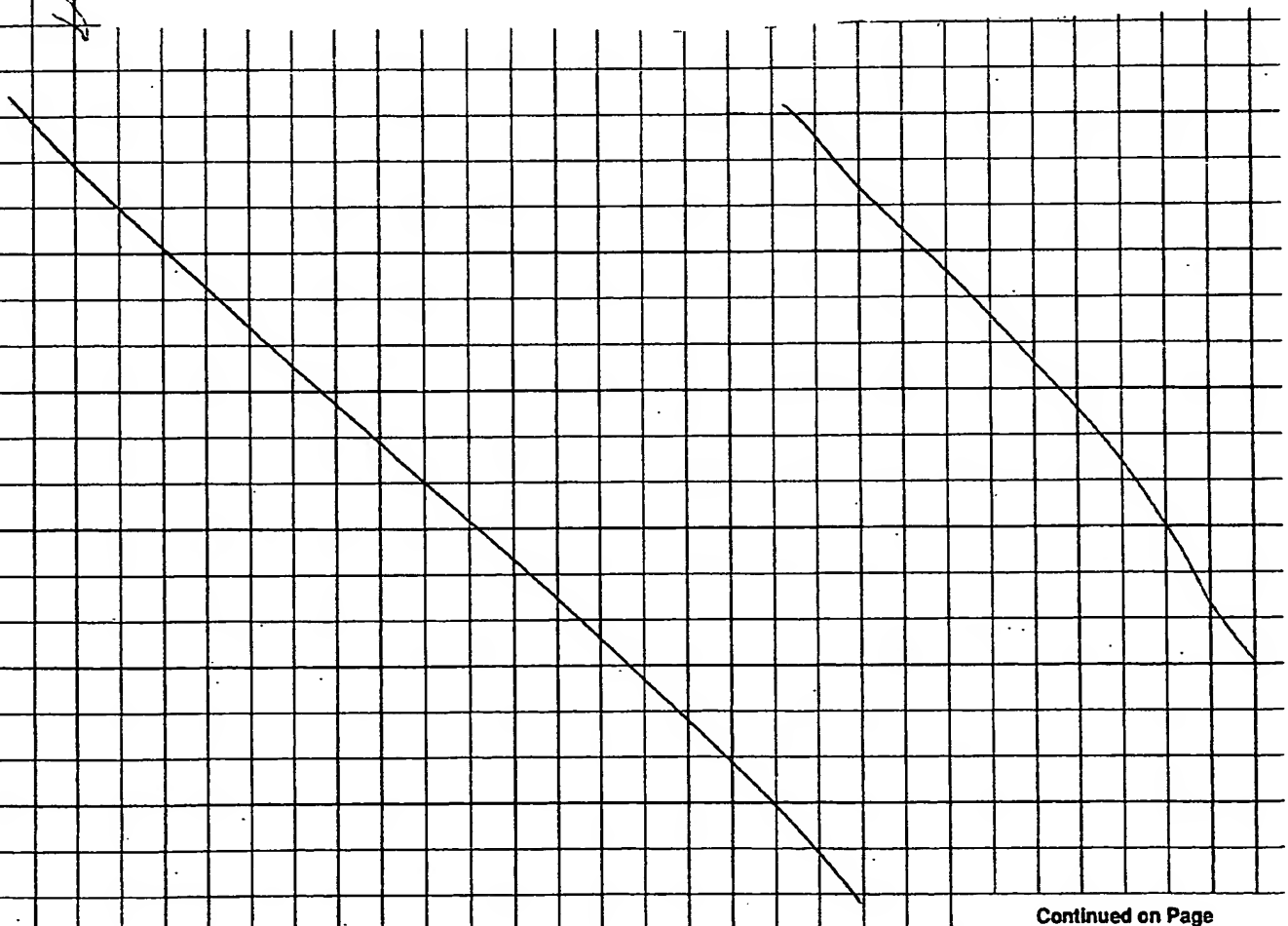

Continued on Page

R ad and Underst d By

Signed	6/3/03 Date	Bala Ohandapani Signed	6/4/03 Date

6/4/03

EUV Program (PR)

•* The predicted vibrational energy of $H_2(1/4)$ is

p	p^2	eV	cm^-1	nm
4	16	8.729332138	70406.23518	142.0328589

The predicted rotational energy of $H_2(1/4)$ is

p	p^2	eV	cm^-1	nm
4	16	0.24144	1947.328977	5135.238569

A series of lines are predicted at

J+1 to J	eV	cm^-1	nm
0	8.729332138	70406.23518	142.0328589
1	8.487892138	68458.9062	146.0730155
2	8.246452138	66511.57722	150.3497479
3	8.005012138	64564.24825	154.8844622
4	7.763572138	62616.91927	159.7012275
5	7.522132138	60669.59029	164.8272029
6	7.280692138	58722.26131	170.2931502
7	7.039252138	56774.93234	176.1340517
8	6.797812138	54827.60336	182.3898594
9	6.556372138	52880.27438	189.1064104
10	6.314932138	50932.94541	196.3365517

These lines may be observed from argon-hydrogen plasma emission when oxygen was added. Run argon-hydrogen. Add oxygen since oxygen will also eliminate the molecular hydrogen peaks in this region. Alternatively, run argon-water vapor plasma. Repeat with helium and neon. The observation of vibration-rotational lines of $H_2(1/4)$ by electron beam excitation will support that the Franck-Hertz experiment will be successful.

BD
6/4/03

*• Electron impact excitation may be possible with spectroscopy in the near-electrode region of a high voltage discharge. Record the vibration-rotational lines of $H_2(1/4)$ from glow discharge plasma of catalyst-hydrogen mixtures such as argon, helium, or neon mixed with hydrogen.

Signed 6/3/03 Date Signed 6/4/03 Date

BD 6/4/03

*• Check the data of the electron bombardment of $CsNO_3$ (10/24/00) for vibration-rotational lines of $H_2(1/4)$.

*• Run condensed gas in 110 -180 nm region to search for $H_2(1/4)$ lines.

*• Run visible spectrum on condensed gas to search for $H_2(1/p)$ vibration-rotational lines.

Continued on Page

Read and Understood By

Signed	Date	Signed	Date
[signature]	6/3/03	Bob Lindgren	6/4/03

6/6/03

In the case that a high pressure noble catalyst-hydrogen mixture such as an argon-hydrogen mixture is used, the formation of a plasma with an electron beam may result in the formation of a high concentration of excimers such as Ar_2^*. The noble catalyst-hydrogen mixture may be maintained in the high pressure range of about 1 Torr to 100 atm, preferably in the range of about 10 Torr to 10 atm, more preferably in range of about 100 Torr to 5 atm, and most preferably in the range of about 300 Torr to 1 atm. In addition to the formation of the catalyst from a source by electron-beam ionization, a source of ionizing ion may be added to form the catalyst from the source of catalyst. In an embodiment, He^+, Ne^+, Ne^+/H^+ or Ar^+ catalysts are formed from a source comprising helium, neon, neon-hydrogen mixture, and argon gases, respectively. The ionizing ion may be ionized by means such as the electron beam and secondarily ionize the source of catalyst to form the catalyst. The ionizing ion may be O^+ from O_2. The ionizing ion may react with noble gas excimers to form the catalyst. The excimers may be He_2^*, Ne_2^*, Ne_2^*, and Ar_2^*, and the catalysts may be He^+, Ne^+, Ne^+/H^+ or Ar^+, respectively.

In an embodiment, the ionization energy of the noble gas atom is higher than the energy released when the ionizing ion is reduced by ionizing the noble gas atom. The ionization of the noble gas atom occurs because the noble gas atom comprises an excimer in an excited state. The excited state energy makes the ionization energetically favorable. In an embodiment, Ar_2^* has an excited state energy of about 9-10 eV; thus, the ionization reaction

BP 6/6/03

$$Ar_2^* + O^+ \rightarrow Ar + Ar^+ + O \quad (1)$$

is energetically favorable wherein the first ionization energies of Ar and O are 15.75962 and 13.61806 eV, respectively.

Continued on Page

Read and Understood By

Signed	Date	Signed	Date
	6/6/03	Bob Dhandapani	6/6/03

6/6/03

In the case that a high pressure noble catalyst-hydrogen mixture such as an argon-hydrogen mixture is used, the formation of a plasma with an electron beam may result in the formation of a high concentration of excimers such as Ar_2^*. The noble catalyst-hydrogen mixture may be maintained in the high pressure range of about 1 Torr to 100 atm, preferably in the range of about 10 Torr to 10 atm, more preferably in range of about 100 Torr to 5 atm, and most preferably in the range of about 300 Torr to 1 atm. In addition to the formation of the catalyst from a source by electron-beam ionization, a source of ionizing ion may be added to form the catalyst from the source of catalyst. In an embodiment, He^+, Ne^+, Ne^+/H^+ or Ar^+ catalysts are formed from a source comprising helium, neon, neon-hydrogen mixture, and argon gases, respectively. The ionizing ion may be ionized by means such as the electron beam and secondarily ionize the source of catalyst to form the catalyst. The ionizing ion may be O^+ from O_2. The ionizing ion may react with noble gas excimers to form the catalyst. The excimers may be He_2^*, Ne_2^*, Ne_2^*, and Ar_2^*, and the catalysts may be He^+, Ne^+, Ne^+/H^+ or Ar^+, respectively.

In an embodiment, the ionization energy of the noble gas atom is higher than the energy released when the ionizing ion is reduced by ionizing the noble gas atom. The ionization of the noble gas atom occurs because the noble gas atom comprises an excimer in an excited state. The excited state energy makes the ionization energetically favorable. In an embodiment, Ar_2^* has an excited state energy of about 9-10 eV; thus, the ionization reaction

$$Ar_2^* + O^+ \rightarrow Ar + Ar^+ + O \qquad (1)$$

is energetically favorable wherein the first ionization energies of Ar and O are 15.75962 and 13.61806 eV, respectively.

BD
8/5/03

Continued on Pag

Read and Understood By

Signed 7/30/03 Dat

Babi Dhandapani 8/5/03
Signed Dat

6/3/03

In an embodiment of the power cell and hydride reactor to form atomic states of hydrogen having energies given by $\frac{13.6\ eV}{\left(\frac{1}{p}\right)^2}$ where p is an integer by reaction of atomic hydrogen with a catalyst, a catalyst is generated by ionization or excimer formation of a source of catalyst. The means to ionize or form an excimer may be an ion beam. The beam may pass through a window into a cell capable of maintaining a vacuum or pressures greater than atmospheric pressure. The beam may be an electron beam. The catalyst may be He^+, He_2^*, Ne_2^*, Ne^+, Ne^+/H^+ or Ar^+ catalysts from a source comprising helium, helium, neon, neon-hydrogen mixture, and argon gases, respectively. The beam energy may be in the range of about 0.1 to 100 MeV, preferably on the range of about 10 eV to 1 MeV, more preferably in the range of about 100 eV to 100 keV, and most preferably in the range of about 1 keV to 50 keV. The beam may maintain a plasma of hydrogen and the source of catalyst. The plasma may provide atomic hydrogen or the atomic hydrogen may be formed by a dissociator such as a filament, or metal such as platinum, palladium, titanium, or nickel.

BD
8/5/03

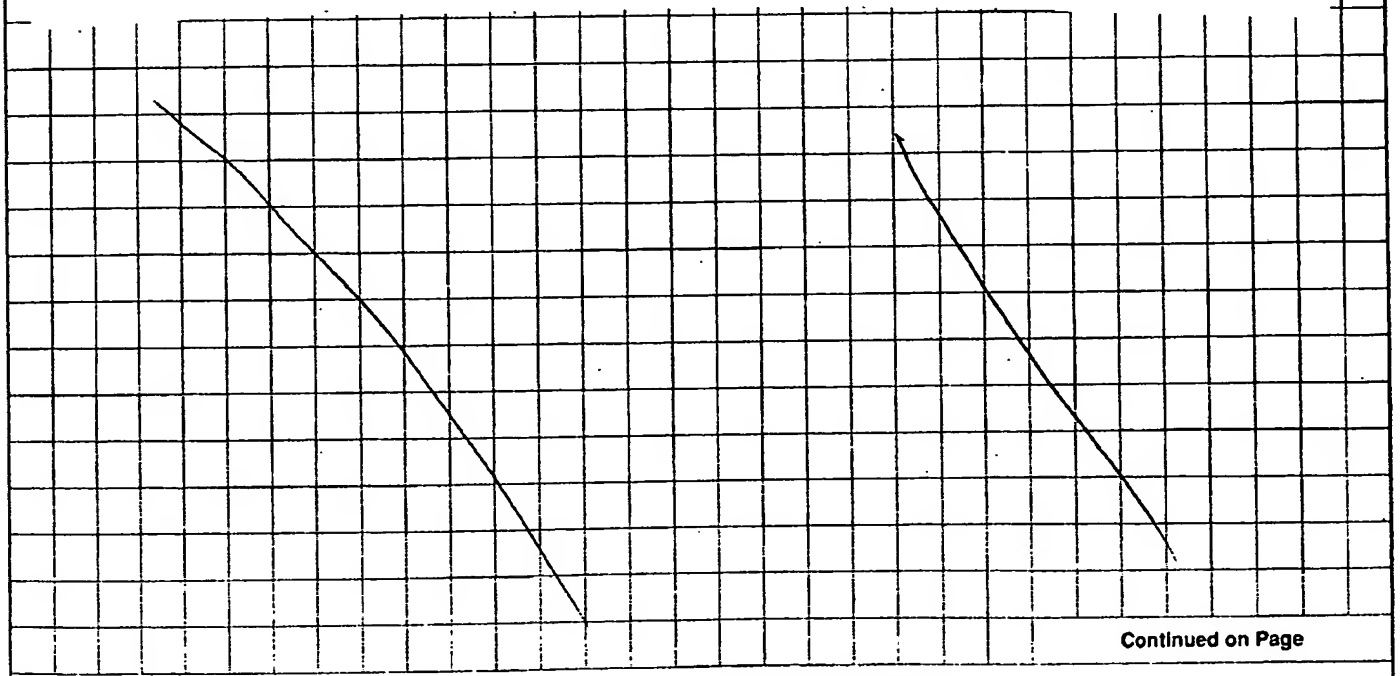

Continued on Page

Read and Understood By

Signed	Date	Signed	Dat
	7/30/03	Bob Dhandapani	8/5/03

7/29/03

The predicted vibrational energy of $H_2(1/4)$ is

p	p^2	eV	cm^-1	nm
4	16	8.254432	66575.93862	150.2043993

The predicted rotational energy of $H_2(1/4)$ is

p	p^2	eV	cm^-1	nm
4	16	0.24144	1947.328977	5135.238569

A series of lines are predicted at

J+1 to J	eV	cm^-1	nm
0	8.254432	66575.93862	150.2043993
1	8.012992	64628.60965	154.7302181
2	7.771552	62681.28067	159.5372456
3	7.530112	60733.95169	164.6525311
4	7.288672	58786.62272	170.1067081
5	7.047232	56839.29374	175.9346081
6	6.805792	54891.96476	182.1760054
7	6.564352	52944.63579	188.8765258
8	6.322912	50997.30681	196.0887642
9	6.081472	49049.97783	203.8736674
10	5.840032	47102.64886	212.3022614

These lines may be observed from argon-hydrogen plasma emission when oxygen was added. Run argon-hydrogen. Add oxygen or alternatively water vapor.

RD
8/5/03

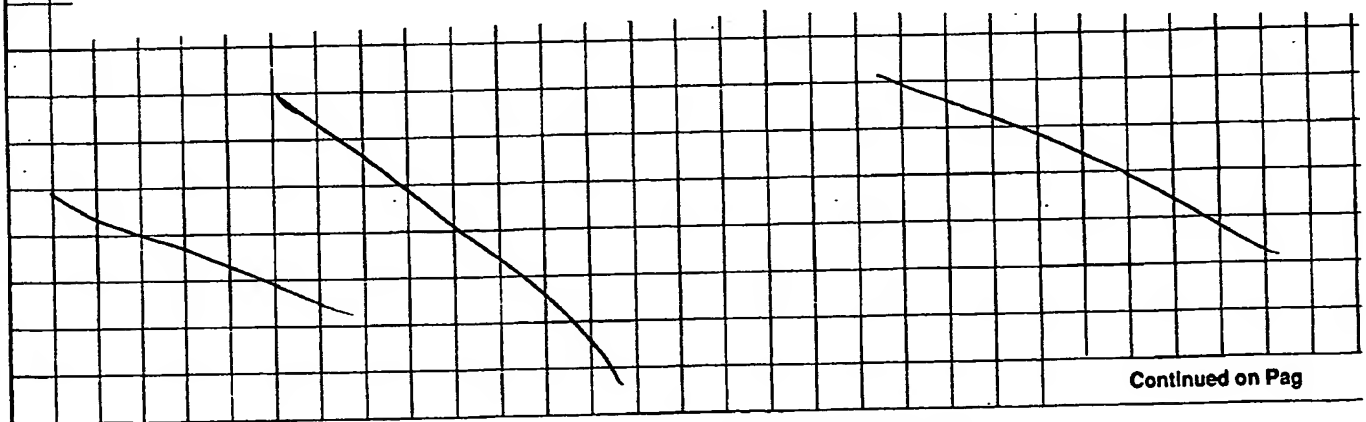

Continued on Pag

Read and Understood By

Signed 7/30/03 Dat

Signed 8/5/03 Dat

9/2/03

A number of experiments indicate that negatively charging the plasma or the reaction mixture will enhance the rate of the hydrogen catalysis reaction. The electrolysis cell that maintains a negative voltage when the power is switched off has a measured gain of at least 10 times the input power. The electron gun experiment shows a high yield of lower-energy hydrogen. The rt-plasma has the greatest intensity when the W filament is hot enough to emit electrons. N. Greenig discharge cell comprised a W filament anode which can emit electrons. The K2CO3 cell run by Conrads et al. used a W wire heated externally wherein the W wire may serve as a source of electrons. The Sr-H2 rt-plasma increased significantly with the application of magnetic electron confinement. Inversion, broadening, and lower-energy hydrogen emission is observed when the wall temperature of the cells maintaining plasmas of catalysts and hydrogen is elevated to boil off hydride ions. This was observed with the RF and Evenson cell plasmas maintained in quartz or Pyrex reactors. Excess heat was observed with an elevated wall temperature in the case of glow discharge cells wherein the elevated temperatures were maintained by an oven.

The negative charge may increase the rate by filling electron energy levels such those below the continuum level. The filling of the level up to the vacuum level may be analogous to the Fermi level of a metal. In this case, the net enthalpy of the catalyst provided by ionization of one or more electrons to the continuum level better matches an integer multiple of 27.2 eV.

In an embodiment of the hydrogen catalysis cell, the plasma has a net negative charge at least in a region where catalyst and atomic hydrogen is present. The negative charge may be provided by at least one of a source of electrons and a means to confine electrons. The means to confine electrons may be a magnetic field such as a magnetic bottle or a selenoidal field. The electron source may be an electron emitter such as a heated filament such as a thoriated W, rhenium, or BaO filament or an alkali (Group I) metal or an alkaline earth (Group II) metal. The source of electrons may be a thermionic cathode. The source of electrons may be an electron gun. Alternatively, the source of electrons may be an electron beam or a discharge electrode such as an anode. The electrons may preferentially be increased in a desired spatial region by an electric field. The electric field may be provided by electrodes. The negative charge may also be provided by a source of negatively charged ions such as hydride ions. In an embodiment, negative ions such as hydride ions are boiled from the surface of the wall of the reactor by maintaining the wall at an elevated temperature.

BD 9/5/03

Signed 9/2/03 Date Bob Greenyer Signed 9/5/03 Date

In a further embodiment of the hydrogen catalysis cell, the plasma has a net positive charge at least in a region where catalyst and atomic hydrogen is present. The positive charge may be provided by at least one of a source of ions and a means to confine ions. The means to confine ions may be a magnetic field such as a magnetic bottle or a selenoidal field. Alternatively, electrons may be confined in a region such that a desired region outside of the electron-rich region is positively charged. The means to confine electrons may be a magnetic field such as a magnetic bottle or a selenoidal field. The source of ions may be an ion beam or a discharge electrode such as a cathode. The ions may preferentially be increased in a desired spatial region by an electric field. The electric field may be provided by electrodes. The positive charge may also be provided by a source of positively charged ions such as a source of alkali (Group I) or alkaline earth (Group II) ions. In an embodiment, positive ions such as alkali or alkaline earth ions are boiled from the surface of the wall of the reactor by maintaining the wall at an elevated temperature. The positive ions may also be provided by boiling off electrons to a different region such that electron-emitting source acquires a net positive charge that positively charges the plasma. Such a source is a thermionic cathode.

RLP
9/5/03

9/2/03

In the electron gun experiment, free electrons may serve as the catalyst wherein the free electrons undergo an inelastic scattering reaction with hydrogen atoms.

Continued n Page

Read and Understo d By

Signed	9/2/03 Date	Signed	9/5/03 Date

Continued on Page

Read and Understood By

Signed	Date	Signed	Date

Document made available under the Patent Cooperation Treaty (PCT)

International application number: PCT/US04/035143

International filing date: 22 October 2004 (22.10.2004)

Document type: Certified copy of priority document

Document details: Country/Office: US
Number: 60/513,582
Filing date: 24 October 2003 (24.10.2003)

Date of receipt at the International Bureau: 06 January 2005 (06.01.2005)

Remark: Priority document submitted or transmitted to the International Bureau in compliance with Rule 17.1(a) or (b)

World Intellectual Property Organization (WIPO) - Geneva, Switzerland
Organisation Mondiale de la Propriété Intellectuelle (OMPI) - Genève, Suisse